An Advanced Electrospinning Method of Fabricating Nanofibrous Patterned Architectures with Controlled Deposition and Desired Alignment

Thesis submitted to

University of Ontario Institute of Technology

in partial fulfillment of the requirements for the award of the degree of

DOCTOR OF PHILOSOPHY

In Mechanical Engineering

Under the Faculty of Engineering and Applied Science

By

Sheikh Md Rasel

Under the supervision of

Dr. Ghaus Rizvi

November 18, 2015

Faculty of Engineering and Applied Science
University of Ontario Institute of Technology

AUTHOR'S DECLARATION

I hereby declare that I am the sole author of this thesis. This is a true copy of the thesis, including any required final revisions, as accepted by my examiners.

I understand that my thesis may be made electronically available to the public.

Abstract

We introduce a versatile advanced method of electrospinning for fabricating various kinds of nanofibrous patterns along with desired alignment, controlled amount of deposition and locally variable density into the architectures. In this method, we employed multiple electrodes whose potentials have been altered in milliseconds with the help of microprocessor based control system. Therefore, key success of this method was that the electrical field as well as charge carrying fibers could be switched shortly from one electrode's location to another, as a result, electrospun fibers could be deposited on the designated areas with desired alignment.

A wide range of nanofibrous patterned architectures were constructed using proper arrangement of multiple electrodes. By controlling the concurrent activation time of two adjacent electrodes, we demonstrated that amount of fibers going into the pattern can be adjusted and desired alignment in electrospun fibers can be obtained. We also revealed that the deposition density of electrospun fibers in different areas of patterned architectures can be varied. We showed that by controlling the deposition time between two adjacent electrodes, a number of functionally graded patterns can be generated with uniaxial alignment. We also demonstrated that this handy method was capable of producing random, aligned, and multidirectional nanofibrous mats by engaging a number of electrodes and switching them in desired patterns.

A comprehensive study using finite element method was carried out to understand the effects of electrical field. Simulation results revealed that electrical field strength alters shortly based on electrode control switch patterns.

Nanofibrous polyvinyl alcohol (PVA) scaffolds and its composite reinforced with wollastonite and wood flour were fabricated using rotating drum electrospinning technique. Morphological, mechanical, and thermal, properties were characterized on PVA/wollastonite and PVA/wood flour nanocomposites containing 0, 5, 10, and 20 wt % of fillers. Morphological analyses carried out by digital optical microscope, scanning

electron microscopy, x-ray computed tomography, and Fourier transform infrared spectroscopy, confirmed the presence and well dispersion of fillers in the composites. In addition, improvement of mechanical properties with increased filler content further emphasized the adhesion between matrix and reinforcement. PVA with 20 wt % wollastonite composite exhibited the highest tensile strength (11.99 MPa) and tensile module (198 MPa) as compared to pure PVA (3.92 MPa and 83 MPa, respectively). Moreover, the thermal tests demonstrated that there is no major deviation in the thermal stability due to the addition of wollastonite in PVA scaffolds. Almost similar trend was observed in PVA/wood flour nanocomposites where tensile strength improved by 228 % for 20 wt % of reinforcement. The PVA/wollastonite and PVA/wood flour fibrous nanocomposite which poses higher mechanical properties might be potentially suitable for many advanced applications such as filtration, tissue engineering, and food processing.

We believe, this study will contribute to further scientific understanding of the patterning mechanism of electrospun nanofibers and to allow for variety of design of specific patterned nanofibrous architectures with desired functional properties. Therefore, this improved scheme of electrospinning can have significant impact in a broad range of applications including tissue engineering scaffolds, filtrations, and nanoelectronics.

Acknowledgements

First and foremost, I would like to express my profound and sincere gratitude, and thanks to my supervisor, Dr. Ghaus M. Rizvi for his continuous invaluable advice, support, and guidance throughout the duration of this work.

I express my deepest appreciation to my Ph.D Committee members for their valuable suggestions and constructive comments.

I would like to give a special thanks to Tahir Siddiqui for his valuable support with the electronic design of the system.

I also extend my thanks to Keval Thaker, an undergraduate student at UOIT, for developing the MATLAB codes of image processing.

My special thanks and appreciation to my colleagues, to Dr. Reza Rizvi and to all of my friends for their help and encouragement throughout my study period.

The financial support provided by Ontario Trillium Scholarships is greatly appreciated.

Finally, my deepest gratitude goes to my parents, for their life-long love, care, and support. It is my privilege to thank my wife Khadiza Akter, for her constant support and encouragement.

Table of Contents

List of Tables

List of Figures

Lists of Publications

1. **Sheikh Rasel** and Ghaus Rizvi, "Fabrication of fibrous patterned architectures with controlled deposition and multidirectional alignment", Polymers for advanced technologies, 16 June 2015, DOI: 10.1002/pat.3606.

2. **Sheikh Rasel** and Ghaus Rizvi, "Functionally graded deposition of polymer nanofibers by an advanced electrospinning method", Materials Letters (under review).

3. **Sheikh Rasel,** Karandeep Samra, and Ghaus Rizvi, "Thermal, mechanical, and morphological properties of PVA/Wollastonite fibrous nanocomposites", Composites Part A: Applied Science and Manufacturing (under review).

Lists of Symbols and Abbreviations

Symbols

H	Distance between needle tip and the ground collector
L	Length of the capillary
R	Needle outer radius
γ	Surface tension of the liquid
μ	Viscosity
G	Elastic modulus
σ	Stress
t	Time
l	Filament length
a	Cross-sectional radius of the filament
$\bar{\sigma}$	Longitudinal stress
L_1	Critical straight length
Q	Flow rate
σ_1	Surface charge
k	Dimensionless conductivity
E	Electrical field
ρ	Liquid density
l_2	Current passing through the jet
r_o	Initial radius of the jet
σ_2	Material conductivity
V	Voltage potential
ε	Material permittivity
σ_t	Tensile strength

ε_b	Elongation at break
T_g	Glass transition temperature
T_m	Melting temperature

Abbreviations

DC	Direct Current
AC	Alternative Current
PHBV	Poly(hydroxybutyrate- co-valerate)
PLA	Polylactic acid
PEO	Polyethylene oxide
PAA	Polyacrylamide
PVA	Poly(vinyl alcohol)
PU	Polyurethane
PCL	Polycaprolactone
PS	Polystyrene
PMMA	Poly(methyl methacrylate)
CA	Cellulose acetate
PET	Polyethylene Terephtalate
PVC	Polyvinylchloride
PVDF	Poly(vinylidene fluoride)
PAN	Polyacrylonitrile
PE	Polyethylene
PP	Polypropylene
PGA	Poly(glycolic acid)
PVP	Poly (vinyl pyrrolidone)
PA	Phthalic anhydride
PMHS	Polymethylhydrosiloxane
RH	Relative humidity

3D	Three-dimensional
ECM	Extracellurlar matrix
MSCs	Mesenchymal stem cells
DDS	Drug delivery systems
V_2O_5	Vanadium pentoxide
MoO_3	Molybdic oxide
WO_3	Tungsten oxide
FET	Field-effect transistors
CVD	Chemical Vapor Deposition
HVFBT	High voltage flyback transformer
PWM	Pulse-width modulation
OT	Overlap time
NT	Net time
OM	Optical microscope
SEM	Scanning electron microscopy
TEM	Transmission electron microscopy
XCT	X-ray computed tomography
FTIR	Fourier Transform Infrared Spectroscopy
DMA	Dynamic mechanical analysis
TGA	Thermogravimetric Analyzer
AFM	Atomic force microscopy
FEM	Finite element method
CNC	Cellulose nanocrystals
$CaSiO_3$	Calcium silicate
LOI	Loss on Ignition

Chapter 1 Introduction

1.1 Introduction

Nanotechnology is a very fast growing scientific area due to its enormous potential applications in almost all engineering and science disciplines. It is used in medical science, materials science, and in electrical, chemical, and mechanical engineering. Nanostructures consist of at least one dimension at the nanometer range, which is one-billionth of a meter in the SI unit system. At nanometer scale, all materials possess very unique physical, chemical, and biological properties which can be beneficial for advanced applications. An example of zero-dimensional nanostructure is a nanoparticle, whereas a nanotube or a nanofiber is one dimensional nanostructure.

One dimensional nanofibers, with diameters ranging from 10 nm to 1000 nm, and aspect ratios (length/ diameter) larger than 100:1 have outstanding characteristics, such as high specific surface area, flexibility in surface functionality, and superior mechanical properties compared with any other forms of the material [1, 2].These exceptional properties make nanofibers a strong candidate for many important and fascinating applications in tissue engineering scaffolds, drug delivery and release systems, sensors, filtrations, energy storage and so on [3, 4]. These nanofibers are also referred as superfine, ultrafine, and submicron fibers in the literatures [5].

To date, numerous approaches have been developed to fabricate nanofibers such as drawing, phase separation, template synthesis, self-assembly, and electrospinning [6]. Drawing is a process that can produce single long nanofiber one by one from polymer solution. The liquid fiber is drawn from a sharp tip and solidified by rapid evaporation of the solvent. Only viscoelastic materials can be drawn by this technique. The viscosity of the droplet continuously changes with time due to evaporation of solvent which affects the fiber diameter and prevents the continuous drawing of fibers [7].

In phase separation method, the polymer gel is prepared from the homogeneous solution of the polymer. The required concentration of polymer solution is then stored in a refrigerator set at the gelation temperature. The gel is submerged in distilled water for solvent interchange followed by the separation from the distilled water, and blotting with filter paper. Then, they are transferred to a freeze-drying vessel which results in a porous nanofibrous matrix [8]. The main drawback of this process is it is time consuming to transfer the solid polymer phase into a nano-porous structure as it involves five major steps.

In template synthesis, a hard nano-porous membrane is used to obtain, nanofibers of polymers, metals, semiconductors and ceramics. Self-assembly is referred to as a 'bottom-up' manufacturing technique where small molecules are added together to assemble a complete nanofiber [9]. Well-defined structures and properties of nanofibers depend on the smaller molecules and the intermolecular forces that bring the molecules together. However, self-assembly is also considered as a time-consuming process.

Electrospinning has proven to be an efficient, versatile and straightforward approach for fabrication of thin fibers from a rich variety of materials including polymers, composites, and ceramics [10, 11]. The resulting electrospun fibers, having diameter in the micro- to nanometer ranges, can be made into large continuous lengths with uniform diameter. Moreover, electrospinning offers some unique possibilities such as adjustable porosity on electrospun fibers, hollow interiors and the flexibility to spin into a variety of shapes and sizes. Table 1.1 shows a comparison of the processing techniques to obtain nanofibers.

1.2 Motivation

Electrospinning involves fabricating a micro- or nanoscale fiber from polymer solution or melts with the use of high voltage electrical field. The high voltage induces charges to the polymer solution. Electrically charged jet is ejected from the spinneret when the electrostatic forces overcome the surface tension of the polymer solution and then undergoes bending instability and solidification of solvent, resulting in the formation of a randomly oriented, nonwoven mat of thin fibers on the collector screen. Electrospinning has the following remarkable advantages [12]:

- The setup is simple and easy to build
- Electrospun fibers can be fabricated from a wide range of materials
- Can develop wide variety of nanostructures including 1D, 2D, and 3D.
- Fiber diameter can be controlled from micrometer to nanometer
- Versatile fiber morphology
- Potential functional properties of nanofibers
- Potential of large-scale production

The fundamental idea of electrospinning can be traced back to the early 1930s. Anton Formhals published a series of patents from 1934 to 1944 describing an experimental setup for the production of textile yarns [13, 14]. In 1969, Geoffrey Ingram Taylor [15] investigated the jet formation from the droplet of the polymer solution and mathematically determined that an angle of 49.3^0 is desired to balance the electrostatic forces with the surface tension of solution, which is referred as "Taylor cone".

In 1966, Simons [16] revealed a technique for the production of patterned non-woven fabrics. In that method, electrically-spun filaments were aggregated into bundles or clusters defining a controlled pattern of aggregates of high-filament density contrasting with controlled areas of low-filament density. In the following few decades, the structural morphologies of electrospun fibers with various polymer materials have been investigated by a number of research groups. Baumgarten et al. [17], in 1971, studied the electrospinning behaviour of acrylic fibers. In 1987, Hayati et al. [18], investigated the effects of electrical field and the factors affecting the jet stability.

Research on electrospinning gained momentum after late 1990s due to increased knowledge on the application of nanofibers in various potential fields. Over the decade, lot of experiments and theoretical studies with various materials have been carried out via electrospinning which are reflected by the numbers of scientific publications and patents.

Table 1.1 Comparison of the processing techniques to obtain nanofibers [12].

Process	Technology	Repeatability	Controllability	Advantages	Disadvantages
Electrospi-nning	Industrial scale	Yes	Yes	Simple and continuous fibers	Jet instability, low productivity
Drawing	Laboratory scale	Yes	No	Simple process	Irregular process
Phase separation	Laboratory scale	Yes	No	Simple equipment required	Only effective for selective polymers
Template synthesis	Laboratory scale	Yes	Yes	Easy to adjust diameter by employing different templates	Complex process
Self-assembly	Laboratory scale	Yes	No	Easy to get smaller nanofibers	Complex process

Usually, the electrospun nanofibers are collected as randomly oriented nonwoven mats [19]. Recently, a number of methods have been developed to accumulate the electrospun fibers as uniaxial array [20-22]. It is well-known that micro/nano patterned structure with proper alignment may possess potential functions which could be useful for many advanced applications for example, tissue engineering and microelectronics. Zhang and Chang [23] employed electro-conductive templates to produce patterned architectures by electrospun fibers. They reported that diameter, spacing, and protrusions play important

roles in controlling the arrangement of fibers. Wang et al. [24] used stainless steel mesh as a template collector and showed well-tailored architectures and patterns can be a potential candidate for tissues or organs, where an order cellular arrangement is needed.

1.3 Applications of Electrospun Nanofibers

The unique features of nanofibers such as high specific surface area to volume, high porosity, and hollow interiors plus the functionalities from the polymers themselves impart nanofibers with many desired properties for advanced applications. An outlook of possible applications is presented in Figure 1.1.

1.4 Problem Statement

Because of tremendous interest in nanoscale materials and their properties, progress on electrospinning has increased dramatically in the recent years. Electrospinning systems are now capable of processing a wide variety of polymers, ceramics, and composite materials into ultrafine fibers with controllable diameter, and surface morphologies. Furthermore, with the modified collectors setup and advanced spinning techniques, structures with different compositions, hollow interiors, complex architectures, unique morphologies, and functional properties of electrospun fibers have been developed [25, 26]. However, many technical issues still exist and a number of fundamental questions need to be resolved.

Ordered architectures of fibrous patterns are very important for many applications, including nanoscale electronic and photonic devices, and tissue engineering scaffolds. Generally, electrospun fibers are collected as a non-woven randomly oriented mat. Li and coworkers [27] produced uniaxially aligned nanofibers using a pair of conductive electrodes, separated by an air gap, but these cannot be employed successfully for producing complex patterned architectures. Therefore, preparation of electrospun nanofibers with ordered architectures still remains a challenge.

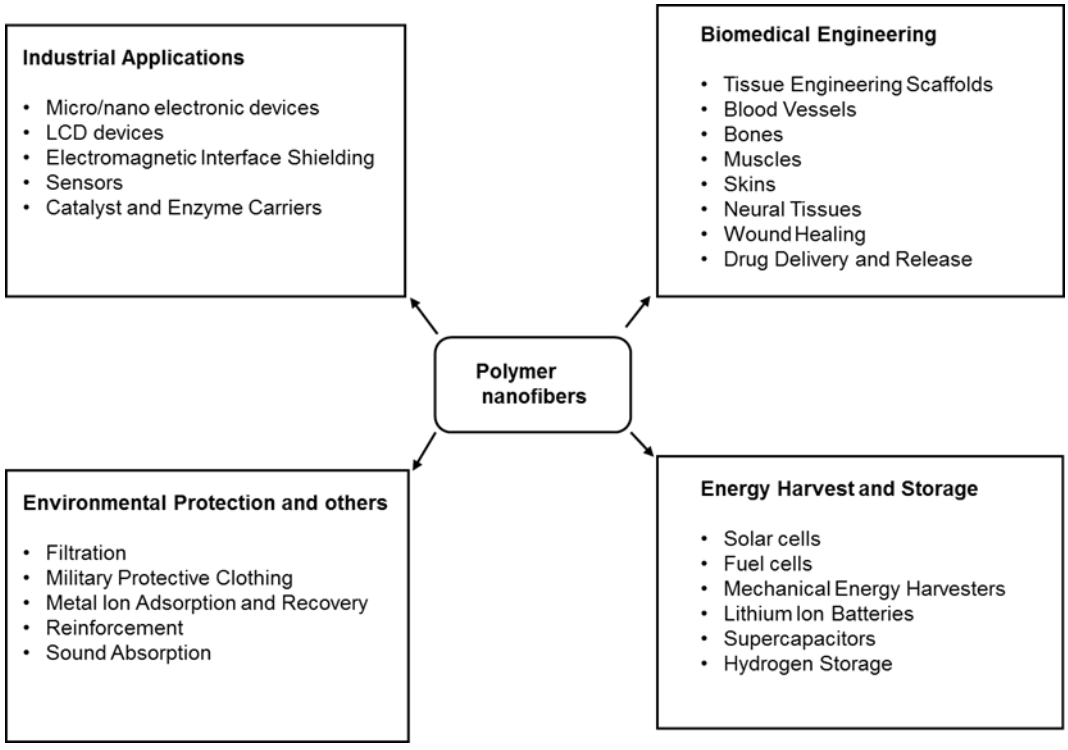

Figure 1.1 Potential applications of electrospun polymer nanofibers.

In addition, controlling the fiber deposition in any desired direction and location within the pattern still remains in rudimentary primary stage of development, particularly for solution electrospinning. A possible mechanism for achieving this is by concentration of electric field in the desired direction of deposition, and the ability to change this direction when needed. But this is difficult to implement. Several studies have been carried out for achieving controlled fiber deposition, for example, by controlling the point of deposition [28], and by using external electrical force guidance [29]. However, the precision and the alignment of fiber deposition have not been satisfactorily implemented.

Normally, nanofibrous patterned architectures are developed by using a patterned conductive electrode as collector which is very expensive and time consuming to construct and can only be used for one type of deposition pattern [30]. Therefore, extensive research is needed in order to develop a versatile, and inexpensive advanced electrospinning method capable of incorporating functional properties into nanofibrous patterned scaffolds

Furthermore, a number of key issues need to be addressed, for instance, how to control the amount of fibers deposition and how to generate multidirectional aligned fibers in a single patterned architecture.

1.5 Research Objectives

The main objective of this research is to develop a system for producing fibrous patterned architectures with controlled deposition and alignment. The following are the specific objectives of this study:

1. Develop an advanced electrospinning setup capable of producing various types of nanofibrous mats.
2. Fabricate and characterize various nanofibrous patterned architectures with the developed advanced setup.
3. Control the deposition directions of electrospun nanofibrous scaffolds
4. Control the electrospun fiber density at desired location within the architecture and produce different kinds of functionally graded scaffolds
5. Investigate the alignment of electrospun nanofibers by controlling the electrical field using microprocessor control system.
6. A parametric study to design the developed advanced electrospinning setup and correlate it with the electrical field simulation.
7. Investigation of thermal, mechanical, and morphological properties of PVA/wollastonite and PVA/wood flour fibrous nanocomposites

1.6 Structure of the Thesis

This thesis is organized into seven chapters:

1. Chapter 2 discusses the basic working principle and various approaches of electrospinning process.
2. Chapter 3 describes the parameters that govern the electrospinning process, materials and solvents that practiced in the electrospinning process by several research groups, properties of electrospun nanofibers and their prospective applications.
3. Chapter 4 provides the details of experimental setup that is constructed in the laboratory and also explains the working principle of a custom measuring tool developed for characterizing the electrospun nanofibers.
4. Chapter 5 reports the experimental finding of various patterned architectures with controlled deposition; the results of alignment of electrospun nanofibers due to controlling the electrical field; fabrication and characterization of uniaxial functionally graded deposition; and a parametric study (shape, size, and gap of electrodes) to design the developed advanced electrospinning setup and electrical field simulations using COMSOL Multiphysics which were correlated with the experimental findings .
5. Chapter 6 presents the thermal, mechanical, and morphological properties of PVA/wollastonite and PVA/wood flour fibrous nanocomposites
6. Chapter 7 includes conclusions and recommendations for future research.

Chapter 2 Electrospinning – The Basics

2.1 Electrospinning Process

Figure 2.1 shows a schematic diagram of typical electrospinning setup. There are three basic components in electrospinning process: a high voltage supply, solution containing pump connected with a pipette or needle to which high voltage is applied, and a conductive collector. Usually, a syringe, acts as a reservoir containing a polymer solution with proper conductivity, viscosity, and surface tension, and its plunger is pushed by a metering pump to generate a constant flow of solution through the needle. A Direct Current (DC) or Alternative Current (AC) high voltage source which induces a high electrical charge on the surface of the solution is applied between the needle and grounded collector, which creates an electrical field between these electrodes. Two major electrostatic forces act on the solution droplet: An electrostatic repulsive force on the surface due to charge having similar polarity and the columbic force arising due to electrical field. With the significantly high electrical field, the electrostatic forces can overcome the surface tension of the solution and form a conical shape named as Taylor cone [31, 32] and ultimately resulting in the ejection of a thin jet from the needle tip. The charged jet then follows a route to ground. Before reaching the collector plate, the charged jet undergoes stretching and a number of whipping motions. During this time the solvent evaporates and the solute is deposited as interconnected webs of continuous fibers of randomly oriented non-woven mat on a grounded collector plate. Hence, the entire electrospinning process may be broken down into several operational regions: (i) formation of the cone-jet, (ii) initiation of the jet, (iii) instability of the jet, (iv) jet solidification and collection.

2.1.1 Formation of the Cone-jet

The jet formation of the polymer solution depends on various important factors such as surface tension, shapes of droplet, rheology, electrical charge, mass, etc. When there is no electrical field in between needle and ground collector, the liquid flows drop by drop. With

increasing voltage potential from zero, the liquid droplet start micro dripping. This phenomena is caused mainly due to attraction of the charged liquid droplet to the ground collector and the reduction of the surface tension which results in accumulation of charges on the droplet surface [33, 34]. At large voltage potentials the liquid droplet continues to deform and forms a conical shape referred as Taylor cone. Both the repulsive force and surface tension acting on the droplet are responsible for the formation of cone-jet [35]. In 1964, G. I. Taylor [15] estimated that the surface tension of liquid droplet is perfectly in equilibrium with the normal voltage creating a conical shape with a half angle of 49.3^0. In 2001, Yarin et al. [33] adjusted the Taylor cone theory based on the experimental results. They reported that the liquid surface develops a critical shape of cone with a half angle of 33.5^0 as shown in Figure 2.2.

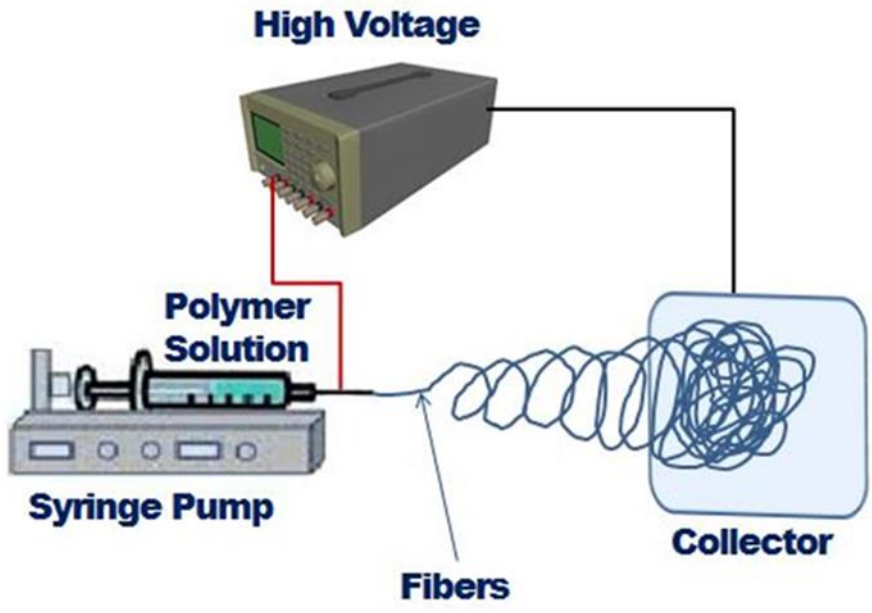

Figure 2.1 Schematic of a typical electrospinning system.

2.1.2 Initiation of the Jet

Since an electrical potential difference is applied between the syringe needle and counter collector, a charge is induced on the surface of the droplet of polymeric fluid with normal and tangential components. Ejection of the fluid jet from the tip of the Taylor cone occurs when the intensity of the electrical field gains a certain critical value that can overcome

the surface tension of the polymer solution. According to Taylor's calculation, the critical voltage *Vc* for electrospinning is

$$V_c^2 = 4\frac{H^2}{L^2}\left(ln\left(\frac{2L}{R} - 1.5\right)\right)(0.117\pi\gamma R) \qquad (2.1)$$

where, *H* is the distance between needle tip and the ground collector, *L* is the length of the capillary, *R* is the needle outer radius and γ is the surface tension of the liquid.

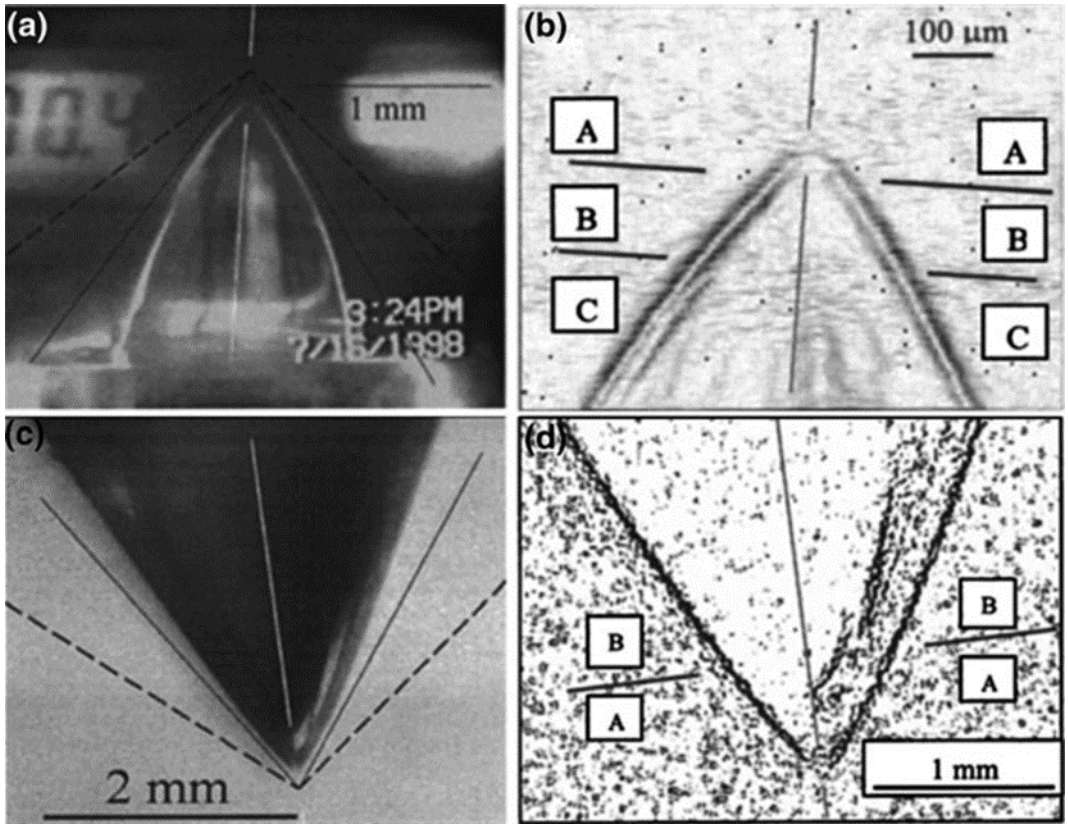

Figure 2.2 (a) Videograph of the critical droplet shape observed for a sessile droplet; (b) Part of the image in (a), processed with Scion Image; (c) Critical droplet shape observed for a pendant drop; (d) The enlarged droplet tip from (c), processed with Scion Image [33].

After ejected from the Taylor cone, the jet travels in a straight line for a certain distance depending on the solution and electrical configuration followed by an array of unstable bending motion with growing amplitudes. Then the jet begins to trail a bending, winding,

spiralling and looping path in space. An example of steady and bending instability of jet in the electrospinning is shown in Figure 2. 3. Numerous theoretical and experimental studied have been carried out to establish these phenomena and are discussed below.

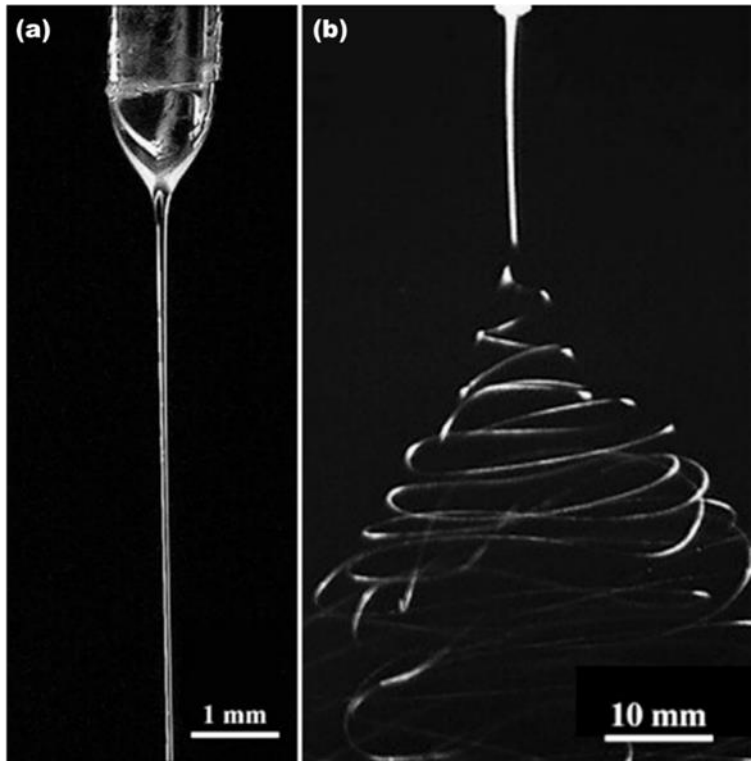

Figure 2.3 Jet travels in a straight line (a), followed by bending instability (b) [36].

2.1.3 Linear Path of the Jet

Reneker and co-authors [34, 37] modeled the linear segment of the jet by a viscoelastic dumbbell as illustrated in Figure 2.4. The dumbbell, AB, models a viscoelastic Maxwellian liquid jet accounting for the elastic component with the spring (elastic modulus *G*) and the viscous component by the dashpot (viscosity μ). According to Maxwell model, the stress σ is equal both at the spring and at the dashpot. Therefore, the total deformation yields [34],

$$\frac{d\sigma}{dt} = G\frac{dl}{ldt} - \frac{G}{\mu}\sigma \qquad (2.2)$$

Where, *t* is time and *l* is the filament length.

The momentum balance for bead *B* is

$$m\frac{dv}{dt} = -\frac{e^2}{l^2} - \frac{eV_0}{h} + \pi a^2 \sigma \qquad (2.3)$$

Where, *a* is the cross-sectional radius of the filament, and *v* is the velocity of bead *B*.

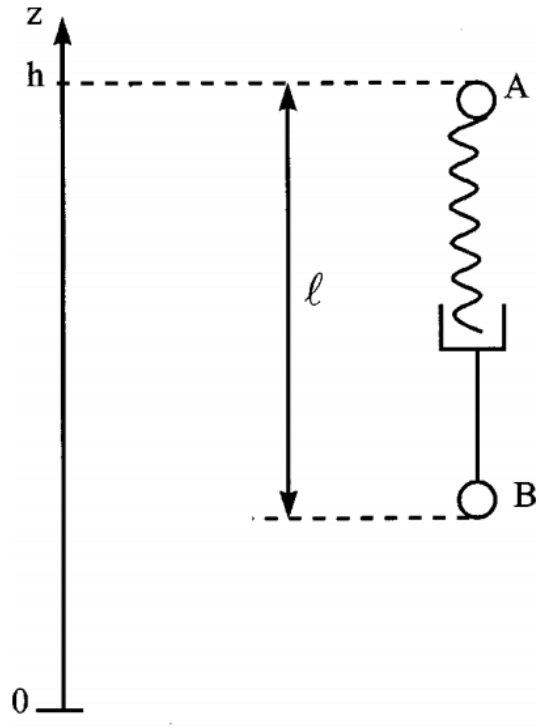

Figure 2.4 Viscoelastic dumbbell model representing a fraction of the rectilinear part of the jet [34].

The numerical results of this expression are displayed in Figure 2.5. The longitudinal stress $\bar{\sigma}$ first raise over time, passes a maximum, and then decreases very slowly (shown in Fig. 2.5 a). The dimensionless longitudinal force, $\frac{F_{ve}\bar{\sigma}}{\bar{l}}$, acting on the jet passes its maximum before $\bar{\sigma}$ does. Therefore, the filament length, $\overline{l^*}$, is identified where $\bar{\sigma}$ passes the maximum and the longitudinal force is quite low. Figure 2.5 b shows that filament length, $\overline{l^*}$, increases with the increases of applied voltage, in agreement with experimental findings.

In another study, He and co-workers [38], measured the critical length of straight jet in electrospinning. The critical straight length L_1 accounts from the capillary orifice or the needle tip to the point where instability starts and is given by,

$$L_1 = \frac{4kQ^3}{\pi\rho^2 {l_2}^2}(R_0^{-2} - r_0^{-2}) \qquad (2.4)$$

Where, $R_0 = (\frac{2\sigma_1 Q}{\pi k \rho E})^{1/3}$,Q is the flow rate, σ_1 is the surface charge, k is the dimensionless conductivity, E is the electrical field, ρ is the liquid density, l_2 is the current passing through the jet, and r_o is the initial radius of the jet. They also verified their theoretical prediction with experimental observations for two materials poly(hydroxybutyrate- co-valerate) (PHBV) and cellulose and claimed good agreement with the model.

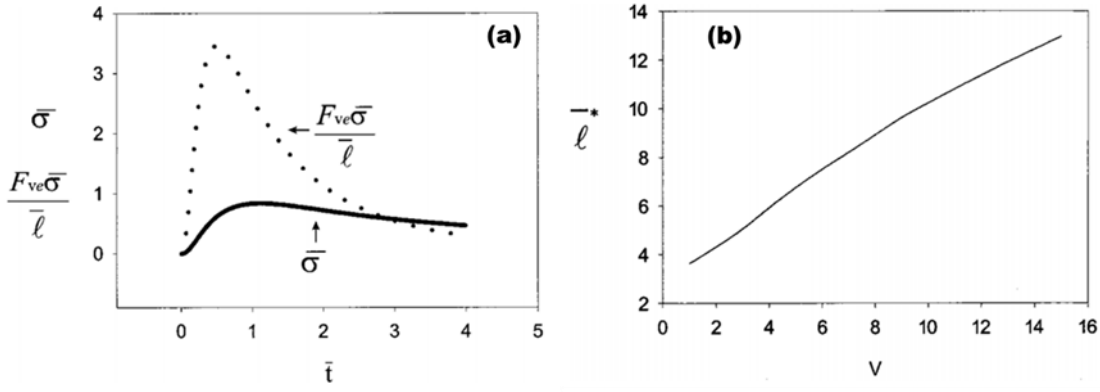

Figure 2. 5 Relation of longitudinal stress with time scale (a), length of the rectilinear part of the jet as a function of the applied voltage [4].

2.1.4 Jet Instability

After straight segment, the jet further elongates and reduces its diameter. In a study, using high speed photographs. Reneker and coworkers [37, 39] reported that the jet in each loop grew longer and thinner while increasing loop diameter and circumference. The elongation of each segment occurs because of induced charges on the jet that are driven by high electrical forces. As the perimeter of the loops grows, the cross sectional diameter of the jet becomes smaller. This breaks the balance force between the surface tension and the electrical forces, and creates an unstable jet. Due to this newly created small diameter, the path of the jet becomes unstable and next cycle of bending instability develops. The

process of bending instability repeats many times on a smaller scale. Three or more smaller diameter bending instability is often observed in the electrospinning process. The solvent in the jet evaporates during its flight from the needle tip to the collector. Finally, the jet is so thin or becomes so stiff that the bending instability can no longer govern the fiber formation process. Figure 2. 6 demonstrates the prototypical instantaneous position of electrospinning jet path (the straight segment is shown red, the first bending coil in yellow, and the third bending coil in blue) [39].

Several research groups have worked on mathematical model of bending instabilities. According to Reneker et al. [34, 39], Hohman et al. [40, 41], and shin et al [42], there are three main types of bending instabilities that have been observed. The Rayleigh instability is the primary mode of instability and occurs due to opposing forces acting on the surface area of the jet. The electrostatic repulsive force acts to increase the surface area of droplet whereas surface tension acts to reduce the surface area. Therefore, instability occurs, which causes the jet to break up into small droplets. This is an axisymmetric, non-conductive mode typically occurring in highly viscous fluids that can lead to bead formation as shown in Figure 2.7. Surface tension, which dominates this kind of instability, can be suppressed by high electrical fields. The second mode of instability is also an axisymmetric instability referred to as the second axisymmetric instability. This type of instability normally occurs at higher electric field strength than the Rayleigh instability.

The third instability called the whipping instability, has a non-axis-symmetric conductive mode and plays a key role in reducing the jet diameter from micrometer to nanometer. High surface charge densities and high fluid flow rates induce a dipole moment into the jet promoting ending motion. The jet undergoes a large deformation as it moves outward and introduces spiral and whipping motions that lead to reduction of the diameter of the fibers.

2.1.5 Jet Solidification and Collection

While the jet travels from needle tip to collector plate, all the solvent evaporates and the jet forms a fairly thin fiber. Finally, electrospun fibers are collected at the target electrode. The target or collector is a conductive electrode having opposite charge, through which

the charges on the fibers dissipate. Different types of targets such as flat plate, metal sheet, rotating cylinder can be used. Based on the collector used in electrospinning, the morphology and structure of electrospun deposited fibers can be modified. In general, a stationary flat plate is used for collecting random oriented fiber mat [43] whereas, rotating drum, parallel plate, and auxiliary electrodes are used to collect aligned fiber array [22, 27] Patterned fiber mat, 3D fibrous scaffolds and fiber yarn or rope can also be developed based on the electrodes employed in electrospinning [4].

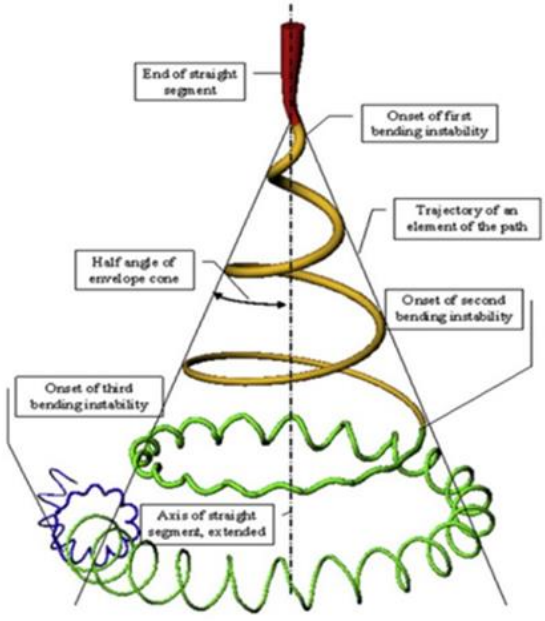

Figure 2. 6 A prototype of bending instability of jet path during electrospinning process [39].

2.2 Various Approaches of Electrospinning Process

Progress in the electrospinning over the last few decades have resulted in numerous new methods for the production and construction of various nanofibrous assemblies. Although electrospun fibers carries many fascinating properties, but initially, they could not catch much industrial attention because of lower production rates and lack of knowledge and interest in the size, shape, and flexibility of electrospun nanofibers. Many advanced electrospinning methods overcome these drawbacks and proved that it is one of the

effective and economic method of producing nanofibers. The recent progress on various approaches of electrospinning is discussed in the following section.

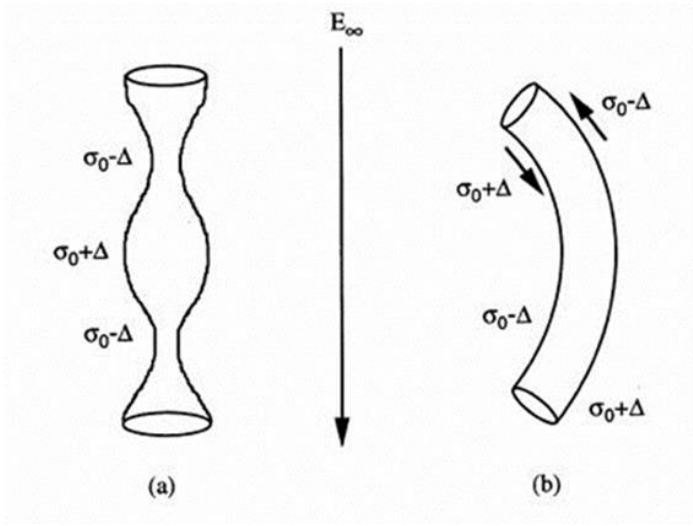

Figure 2.7 Axisymmetric (a) and non-axisymmetric instabilities of the jet caused by an external electrical field [39].

2.2.1 Nonwoven Electrospun Nanofibers

In a typical electrospinning process, a flat counter electrode is placed at a certain distance from the needle tip to which high voltage is applied. This results in a uniform electrical field being generated. Electrospun nanofibers are collected on the plate as random or nonwoven mats [44, 45]. Some potential applications of nonwoven mats are: filtration, adsorption of biological and chemical warfare gases, protective clothing, thermal insulation, artificial blood vessels, wound dressing, drug delivery systems, and fiber-reinforced materials [3, 46].

2.2.2 Fiber Alignment

The orientation of nanofibers along a certain direction is often required for the fabrication of electronic and photonic device, fiber-based reinforcement or for tissue engineering. Numerous approaches, described in the following sections, have been used to produce well-aligned and unidirectional electrospun nanofibers.

Rotating Drum Collector

A continuous and uniform film of fiber can be formed by rotating the collector drum at very high speed and translating the spinneret or the drum. The key factors for controlling fiber diameter and alignment in this process are the rotational speed and the relative rate of translation between the spinneret and the drum. Figure 2.8 illustrates a schematic of electrospinning with rotating drum. This technique is widely used to obtain aligned electrospun nanofibers [47, 48]. The fiber alignments can be achieved only to some extents. The main advantages of this process are high production rate, low cost, better process control and alignment.

Rotating Disk Collector

The rotating disk collector is a slightly modified setup of rotating drum collector. Here a tapered, wheel like disk is used as collector (shown in Fig. 2.9). The advantage of using a rotating disk collector over a drum collector is that most of the fibers are deposited on the sharp edge and the degree of orientation of the collected fibers is significantly improved. Several researchers have showed that the field strength is much higher near the edge of the disk [49, 50]. As a result, the charged fibers were continuously deposited parallel to each other along the edge. A small quantity of thick aligned fibers can be produced in this way.

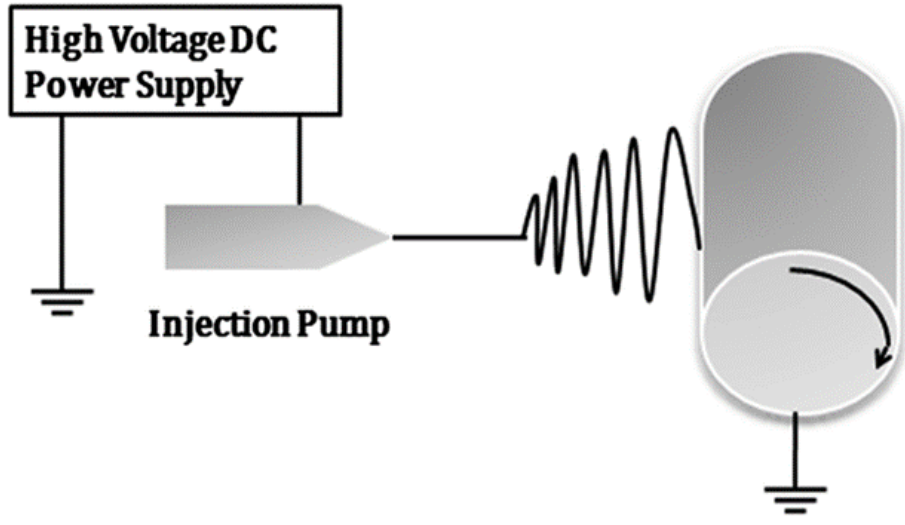

Figure 2.8 A schematic of rotating drum electrospinning method [28].

Pair of Parallel Electrodes

Li et al. [21, 27] reported that the geometric arrangement of conductive collector had a great effect on the orientation of electrospun nanofibers. When two conductive strips are placed in parallel having a gap of variable widths as shown in Figure 2.10A, it is possible to collect highly uniaxial aligned nanofibers (Fig. 2.10B). The arrangement of parallel electrode collectors with a gap or insulating section between the electrodes alters the electrostatic forces that assist the charged fibers to span across the gap (Fig. 2.10C). The authors claim that increasing the gap distance improves the alignment of the nanofibers until fibers break down. The degree of orientation of the nanofibers can be fairly improved by this process.

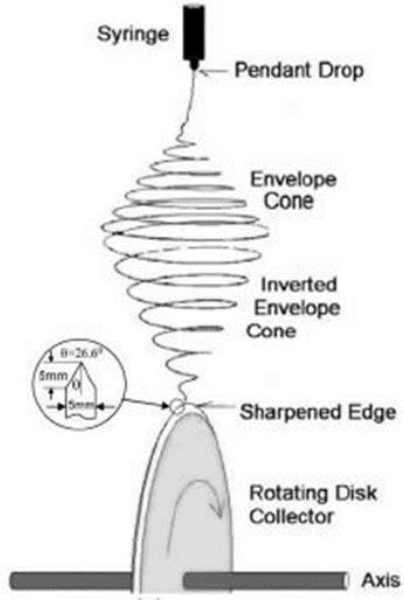

Figure 2.9 Schematic of electrospinning with rotating disk [28].

Magnetic Electrospinning

Magnetic electrospinning setup is the same as the conventional setup except for the use of two permanent magnets placed parallel to each other to generate a magnetic field between them (sketch is shown in Fig. 2.11). Yang et al. [51] have used this technique to obtain well aligned PVA electrospun fibers. They used small amount of magnetic nanoparticles into the polymer solution to magnetize and claimed that embedded small amount of

magnetic nanoparticles do not hamper the morphology of the fibers. They demonstrated that the magnetic field springs the fibers across the gap making parallel array.

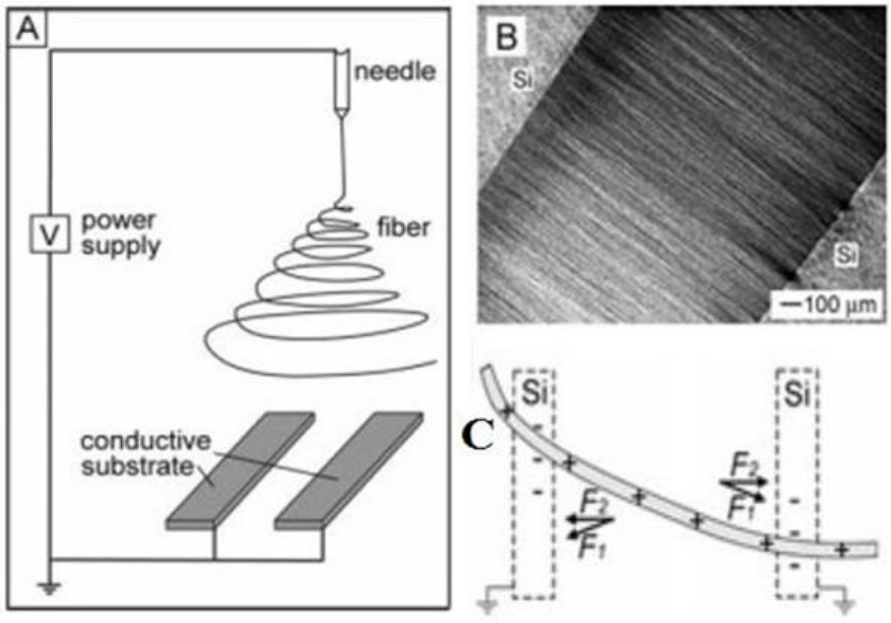

Figure 2.10 A) Schematic setup of parallel electrodes separated by a void gap. B) Optical micrograph of PVP nanofibers collected across the void gap between two silicon strips. C) The electrostatic force analysis of charged nanofibers between the electrodes [27].

2.2.3 Advanced Electrospinning Processes

Coaxial Electrospinning

Coaxial electrospinning is an extended form of electrospinning and consists of two concentrically aligned nozzles (sketch shown in Fig. 2.12). Two polymeric solutions are separately supplied into the central tube nozzle for developing core-shell nanofibers. The same high voltage is applied to both nozzles which leads to the formation of a compound droplet. Due to high electrostatic field, a compound jet emerges which consists of core material surrounded by shell material. The jet experiences similar bending instability and solidification discussed earlier, during its travelling and finally, nonwoven nanofibers are collected on the collector screen. This coaxial electrospinning has been widely applied for

controlled drug release [52], enclosing functional liquids within the fiber matrix [53], and highly sensitive biochemical sensors [54].

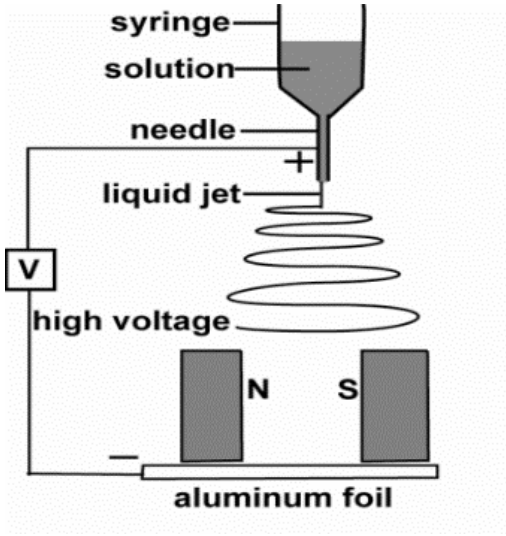

Figure 2.11 Schematic of magnetic electrospinning to generate aligned fibers [51].

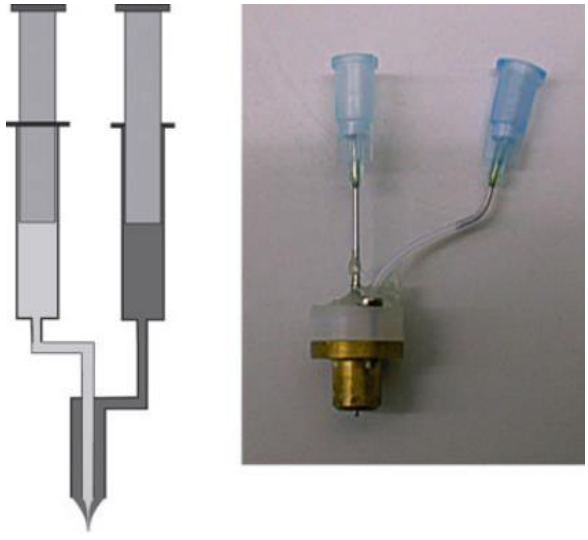

Figure 2.12 Schematic view of coaxial electrospinning [52].

Needleless Electrospinning Process

One of the barriers of conventional electrospinning method is low production rate. In order to avoid this limitation various efforts have been made, such as increasing the number of

needles [55], increasing flow rate of solution using air jacket [56]. Needleless electrospinning process is considered a substitute for overcoming the issues of low production and a large operating space. A schematic setup of needleless electrospinning is depicted in Figure 2.13. A bath is filled with polymer solution which is charged by dipping an electrode in it. A spiral coil is employed into the liquid bath to create multiple spinnerets. Numerous jets initiate simultaneously from the liquid bath and deposit on collector screen. This needleless electrospinning is very problematic to control as the jets initiation process from liquid bath is self-organized [57].

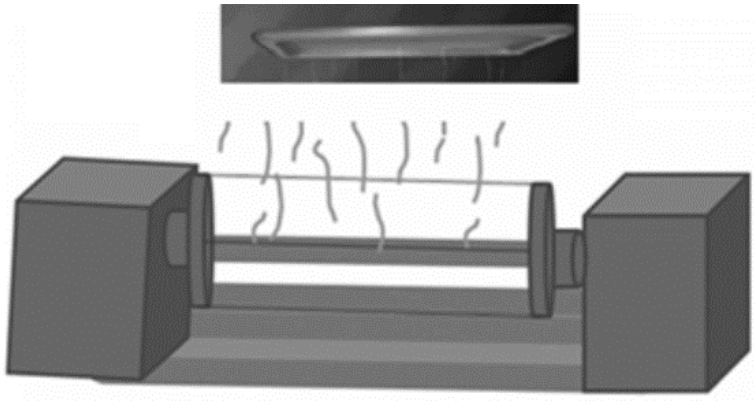

Figure 2.13 Schematic setup of needleless electrospinning [55].

Multijet and Mixed Electrospinning

In order to fabricate multilayer nanofibers two or more syringes with different polymer solutions are placed in parallel (Fig. 2.14A) from where multiple jets are ejected when the same high voltage is applied to the needle tip. In mixed electrospinning, two or more different polymer solutions are mixed prior to application of high voltage to the needle to form compound solutions from two or more different syringes under different processing conditions (Fig. 2.14B). Kidoaki et al. [58] first introduced mixed and multilayer electrospinning technique. Moreover, various materials such as PCL, PLA, PDO, gelatin, and elastin have been studied using multilayer electrospinning [59, 60]. These electrospinning methods not only increase production rate but also open many more potential applications for biomedical and advanced nanocomposites.

Manipulation of Electrical Field

The electrostatic charge distribution along the jet path in electrospinning has been studied by many researchers [61-63]. The deposition of electrospun fibers can be altered, with even a slight variation in the electrical field profile. Therefore, an external electrical field can be added in this system to control the deposition location and area [63] of electrospun fiber. By manipulating the electrical field, it is possible to deposit electrospun fibers in uniaxial array [64] and to develop pattern structures [65]. The auxiliary electrodes system can have the base electrode, steering electrodes, focusing electrodes, the collector and guiding electrodes as shown in Figure 2.15.

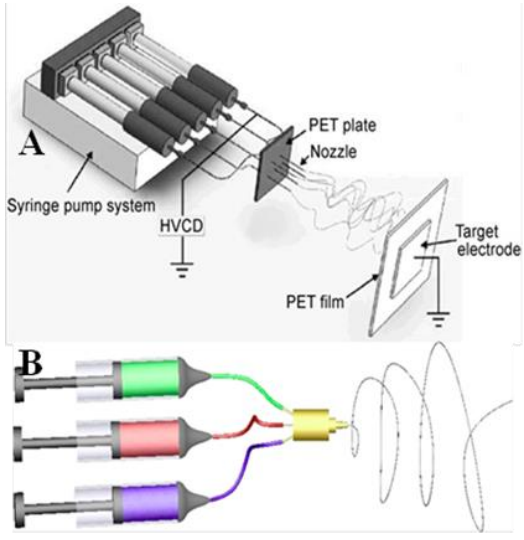

Figure 2.14 Multiple syringes arrangement for A) multilayer B) mixed electrospinning [58].

Usually, the base electrode is a conductive plate which generates a uniform electrical field between spinneret and the collector screen. The function of the focusing electrodes is to monitor the jet so that deposition of electrospun fiber is more localized. One or more ring, cylindrical, rectangle, or conical shape focusing electrodes are placed closed to spinneret to reduce the spread area of jet. Deitzel et al. [64] used ring type focusing electrodes, placed evenly between spinneret tip and collector screen. They generated a cylindrical electrical field applying the same positive voltage on the needle tip and rings and a negative charge to the collector as shown in Figure 2.16 (A). Due to auxiliary electrodes, the electrical field profile converged to the centerline (Fig. 2.16 (B)) which significantly reduced the

deposition area of electrospun fiber. Using this technique, randomly oriented nanofibers can be fabricated on a small spot. Steering electrode is used in order to have more precise control over jet.

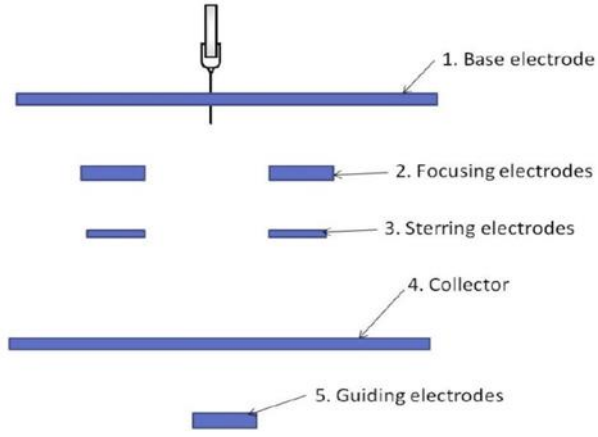

Figure 2.15 Arrangement of auxiliary electrodes for controlling the electrical field profile [64].

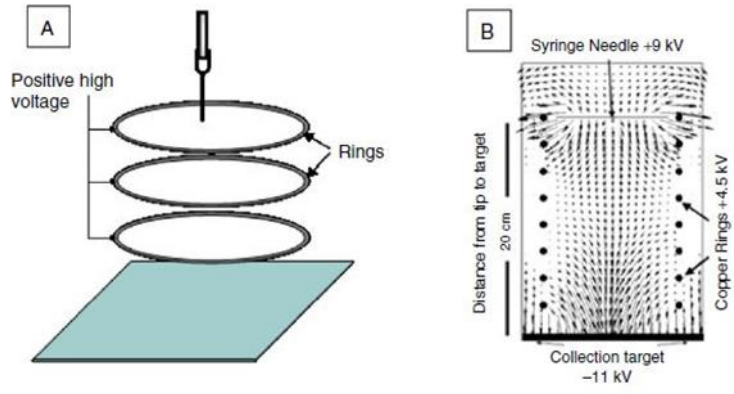

Figure 2.16 Auxiliary electrodes set-up (A) for controlling fiber deposition, and corresponding electrical field profile (B) [64].

2.2.4 Nanofibrous Patterned Architectures

In the recent years, patterning of electrospun nanofibers has been receiving attention for various applications, such as micro or nano-devices, microelectronics, photonic and biomedical fields. One of the most simple and effective methods for developing

nanofibrous structures is to use a patterned electrode as collector. Zhang and Chang [23] employed an electroconductive template with woven structure and found a patterned architecture similar to the patterned template collector after electrospinning. Changing wires with different diameters within the template collectors, they reported that the patterned collector directly affects the deposition and arrangement of the fibers, as well as the architecture of the electrospun mats. Using the patterned electrode Ye et al. [66] fabricated the Bird's Nest patterned architectures from various non-polar and polar polymer materials (illustrated in Fig. 2.17).

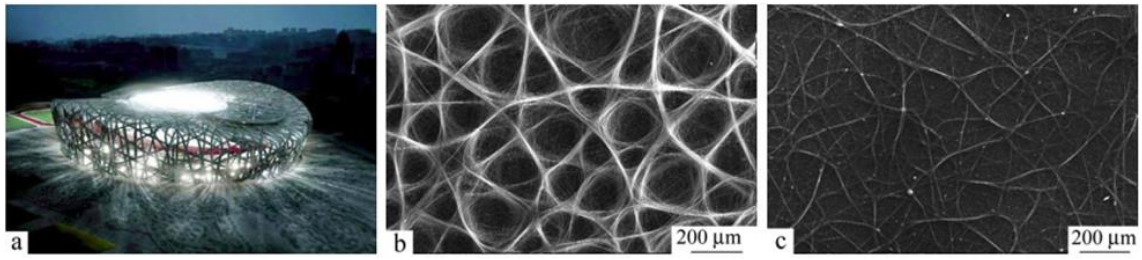

Figure 2.17 Images of (a) Beijing National Stadium-Bird's Nest, patterned structure of (b) chlorinated polypropylene nanofibrous membrane, and (c) polystyrene nanofibrous membrane.

Chapter 3 Electrospinning Process

3.1 Materials and Solvents

In general, polymers are the preferred material, both for academic and industrial researchers because they have beneficial mechanical, chemical, and electrical properties, like light weight, flexible, durable, high tensile strength, chemical resistance, and physical-chemical stability. The functionality and applicability of polymers can be further enhanced by producing micro or nano structures using electrospinning method. Almost all soluble polymers can be processed to form micro nanofibers by this technique. A comprehensive summary of polymers which have been successfully electrospun to-date is listed in Table 3.1. Also given in the table are the solvents which have been used and chemical formula for the corresponding polymers.

Table 3.1 Different polymers used in electrospinning

No.	Polymer	Solvent	Ref.
1	Polylactic acid, PLA	Chloroform, Methlyene chloride and Dimethyl formamide	[22, 67]
2	Polyethylene oxide, PEO	Ethanol/Water, Chloroform ($CHCl_3$), Acetone	[44, 68]
3	Polyacrylamide, PAA	Ethanol/Water	[69]
4	Poly(vinyl alcohol), PVA	Ethanol/Water	[70]
5	Polyurethane, PU	THF/ethanol, Dimethyl formamide	[44]
6	Polycaprolactone, PCL	Acetone	[44]

7	Polystyrene (PS)	Tetrahydrofuran (THF), Dimethylformamide (DMF), Carbon disulfide (CS_2), Toluene	[71]
8	Poly(methyl methacrylate) (PMMA)	THF, Acetone, and $CHCl_3$	[72]
9	Nylon 6	Formic acid and acetic acid	[73]
10	Cellulose acetate, CA	Acetone, acetic acid, dimethylacetamide	[74]
11	Silk	Formic acid	[75]
12	Gelatin	Formic acid, acetic acid	[76]
13	Polyamide, PA-6	Formic acid, Formic acid/dichloromethane, Formic acid/acetic acid, Formic acid/chlorophenol, Chlorophenol, Hexafluoroiso propanol	[77]
14	Polyethylene Terephtalate, PET	Trifluoroaceticacid (TFA)/1,2-Dichloroethane (3:2, v/v)	[78]
15	Polyvinylchloride, PVC	Tetrahydrofuran/dimethylforma mide	[79]
16	Collagen	Hexafluoro-2-propanol	[80]
17	Poly(vinylidene fluoride) , PVDF	Dimethylformamide:dimethylac etamide	[81]
18	Polyacrylonitrile, PAN	Dimethyl formamide	[82]

Polymers melts do not require use of solvents, which is beneficial for environment, and can be employed to produce nanofibers through electrospinning. Instead of solution, molten polymers at high temperature are introduced into the syringe and the fabrication has to be performed under vacuum conditions. Polyethylene (PE), polypropylene (PP), PLA, PET, PCL, PEG, and PU have been successfully electrospun by melt electrospinning technique [83, 84].

3.2 Effect of Working Parameters on Electrospinning

Understanding the effect of a wide range of working parameters such as solution parameters, process parameters, and ambient parameters are very crucial for the process of electrospinning and the transformation of polymer solutions into nanofibers. By proper control of these parameters, desired morphologies, properties, and diameters of fibers can be achieved. Numerous research groups investigated the effect of such parameters on electrospinning process and reported that the morphologies of electrospun fibers are greatly dependent on each of the parameters.

3.2.1 Solution Parameters

Surface Tension

Surface tension is one of the important factors in electrospinning. Fong et al. [85] conducted experiments with PEO as model with distilled water, NaCl, and ethanol to determine the influence of surface tension. They reported that by holding the PEO concentration constant and reducing the surface tension of the solution, smooth fibers with larger diameters can be produced. In general, surface tension should be low enough compared to charges present on the polymer solution to initiate the electrospinning. If all the parameters of electrospinning remain constant, surface tension creates a window of upper and lower boundaries of electrospun fiber [86, 87].

Viscosity

Solution viscosity is a vital parameter determining the fiber morphology [44, 85, 88]. As viscosity is directly proportional to concentration in a binary polymer-solvent system, adjusting the polymer concentration of the solution, fiber morphology can be controlled. Continuous and smooth fibers can be obtained at relatively high viscosity of polymer

whereas low viscosity results in thin fibers with beads [44]. Solution cannot be pressed through tiny needle when the viscosity is too high. It is well-known that polymeric molecular weight, viscosity, and solution concentration are closely related to each other. For example, when the solution viscosity is low, the surface tension dominates in electrospinning, as a result, beaded fibers are formed. In contrast, if the solution has proper viscosity, continuous and uniform fibers can be acquired.

Concentration

The concentration of polymer solution is also a key factor in determining the fiber formation during the electrospinning process. At very low concentration of polymer, electrospun fibers are no more continuous, rather electrospray occurs due to low viscosity and high surface tensions of the solution [86]. With the slight increase in concentration, formation of electrospun material changes from polymeric micro (nano)-particles to a mixture of beads and fibers [89]. With further increase in concentration, uniform and smooth fibers are obtained. By increasing the concentration of solution, the fiber diameter is also increased if the solution concentration is suitable for electrospinning process [89, 90]. Finally, micro-ribbons type's electrospun fibers are produced at very high concentration of polymer solution [91].

Molecular Weight

Molecular weight of the polymer is a significant parameter which affects the morphologies of electrospun fibers. In general, higher molecular weight reflects more entanglements of polymer chains in solution which prevents the breakage of the fibers. Hence, smooth fiber is more common for a fixed concentration of solutions with higher polymer molecular weight. Lowering the molecular weight of the polymer results in non-uniform or beaded fibers [89] and too high molecular weight trends to form micro-ribbon [91].

Solution Conductivity

Conductivity of solution is related to the presence of charges at the surface of solution which is responsible for stretching of the polymer solution during the electrospinning process. Generally, polymers are polyelectrolytic in nature, in which adding charges on the surface mean higher conductivity of the solution and hence, under the higher electric field, the movement of charged jets increase, resulting in greater elongation. The electrical

conductivity favors the formation of thinner fibers [85, 89], which can be improved by adding salts or electrolytes which produce ions.

3.2.2 Processing Parameters

Voltage

Applied voltage is one of the critical factors within the electrospinning process. It is reported that diameter of electrospun fibers is not significantly affected by the applied voltage [88]. Depending on polymers, applied high voltage generates controversial results. Several research groups reported that higher applied voltages can raise the electrostatic repulsive force on the charged jet which reduces the fiber diameter [92]. Studies also report that a higher voltage can favour the formation of large fiber diameter because more fluid is ejected [93]. Some groups also demonstrated that too high voltage causes multiple jets which provide non-uniform fiber diameter and the beads formation [89]. Thus, voltage effects show different tendencies on electrospun fiber's diameter, the level of significance varies with the polymer solution concentration, mass of polymer fed out from needle tip, elongation level of a jet by an electrical force, morphology of a jet (a single or multiple jets), etc. However, voltage itself does not have a very significant role in controlling the fiber morphology.

Flow Rate

Flow rate determines the amount of solution ejected from the charged needle tip in the electrospinning process. Studies have reported that the flow rate is inversely proportional to the rate of jet thinning. Higher the flow rate results in reducing the rate of jet thinning, and as a result, thicker or non-uniform electrospun fibers may be produced and vice versa [94]. Higher flow rate carries more polymer materials at the tip of the needle which helps to form larger Taylor cone. Therefore, solutions do not have much time to elongate or solvent may not evaporate completely as the solution moves faster and leaves beads, non-uniform and larger diameter on electrospun fibers. On the other hand, smooth fibers with thin diameter are more common when relatively lower flow rates are applied, due to low stretching force of shooting jet and short drying rate of solvents.

Distance between Tip and Collector

The distance between tip of the syringe and collector is another important parameter affecting electrospun fiber diameter and its morphologies. Generally, lesser the distance, lower the flight time and higher the electrical field. As a result, the solvent will not have enough time to evaporate before reaching the collector which lead to bead formation with flatten cross-section [95]. In contrast, too large distance decreases the electrical field strength and causes both increase [96] and decrease [88] the fiber diameter. The larger distance enhances the evaporation rate of solvent, so that smooth and thinner fibers can be obtained but this evaporation depends on humidity and volatility of solvent [95]. The larger distance also generates insufficient electrical field between the needle tip and collector electrode. Sometimes these contradictory phenomena may favour the development of higher diameter of fibers. It has been proven that optimum distance provides smooth and thinner electrospun fibers for each polymer.

Collector Plate

Usually, collector electrode is grounded to maintain proper potential difference between the collector and needle tip, and collects the electrospun fibers. A non-conducting plate may yield lower packing of fibers compared to conductive plate. In the literature, various collectors such as aluminum foil, glass plate, wire mesh, rotating drum, pin, and liquid bath etc. have been practiced [28, 97].

Diameter of the Needle

It has been shown that the diameter of the needle directly affects electrospun fibers. Smaller diameter of the needle restricts solution flow at the tip and forms smaller droplet with higher surface tension. As a result, time for jet thinning increases and beads and thin fibers are observed. On the other hand, increasing the needle diameter, bigger droplet forms which can be non-uniform with beads.

3.2.3 Ambient Parameters

Humidity and Temperature

Ambient parameters such as humidity and temperature also play a great role in the formation of electrospun fiber diameters and morphologies. Low humidity favors

generation of smooth and thin fibers as solvent evaporation is faster when fibers move towards the collector plate. Whereas, high humidity helps in condensing water on the fibers, leading to porous and thicker fiber [98]. As for temperature, fiber diameters slightly decreases with increasing temperature [94]. The reason behind this phenomenon is that the solution viscosity decreases with increasing temperature for a fixed concentration of solution.

3.3 Properties of Electrospun Nanofibers

Nanofibers formed by electrospinning exhibit various distinct features and properties that are not usually seen in conventional one-dimensional structures produced by other techniques. In this section, we discuss some of the unique properties of polymer nanofibers.

3.3.1 Fiber Dimension and Morphology

The diameter of polymer fibers produced by electrospinning ranges from nanometer to several micrometers which is the key parameter for many applications. The major advantages of electrospun nanofibers are large surface area to volume ratio, high degrees of porosity, superior mechanical properties and modified surface functionalities. However, for a variety of applications, for instance, tissue engineering, filtration, sensors, fuel cell, catalysis, drug delivery, and nanofiber reinforcement, it is desirable to have a porous, hollow tube, or non-smooth surface structures on the electrospun fibers.

3.3.2 Porous Nanofibers

The formation of pores in the nanofibers greatly increases its surface area which is advantageous in many applications. Numerous attempts have been reported by number of groups for generating a porous nanofiber. One of them is based on phase separation of polymers caused by selecting appropriate parameters of electrospinning process. During the evaporation of the solvent, the solution becomes thermodynamically unstable, yielding polymer rich regions and polymer deficient regions, which results in formation of pores in the solid phase [99].

Electrospun porous nanofibers can also be obtained from a solution of mixtures of two immiscible polymers in the common solvent followed by one of the polymers being dissolved from the spun material [99]. Evaporation of the solvent causes phase separation within the nanofibers, leading to bimodal or porous structures.

Another method for producing porous structures is using a ternary system comprising of a highly volatile and a less volatile solvent mixed with the polymer. The difference in the evaporation rates of solvents generates the phase separation in this system. Qi et al. [100] demonstrated a ternary system of BuOH/DCM/PLLA and obtained porous fibers (shown in Fig. 3.1). This is obtain if the solvent is more volatile than the non-solvent in the spinning solution.

A more commonly used method is the selective removal of one of the phase component from electrospinning blend materials. You and co-workers [101] have successfully prepared porous ultrafine poly(glycolic acid) (PGA) fibers from ultrafine PGA/poly(L-lactic acid) (PLA) blend fibers after removing the PLA by selective dissolution technique with chloroform.

McCann and co-workers [102] have developed highly porous fibers by modifying collector setup. Instead of conventional setup they used a liquid nitrogen bath to collect polystyrene, polyacrylonitrile, polycaprolactone, and polyvinylidenfluoride fibers and then reheated rapidly to room temperature. This freeze-dry approach causes an instant phase separation into solvent and solid polymer leaving highly porous surface on the electrospun fibers.

It is evident that the amount of moisture in the environment affects the surface morphology of electrospun fibers; therefore, by controlling humid environments a porous structure can easily be developed. In this approach, the relative humidity (RH) is controlled using a humidifier tool placed inside the electrospinning box. When the spinning fiber experiences solvent evaporation process, the tiny droplets of water precipitates onto the streaming fiber. These water droplets leave porous structures on the solidified fibers. Casper et al. [98] worked with PS and revealed that greater than 30% humidity in air initiated pores on the surface of electrospun fibers. They also claimed that increasing the amount of humidity

caused an increase in the number of pores on the surface, the pore diameter, and the pore size distribution.

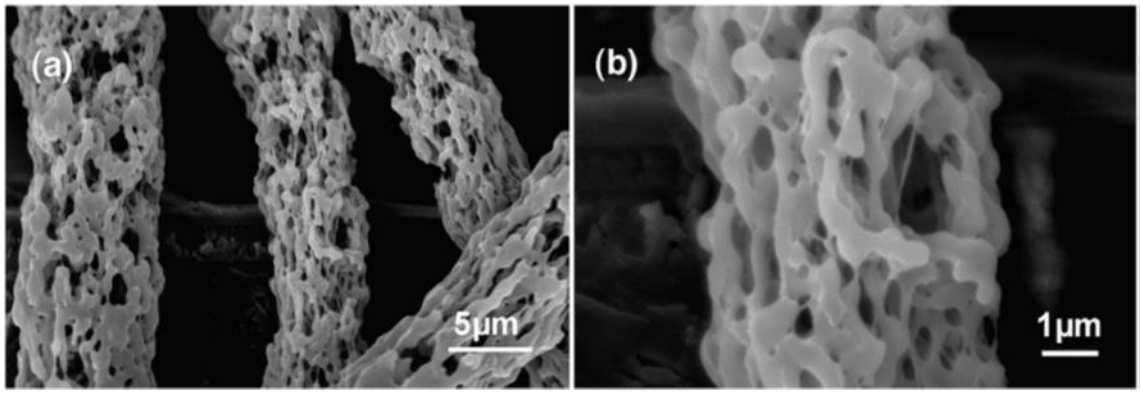

Figure 3.1 Fabrication of porous fibers prepared from the solution of 8 wt.% PLLA with DCM/BuOH (60/40): (a) low magnification, (b) high magnification [100].

3.3.3 Hollow Nanofibers

One dimensional nanofibers with hollow interiors are very attractive for a range of applications such as nanofluidics and hydrogen storage. Couple of methods have been employed for fabrication of this kind of nanostructures. One of them is based on the removal of template materials. In this method, conventional electrospinning is used to make a precursor polymer in to nanofiber or a ‘‘template’’. After that, a second material is deposited onto the template surface with an inorganic ceramics or metals either from solution or melt, via layer by layer techniques or from the vapor phase and this is followed by selective removal of the polymer cores or template, resulting in the desired hollow nanofibers. Donmez et al. [103] for instance, successfully fabricated hollow Hafnia (HfO_2) nanofibers using removal of nylon 6, 6 nanofibers as sacrificial template.

Another popular method for producing hollow nanofiber is based on coaxial spinning (Fig. 3.2A). The basic concept of this approach is to prepare the nanofibers by coaxial electrospinning from two immiscible liquids, followed by removal of the core material by selective solvent. Applying the same technique, Xia and Li [104] fabricated TiO_2/PVP poly (vinyl pyrrolidone) hollow nanofibers (Fig. 3.2B) by removing the oil phase from the core. Highlighting a problem of unstable Taylor cone in the formation of core-shell or hollow nanofibers, the same authors showed in another paper, that adding a sol-gel

precursor such as $Ti(OiPr)_4$ to the PVP solution during the spinning process can prevent structural breakdown. Using this technique, they developed a stable morphology of electrospun fiber [105]. Polycrystalline ceramic nanotubes were obtained by removing both PVP and oil through calcination at elevated temperature (Fig. 3.2 C and D).

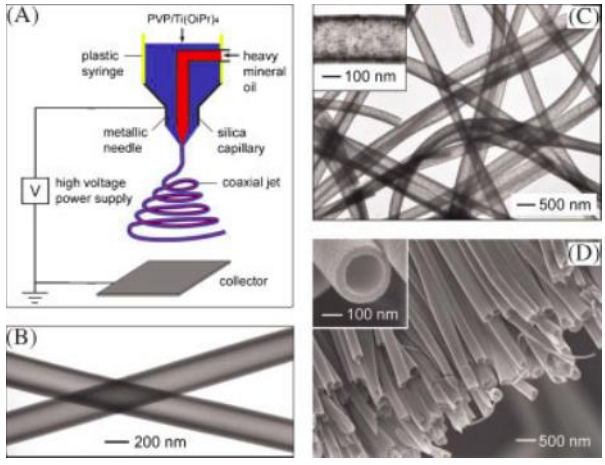

Figure 3.2 (A) Schematic setup of electrospinning with a co-axial spinneret. The heavy mineral oil (core phase) and the ethanol solution (shell phase) containing PVP and $Ti(OiPr)_4$, were simultaneously ejected through a coaxial spinneret. TEM images of hollow nanofibers after the oily phase was selectively removed (B) by extraction (C) by calcination. (D) SEM image of a uniaxial aligned array of nanotubes made of anatase [104].

With the similar setup, Park et al. [106] successfully fabricated hollow carbon nanofibers (HACNFs) using poly(methyl methacrylate) (PMMA) as a pyrolytic core precursor with either polyacrylonitrile (PAN) or PAN/PMMA blended polymer as a carbon shell precursor.

3.3.4 Core-shell Nanofibers

Having intrinsic functional properties from two materials, nanofiber with core and shell can be fabricated by slight modification of spinneret in the conventional electrospinning process. Two immiscible [107] or miscible [108] polymers or polymer with ceramic [105] or metals are ejected through outer and inner capillaries of a coaxial spinneret (shown in Fig. 3.3) simultaneously and formed a coaxial jet containing both materials side by side.

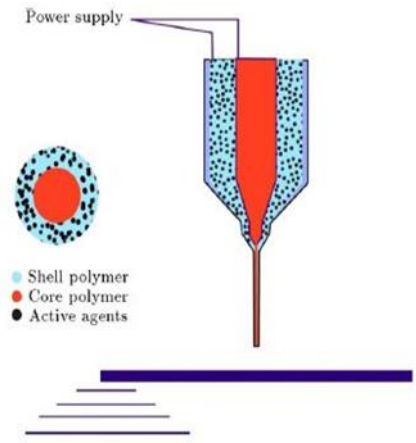

Figure 3.3 Schematic illustration of the coaxial electrospinning for spinning core-shell nanofibers [109].

The fabricated core-shell nanofibers have advantages accruing from both materials simultaneously. For instance, Lee and co-works [109] synthesized Si core/C shell nanofibers as an anode material for Lithium batteries using co-axial electrospinning and showed they are promising anode materials satisfying both productivity and electrochemical requirements. Moreover, the coaxial electrospinning can be widely applied in encapsulating drugs into polymer nanofibers, enclosing functional liquids, and controlling the secondary structures of nanofibers.

3.3.5 Three-Dimensional Structural Nanofibers

Electrospinning has been adopted as a versatile method which is capable of producing complex three-dimensional (3D) nanofibrous structures. These 3D nanofibrous macrostructures are very attractive for tissue engineering, filtration, and energy storage applications. Yan et al. [110] reported 3D honeycomb structures with various polymers (shown in Fig. 3.4). They observed that humidity is a key parameter for developing these self-assembled 3D honeycomb structures. When the humidity drops at a certain level, the low concentration solution remains wet after electrospun which may cross or contact each other at certain point. With the additional support from surface tension and repulsive force, electrospun nanofibers grow high into the walls of the 3D honeycomb structure.

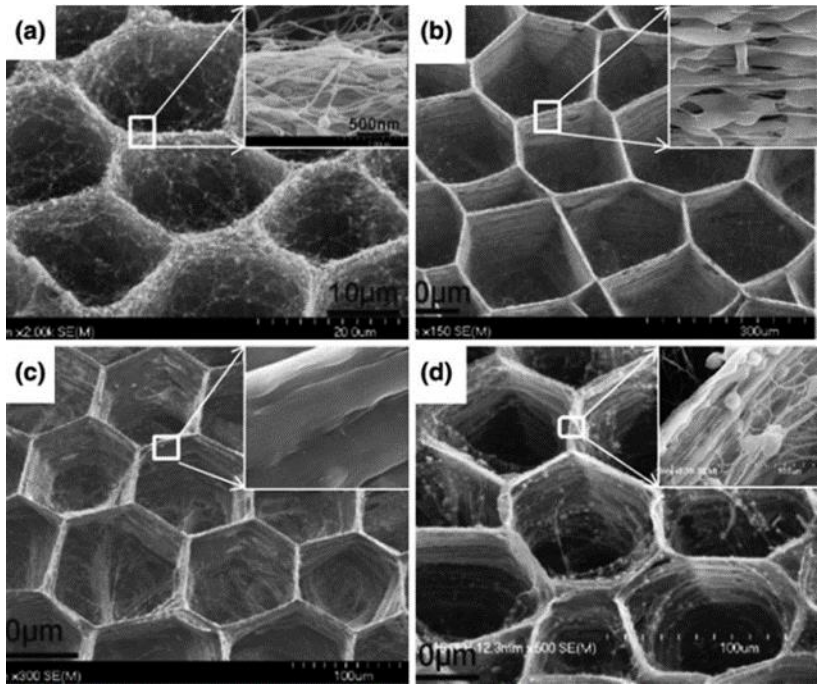

Figure 3.4 SEM images showing the surface morphology and wall structures of 3D honeycomb structures from (a) 3 wt. %PAN/DMF solution at the voltage of 22 kV (b) 6 wt. %PVA/aqueous solution at the voltage of 22 kV (c) 16 wt. %PEO at the voltage of 22 kV and (d) 16 wt. %PEO at the voltage of 19 kV [110].

Three-dimensional complex structures can also be developed by modifying the fiber collection method. Zhang and Chang [111] recently developed 3D fibrous tubes and interconnected 3D tubular structures (as displayed in Fig. 3.5).

Besides direct fabrication method of 3D structures using electrospinning, the 2D layers of electrospun fibers can be turned into desired 3D fibrous structures, by a subsequent post-process such as folding or rolling up. Figure 3.6 shows some examples of 3D fibrous structures obtained by post-processing after electrospinning.

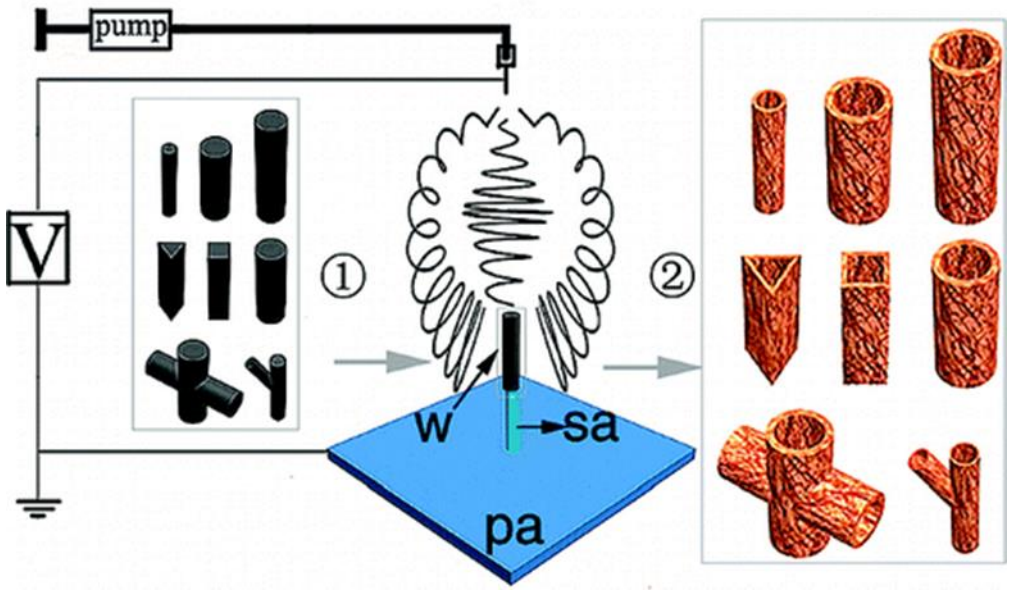

Figure 3.5 Schematic sketch of the process for fabrication of 3D fibrous tubes and other tubular structures [111].

3.4 Applications of Electrospun Nanofibers

The unique features of nanofibers such as high specific surface area to volume, high porosity, and hollow interiors plus the functionalities from the polymers themselves impart nanofibers with many desired properties for advanced applications. An outlook of possible applications is presented in the following section.

Filter applications

Fiber-based filter shows significant improvement in filtration efficiency compared with conventional filter. The three key features of nonwovens electrospun fibers are the overall porosity; defined as the ratio of the pore volume to the overall volume, the average pore size (the pore size distribution), and the inner specific surface area (defined as the surface area divided by either the overall volume or the overall mass).To obtain higher filter efficiency, it is generally necessary that the sizes of the pores in the filter materials should be in the nanometer ranges. The filtration efficiency also depends physical structure of the filter, for instance, fiber fineness, thickness, and base structure; electronic properties of fiber surface, and its surface energy. These parameters determine the circulation of gas through the fibers, the resistance to airflow, and the filter effectiveness. The mechanisms

of capturing particles by the filter media can be broken down into four mechanisms based on the particles size. Large particles than the pore size of the filter media are easily blocked by the sieve effect whereas smaller particles could be captured by the fibers, through interception, impaction, or static electrical attraction mechanism.

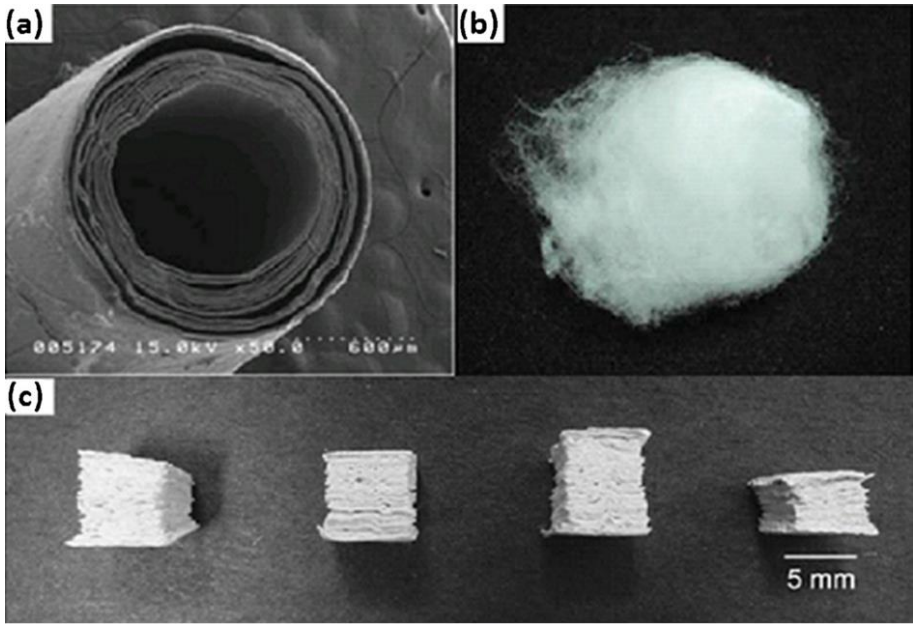

Figure 3.6 3D nanofibrous structures acquired by post-processing after electrospinning (a) Oriented chitosan mesh tube [112], (b) 3D scaffolds after mechanical expansion [113], and (3) 3D composite scaffolds [114].

It is shown by experimental measurements and theoretical calculations that electrospun nanofiber scaffolds are very efficient for capturing airborne particles ranging from 0.5 µm to 200 µm [115]. Nanofiltration membranes composed of nanofibers are frequently used in moderating of ground water and the distillation of surface water for drinking water requirement [116]. Nanofiber filters are also used to protect and isolate garments and bags from virus, bacteria, and decontaminate aerosol dusts [117].

As fiber-based filters are capable of blocking most of the tiny particles from waste liquids and air, therefore, they are strong candidate of filter media in industrial applications, particularly as wastewater treatment for textile industries, and for the noise reduction problem of aircraft, vehicles and infrastructures. Donaldson, AMSOIL, and DuPont

Company have produced nanofiber-based filter products for industry, consumer, and defense applications

Nanofiber Reinforcement

The dominating parameters that effect the fiber reinforced composite are the mechanical properties of the fibers, their aspect ratio and the mechanical bonding between the fibers and the matrix [1]. Because of the high surface to volume ratio, the use of nanofibers exhibits better interaction between the fibers and matrix materials, hence, enhances the mechanical properties. As nanofibers have small diameters, the light reflection is negligible. Therefore, transparent matrices with reinforced nanofibers remain transparent, even though their refraction indices do not match with each other. The impact strength of the reinforced matrix can be improved significantly by adding nanofibers, due to large specific surface area between matrix and nanofiber. Tang and Liu [118] prepared cellulose nanofibrous reinforced PVA nanocomposite and showed that the composite film exhibited good transparency to visible light. The mechanical strength and Young's modulus were also increased considerably compared with the pure PVA film

Tissue Engineering

In tissue engineering, the electrospun scaffolds are used on human body cells so that they can mimic the structure and biological functions of the natural extracellurlar matrix (ECM). The nanofibrous scaffolds are expected to facilitate the growth, migration, and proliferation of the cells to regenerate the three-dimensional structure of the tissue. Moreover, they are able to fulfil a diverse range of requirements concerning biocompatibility, biodegradability, architecture, large surface to volume ratio, high porosity, variable pore size distribution, and the ability to be tailored into a variety of sizes and shapes, and mechanical properties. A schematic illustration of general principal of tissue engineering is shown in Fig. 3.7. Numerous researchers are making extensive efforts for producing such scaffolds with synthetic biopolymers and/or biodegradable polymer nanofibers that can mimic native structures [4, 119].

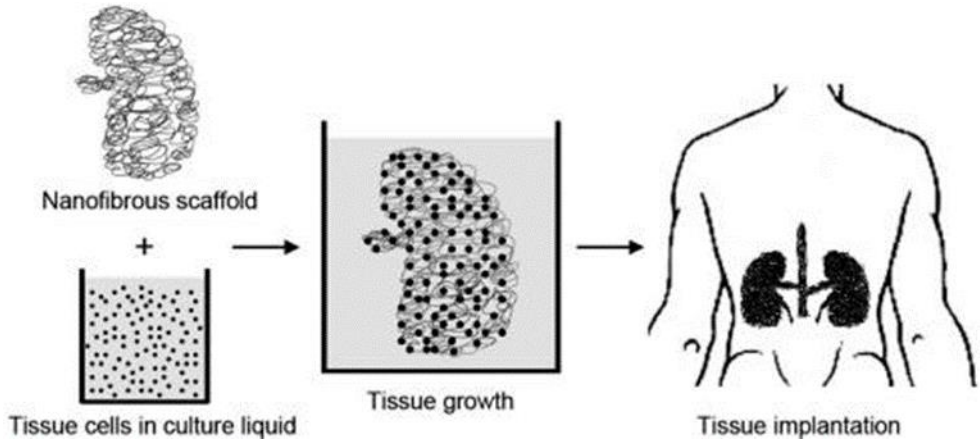

Figure 3.7 A schematic illustrations of tissue engineering [3].

Wound Dressing

A potential application of electrospun nanofibers in biomedical field is in the treatment of large wound healing, such as burns and abrasions. Wound healing recovers the damaged organs by a native process of regenerating dermal and epidermal tissues. Normally, the injured body cannot heal a deep dermal wound. Therefore, with the aid of electrospinning method, a thin layer of nanofibrous web especially from biodegradable polymers is directly sprayed or spun onto the affected zone which lets wound heal by encouraging the formation of normal skin growth and eliminates the formation of scar tissue that occurs in a traditional treatment method [120]. Such nanowebs carry enough pores, ranging from 500 nm to 1 μm, for the exchange of liquids and gases with the environment, but they are small enough to protect the wound from bacterial penetration via aerosol particle capturing mechanisms.

Bones

The functional properties of bone tissue scaffolds are that they should be porous, and made of biodegradable materials that shelter various growth factors, drugs, genes, or stem cells. Nanofibrous poly(e-caprolactone) (PCL) scaffolds have been extensively studied in bone tissue engineering [121, 122]. Yoshimoto et al. [122] cultivated, expanded and seeded mesenchymal stem cells (MSCs) derived from the bone marrow of neonatal rats on electrospun PCL scaffolds and observed that penetration occurred into the PCL matrix after one week and type I collagen occurred at 4 weeks.

Zhang et al. [123] prepared hydroxyapatite/chitosan (HAp/CTS) biomimetic nanocomposite fibers by combining an in situ co-precipitation synthesis approach with an electrospinning process. It had been demonstrated by biological in vitro cell culture with human fetal osteoblast (hFOB) cells for up to 15 days that the integration of HAp nanoparticles into chitosan nanofibrous scaffolds can lead to significant bone formation oriented outcomes compared to that of the pure electrospun CTS scaffolds.

PLC/ Bioactive glass, PCL–HA–collagen, poly(ethylene oxide terephthalate)-poly(butylenes terephthalate) (PEOT/PBT) fibers), silk fibron/ bone morphogenetic protein-2 (BMP-2) or Hap, poly(lactic acid)/gelatin, and collagen–hydroxyapatite have also been widely studied for bone tissue regeneration [124, 125].

Blood Vessels

To mimic the native blood vessel, the electrospun nanofibers should carry desired morphological and mechanical characteristics. Vaz et al. [126] fabricated a bi-layered tubular scaffold composed of a stiff and oriented PLA fibrous outer layer and randomly oriented PCL fibrous inner layer (PLA/PCL) and achieved desired levels of pliability. They suggested that PLA/PCL bi-layered electrospun scaffolds have appropriate characteristics to be considered a candidate for blood vessel tissue engineering. Small diameter vascular grafts were prepared with a composite scaffold incorporating a highly porous poly(ester-urethane)urea (PEUU) inner layer and an external PEUU electrospun nanofiber layer by Soletti and coworkers [127] (as presented in Fig. 3.8). The bilayer scaffold showed comparable mechanical properties with those of native vessels, and better cell integration and growth.

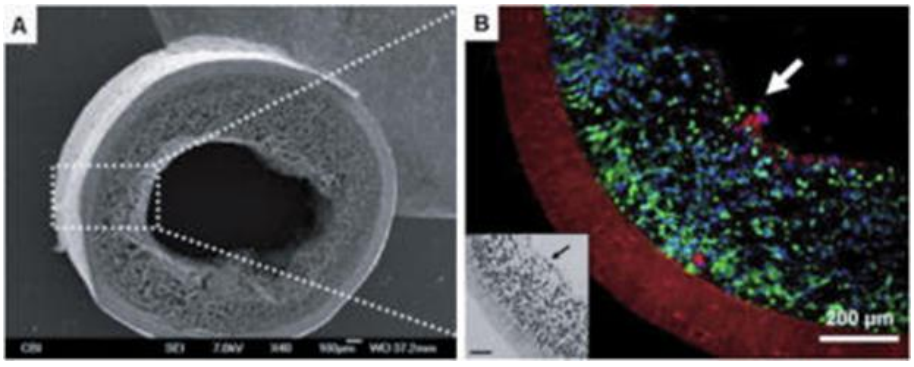

Figure 3.8 A bi-layered small diameter PEUU vascular graft (a) before and (b) after cell cultivation [127].

Drug Delivery and Release Control

In the last few decades, researchers have showed tremendous attention for transporting, releasing, and controlling of drug delivery systems (DDS) as it is a crucial concern in medicine. In medical service, controlled release of drug is considered to be an efficient process. DDS fabricated by electrospinning have many advantages over conventional doses, for example, improving therapeutic efficacy and reducing toxicity by delivering drug at a controlled rate over a longer period of time. Furthermore, they are able to penetrate certain membranes or barriers, e.g., the blood–brain barrier, and can be released only on the targeted cells. However, degradation rate of polymer regulates the type of a drug loading into delivery system. According to drug loading and carrier materials, likely modes of DDS are: (1) Post spinning nanofibers- drug as particles attached to the surface of the carrier (2) both drug and carrier are nanofiber-form, hence the end product will be the two kinds of nanofibers interlaced together, (3) the blend of drug and carrier materials integrated into one kind of fibers containing both components, and (4) core-shell electrospinning where the carrier material is electrospun into a tubular form and the drug particles are encapsulated. DDS can be used to treat many diseases, such as cardiovascular diseases and diabetes, cancerous tumors, metastases, pulmonary hypertension, and asthma.

Solar Cells

Electrospun nanofibers with metal oxide have shown great application potential in solar energy sector as they have characteristics of better electrical conductivity with higher specific surface area than nanoparticles, and interconnected pores in nanofibrous mat

enhanced penetration of viscous polymer gel electrolyte. The solar–electric energy conversion efficiency have been achieved over 90 % from electrospun TiO_2 electrodes with a poly(vinylidenefluoride–co–hexafluoropropylene) (PVDF–HFP) gel electrolyte than conventional liquid electrolyte system [128]. To improve electrical conductivity, the electrospun TiO_2 electrode was further treated with $TiCl_4$ aqueous solution so that an additional rutile TiO_2 layer can form on the fiber surface. Such a rutile TiO_2 reduced the pore volume of nanorod photoelectrodes while improving inter-rod connectivity and enhancing electron diffusion [129]. By doping of materials onto electrospun fibers, charge generation and transport can also be improved. For instance, strontium doped TiO_2 ($SrTiO_3$) enhanced photocatalytic activity by improving charge separation derived from the coupling effect of TiO_2 and $SrTiO_3$ nanocomposite [130].

Fuel Cells

Electrospun materials can be used as catalyst in fuel cells because they have high catalytic efficiency, excellent durability, and affordable price. Pt based catalyst, for example, PtRh and PtRu nanowires were prepared by electrospinning, and exhibited higher catalytic performance than commercial nanoparticle [131]. Electrospun nanofibers can also be employed as catalyst-supporting materials instead of direct use as catalyst. Li et al. [132] electrodeposited Pt clusters on the carbon nanofiber mats and showed that the catalytic peak current of the composite catalyst reached up to 420 mA/mg as compared with 185 mA/mg of a commercial Pt catalyst.

Hydrogen Storage

Hydrogen, a zero-emission fuel, is considered to be a future energy source. Researchers are investigating to find efficient methodologies to produce and store hydrogen. Hydrogen can be absorbed by the materials based on the materials' porosity in the form of metal hydrides. The smallest pores are most efficient for hydrogen storage; therefore, using electrospinning method, desired pore size and morphology of nanofibrous materials can be fabricated for hydrogen storage. Electrospun carbon fibers [133], and graphite nanofibers [134] have shown high hydrogen storage capacity.

Supercapacitors

Electrospun nanofiber-based supercapacitors show excellent capacitive behavior due to high specific surface area and controllable pore size on the electrospun fibers. Wee et al. [135] synthesized vanadium pentoxide (V_2O_5) nanofibers using electrospinning and showed a maximum specific capacitance of 190 F g^{-1} in aqueous electrolyte (2 M KCl) and 250 F g^{-1} in organic electrolyte (1 M $LiClO_4$ in PC) with promising energy density of 5 Wh kg^{-1} and 78 Wh kg^{-1} respectively. Porous carbon nanofiber composites (NFCs) were produced with polyacrylonitrile (PAN) and polymethylhydrosiloxane (PMHS) by Kim and coworkers [136] and demonstrated with 5 wt% PMHS had the highest specific capacitance, 126.86 F g^{-1}.

Catalyst and Enzyme Carriers

One of the main difficulties in catalysis is the elimination and recycling of the catalytic agent after the reaction. The addition of homogeneous or heterogeneous catalysts into nanofibers plays a vital role in resolving these issues. The reaction can be carried out by either circulating the mixture around the fibers (as is the case in the continuous flow mode to shorten reaction time) [137], or the fibers fixed on a carrier can be immersed repeatedly into a reaction vessel to catalyze the content of the vessel. The polymer nanofibers mixed with metal (Rh, Pt, Pd, Rh/Pd, and Pd/Pt) nanoparticles has been widely used for improving the efficiency of catalyst. Formo et al. [137] have demonstrated a simple polyol method for depositing Pt, Pd, and Rh nanoparticles with different sizes on nonwoven mats of TiO_2 and ZnO_2. They found that Pt nanoparticles coated on nanofibers membranes exhibited an excellent catalytic ability for a number of reactions.

Sensors

Besides high sensitivity, fast response, and reliability, a good sensor should have small dimension but large specific surface area, low manufacturing cost, and multiple functions. Therefore, electrospun nanofibers are very strong candidate to form a highly sensitive and fast response sensor. Various approaches have been reported for making nanofibrous sensors such as using polymeric sensing material, incorporating sensing molecules into other polymer nanofibers, coating/grafting sensing material on electrospun nanofiber surface. Nanofiber based sensors can be employed both in liquid and gas environment.

Gouma et al. [138] reported that electrospun fibers with molybdic oxide (MoO_3) and tungsten oxide (WO_3) could be engaged for detection of NO_2 and NH_3 in air, respectively.

Transistors

The electrospun nanofibers having tunable, optical, and electrical properties can be effectively used in field-effect transistors (FET). Babel and coauthors [139] investigated the optical and electrical properties of two series of binary blends of poly[2-methoxy-5-(2-ethylhexoxy)-1,4-phenylenevinylene] (MEH−PPV) with regioregular poly(3-hexylthiophene) (PHT) and with poly(9,9-dioctylfluorene) (PFO) and claimed that they can be exploited in field-effect transistors. Polyaniline/polyethylene oxide (PEO) nanofibers were electrospun and overserved the effect of field-effect transistor (FET) by Pinto et al [140]. They proposed one dimensional electrospun nanofibers can be successfully employed in FETs.

Other Applications

Electrospun nanofibers can be used as templates in the Chemical Vapor Deposition (CVD) to produce hollow ceramic or metallic fibers [141]. In this method, the electrospun biodegradable or soluble polymer nanofibers are coated by a range of polymers, metals and ceramics materials. A hollow nanotube is formed after degradation of the template polymer fibers.

Using various advanced methods of electrospinning, the properties of nonwoven nanofibers can be greatly altered and combined with conventional textiles to provide higher performance textiles such as for increase in wind resistance, regulation of the water-vapor permeability, optimizing the thermal insulation behavior, and support of textiles with specific functionalities, for instance, self-cleaning effect, aerosol filtering, and protection against chemical or biological hazards [142].

Electrospun polymer nanofibers have huge potential in sound absorption. Liu and coworkers [143] worked with electrospun polyacrylonitrile (PAN), thermoplastic polyurethane (TPU) and thermoplastic polyester elastomer (TPEE) nanofibers and showed PAN membrane had higher sound absorption coefficients in the frequency of 100–2500 Hz.

Electrospun nanofibers with electrical and electro-optical behavior play significant role in developing nanoscale electronics and photonics device [144], for instance, nano-diodes, field emission, optoelectronics, and electrochromic display. Another potential application of polymers nanofibers with piezoelectric effect such as polyvinylidene fluoride is piezoelectricity [145].

Chapter 4 Experimental Setup

4.1 High Voltage Power Supply Generation

The high voltage is one of the basic requirements in electrospinning process which creates an electric field between the tip of a needle and a collector plate. When the applied high voltage reaches a significant value that can overcome the surface tension of the solution, only then the fiber jet ejects from the Tylor cone. Generally, more than 6 KV positive or negative high voltage is needed in order to initiate the jet from the solution droplet [146]. However, depending on the other processing, solution, and environmental parameters of electrospinning, a higher voltage may be required. High voltage plays a significant role in order to develop fiber diameter and morphology.

We developed a stable high voltage direct current (DC) power supply in the laboratory which can generate up to 30 KV. This system is based on high voltage flyback transformer (HVFBT), which was selected because it is easy to find, inexpensive, and compact.

A typical flyback transformer and its circuit are shown in Figure 4.1. A DC power supply drives the primary winding of the flyback transformer. When the switch is turned on, energy is stored in the primary core material. An integral diode and polarity dots on the transformer are placed in such way that no energy can transfer to the load. When the switch is turned off, the polarity of the transformer winding converses due to the failing magnetic field in the primary winding, and the energy that was stored in the core material is transferred to the load. This activity is repeated and the duty cycle is adjusted till the required voltage is achieved.

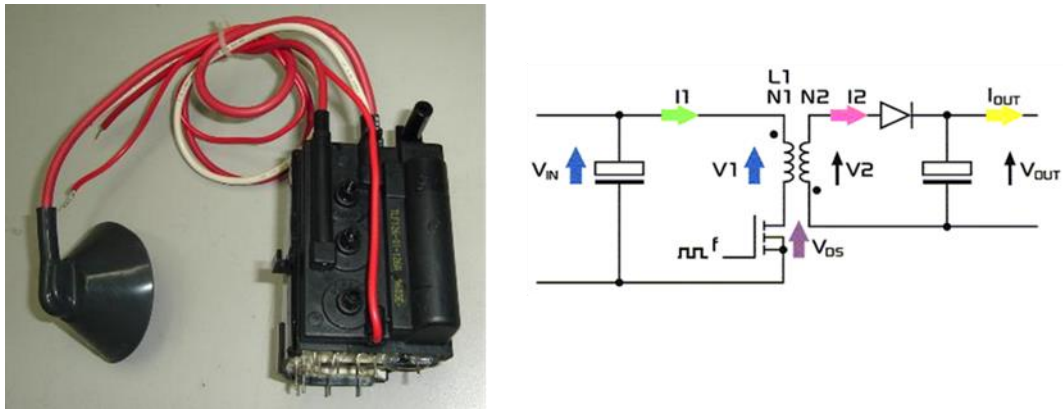

Figure 4.1 A typical flyback transformer and its circuit [147].

4.1.1 Design of HV Circuit

The high voltage power supply consists of a HVFBT as the main component, a PWM circuit, and a feedback circuit (as illustrated in Fig. 4.2). A pulse-width modulation (PWM) with controllable frequency and duty cycle was used as an input to the HVFBT.

The PWM circuit was comprised of a SG3525 IC, a duty cycle control circuit with 15 kΩ variable resistor, and a frequency control circuit. The duty cycle and frequency of the PWM wave need to be adjusted in order to achieve desired output voltage in the HVFBT. The drain pin of IXFH8N90 MOSFET was hooked to the primary side of the HVFBT. The high frequency generated by PWM triggers the MOSFET and allows the current to flow through the primary winding of HVFBT. Two MOSFET were connected in parallel to double the input frequency of PWM. The maximum input voltage of the primary winding of the HVFBT for this design circuit is DC 60V.

To monitor the output voltage, one end of a high voltage resistor was connected to the high-voltage output pin of the secondary winding of HVFBT. We have used a 500 MΩ resistor so that the current flow through the monitoring circuit remained as small as possible. The divided voltage was then buffered and converted into digital data which was displayed by the LCD. Finally, the divided voltage was multiplied by a known calibration factor (voltage dropped across a known resistor) in order to calculate the actual high voltage output. A feedback from the output high voltage is also connected to the input PWM circuit. Using a variable potentiometer from the feedback circuit, the high voltage

output can also be adjusted. A high voltage capacitor was hooked in between a ground pin and high voltage output pin of HVFBT to maintain a smooth and continuous high voltage output.

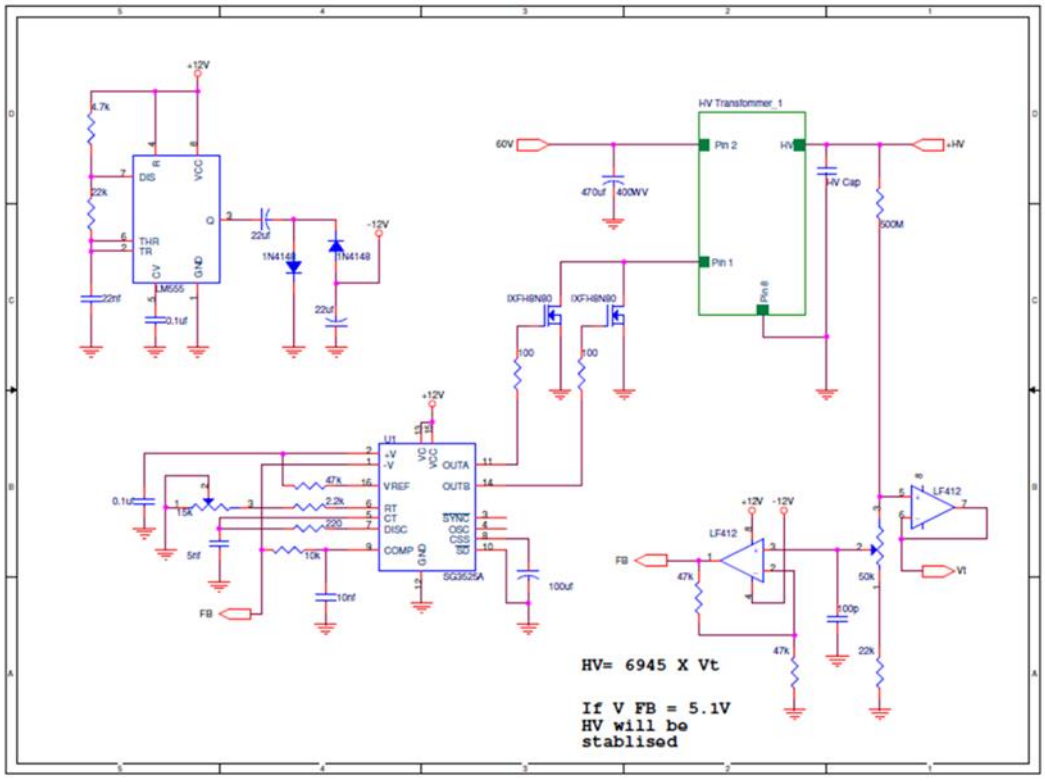

Figure 4.2 A circuit diagram of high voltage power supply using HVFBT

Any kind of leakage, dry soldering, electromagnetic radiation from high voltage output, improper adjustment of duty cycle and frequency to the PWM can induce noise in to the high voltage signal which can make the entire system unstable. Therefore, the HVFBT and high voltage control circuit were submerged in mineral lubricant oil to avoid any disturbance. All the electronics design work regarding this advanced electrospinning setup has been carried out in collaboration with Mr. Tahir Siddiqui.

4.2 Electrode Control System

Typically, in electrospinning process, conductive electrode is used to collect the electrospun fibers. An opposite high voltage potential is connected with the electrode to create a continuous path for the movement of charges. There are numerous type of

collectors used in electrospinning methods including aluminum foil, flat conductive plate, wire mesh, grids, parallel plate, rotating drum, liquid bath and so on [28, 148]. Electrospun nanofibers deposition pattern varies based on the collector used in the electrospinning system. Li and co-workers [27] have suggested that electrospun nanofibers can be prepared as uniaxial aligned arrays by using two parallel conductive collectors separated by air gap. They connected both conductive collectors to the fixed ground potential and showed the electrical field splits into two equal parts between the collectors, and as a result, electrospun nanofibers receive some degree of alignment.

One of the objectives of this research is to produce aligned fibers. Therefore, we started our works by modifying the conductive electrode system in order to develop a versatile system of electrospinning so that it can be capable of producing any kind of patterned architectures with desired alignment. We hypothesised that by switching the high voltage potential of electrodes, the electrical field as well as electrospun charged fibers could be moved from one location to another location. But altering one high voltage potential to other is quite a difficult task because they might create sparks between the opening contacts of switches or relays.

We replaced a single conductive electrode, typically used in an electrospinning process, with multiple electrodes as depicted in Figure 4.3. The voltage potential of these electrodes are altered with the help of microprocessor based control system. An important component in this control system are the relays. Each collector electrode is operated by an individual relay. The characteristics of these relays are that they should have high switching voltage to avoid spark between the opening contacts and the contact release time should be as low as possible. To satisfy these characteristics we have employed 9104 series high voltage SIP reed relays. The key features are:

- High voltage switching up to 1000 V
- High dielectric strength (2000 V DC)
- High insulation resistance – 1011Ω minimum
- High speed switching (0.5 ms) which is quite high compared to electromechanical relays

- Magnetic Shield – reduces interference

In short, the electrode control system consists of multiple conductive electrodes which are connected to individual high voltage relays. The relays are operated by microprocessor control system. ARDUINO codes have been developed which were uploaded to the microprocessor. We interface the high voltage system to the personal computer via HyperTerminal.

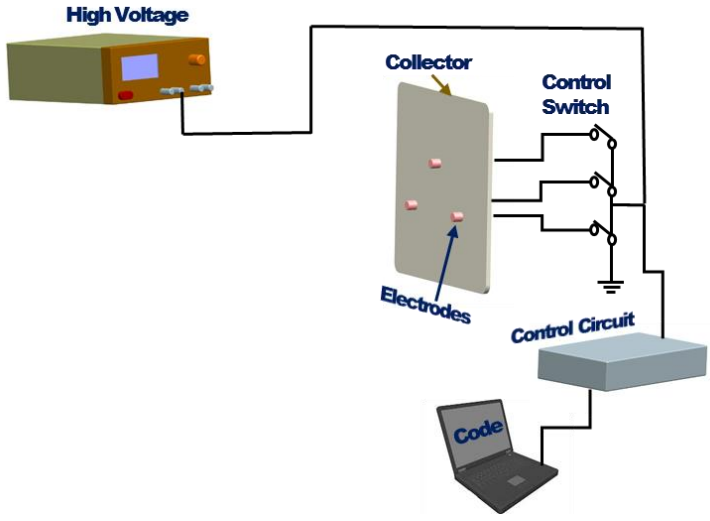

Figure 4.3 A schematic sketch of electrodes control system.

4.3 Program Development

The main purpose of this research is to develop various fibrous patterned architectures, controlled deposition at desired locations, and improve the alignment of electrospun nanofibers with the help of multiple electrodes and switching their zero voltage potential. Based on the required deposition pattern, number of conductive electrodes are needed to engage and arrange them in desired location. Finally, the zero voltage potential of electrodes switches in a sequence of preferred direction by microprocessor control system. For example, in order to develop rectangular functionally graded scaffolds, we may employ three pairs of electrodes (six electrodes) (a schematic of electrodes configurations is shown in Fig. 4. 4A) where electrodes are placed in a column and row a certain distance apart from each other.

Figure 4.4B shows the switching times of these electrodes. The voltage potential of electrodes are switched in a pattern in which two electrodes are active concurrently. This is called overlap time (OT). Then the 1st electrode is switched off while only the 2nd remained active for certain time called net time (NT) after which the 3rd electrode is activated. Following another OT the 2nd electrode is deactivated and after NT, the 4th electrode is activated and the cycle progressed in a clockwise direction following the electrodes switching sequence of 1-2-3-4-5-6-1.

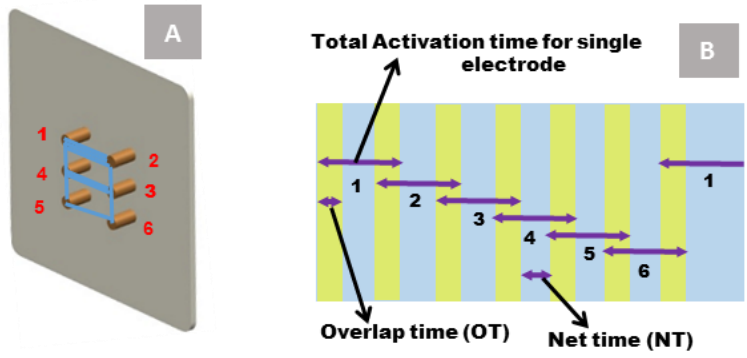

Figure 4.4 Schematics of A) electrodes configuration and B) control timing for driving electrodes to generate a desired pattern.

With this electrodes configuration, the required functionally graded scaffolds can be produced in two different ways. Changing overlap time between each pair of electrodes (electrodes 1 & 2, 3 & 4, and 5 & 6), deposition time of fibers can be varied at those locations and as a result, functionally graded scaffolds are developed. In another direction, keeping overlap and net time constant, we can prolong the electrical field potential between active electrodes pairs 1 & 2, 3 & 4, and 5 & 6. Thus, functionally graded scaffolds are created by varying the cycling ratios among the electrodes.

Therefore, switching the voltage potential of electrodes is the key element for generating various shapes of nanofibrous patterns. We developed microprocessor based system for controlling the electrodes. For each desired shape of nanofibrous scaffolds, we wrote separate codes which were uploaded to the ARDUINO microprocessor. Program was controlled from personal computer with the help of hyper terminal.

4.4 Chamber Fabrication

During the experiment the associated current in the system can be up to few micro amperes at very high voltages. Therefore, this can be very dangerous for the human body because any untimely contact, during operation, may affect the heartbeat, resulting in possible fatality. Also, high voltage applied between two electrodes with an air gap may produce ozone and röntgen radiation. Another harmful item is the solvent, which evaporates during the travelling of jet from the spinneret to collector screen and hazardous fumes may escape from the setup. Therefore, special safety precautions need to be employed in the experimental test equipment design.

Figure 4.5 illustrates the designed test equipment enclosure with a protective cover of transparent acrylic sheet. A protective magnetic switch is equipped on the door. If the door is opened during operation, magnetic sensors are triggered and the whole system shuts down within a few microseconds which prevents any direct human contact from live charges. In addition, the transparent sheet yields a clear view of the electrospinning process and prevents air drafts from outside of the cabinet which may disturb the fiber deposition from the target position.

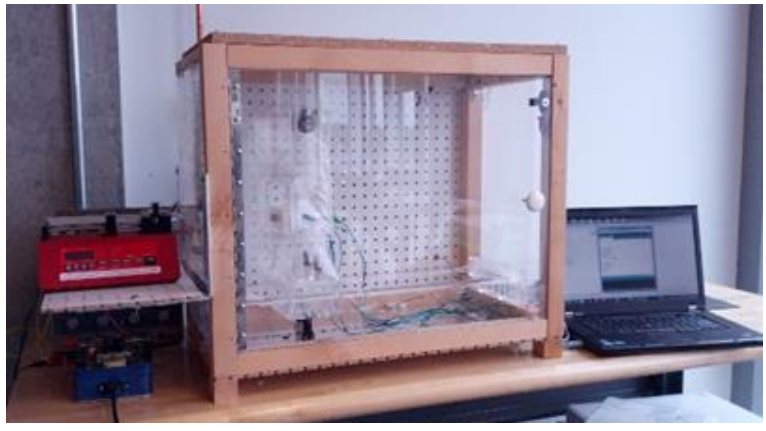

Figure 4.5 An illustration of experimental test equipment setup.

4.5 Measuring Tool Design

The fibers produced by electrospinning are small in size and are deposited on the collector in various patterns such as random, unidirectional and aligned multidirectional. It is important to understand how fibre diameter and its distribution are affected by the electrospinning variables. Generally, the characterization involves area, diameter, length, and orientation measurements of electrospun fibers. To characterize the electrospun fibre diameter and distribution, micrograph images of the deposited fibers are required. These micrographs are usually obtained by optical microscope (OM), scanning electron microscopy (SEM), transmission electron microscopy (TEM) or atomic force microscopy (AFM). There are number of difficulties involved in processing these images. One of major issues is the non-uniformity of nanofibers throughout the image. The diameters may vary from point to point in the same fiber which make the diameter measurement very problematic based on area and perimeter calculations. Another problem is the overlapping of fibers which enhances the complexity in distinguishing the original fiber diameter. Moreover, Electrospun nanofibers are very long and continuous, leaving open boundary area at the edges on the micrograph image. Most commercially available measurement equipment cannot deal with nanofibers.

However, fiber diameters can be measured by using manual method that can lead to high human errors in the output results. In this method, first the micrograph scale bar is measured manually in terms of pixel. Then individual fiber diameter is counted selecting two edges of the fibre perpendicular to the fibre axis. Finally, measured pixel number is converted to nanometres using the scale. Therefore, this manual method is not considered as user friendly, time effective or productive. Identifying the edges of the fibers need great attention and the measurements should be exactly perpendicular to the fiber axis which are very difficult to achieve. Moreover, as it is an operator-based method, fatigue can reduce the accuracy.

The aforementioned problems can be eliminated by introducing automating measurement of fiber diameter. Therefore, we developed an image processing tool using MATLAB algorithm in order to minimize operator errors as well as to accelerate our research works.

The developed tool can read the electrospun fiber's micrograph images and can automatically measure their characteristics including diameters of fibers, and their orientations with respect to horizontal axis along with the statistical variations. The development of the MATLAB codes was carried out by collaboration with Keval Thaker, an undergraduate student at UOIT.

Figure 4.6 presents a flow chart of MATLAB algorithms for image processing of electrospun fibers. The input to the MATLAB was a pixel based image (RGB image) and stores as three-dimensional arrays (i.e., matrices), in which each element of the matrix corresponds to a single pixel in the displayed image. To reduce memory requirements, image was converted to 8 bits grayscale image in where each pixel is a shade of grey, normally from 0 (black) to 255 (white) followed by Median filtration technique which was employed to reduce noise and improve smoothness. After that, image was transformed to binary data where edge corresponds to sudden change in intensity level from 1 to 0 and vice versa (shown in Fig. 4.7A). A morphological operation was performed using marker and mask images in order to reconstruct the fibers (see Fig. 4.7B). Then the skeleton of the objects is created from binary image. Generally, two or more fibres overlap each other throughout the image. Therefore, after identifying overlapping regions by neighbourhood operation, they have been removed from the reconstructed image.

To measure the fiber diameter and angle, reference lines at 100 pixel intervals were sketched along the horizontal axis of the image. These reference lines intersected with fiber's skeleton. At intersect points perpendicular lines were constructed based on the negative reciprocal of the linear fit of skeleton. Continuous fibrous region (white pixel) was counted along the perpendicular line. Finally, the number of white pixels converted to micrometers by multiplying with the conversion factors which provided the diameter of the fiber. As the edges of fibers were created by rectangular pixels, the average of five diameters at each measuring point in short intervals has been used (presented in Fig. 4.7C) to improve measurement accuracy. Prior to commencing the measurement process, it is required to calibrate the custom measuring tool with the image scale bar.

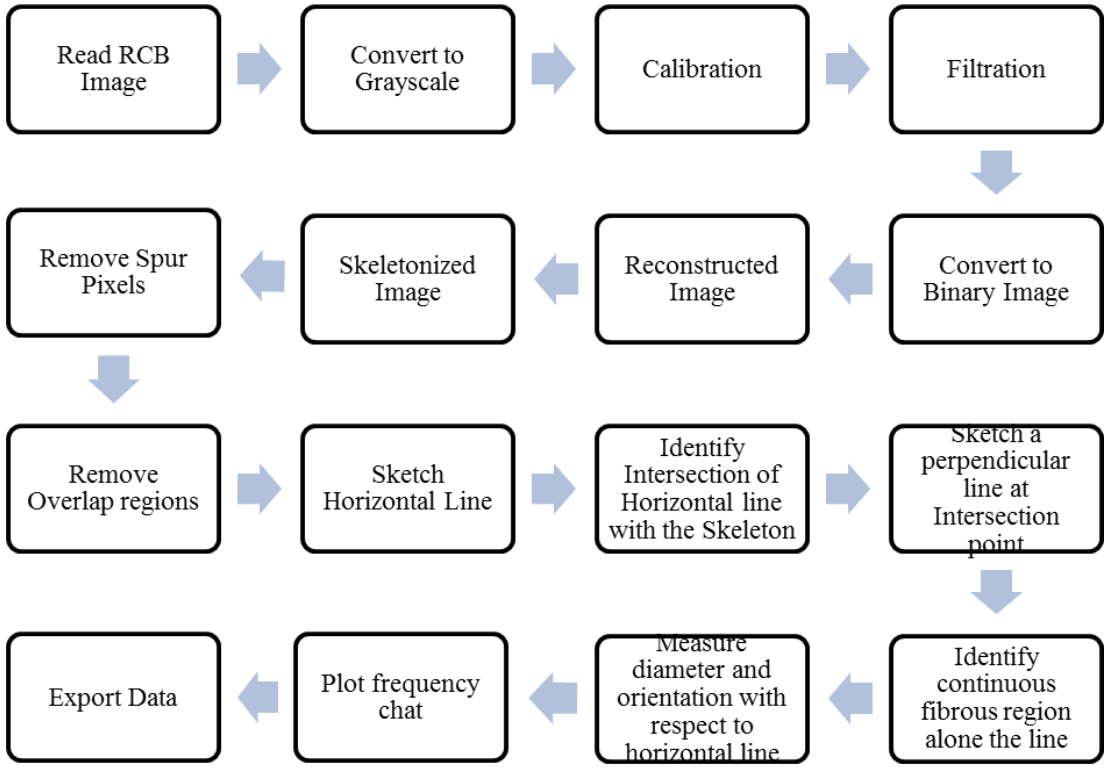

Figure 4.6 Flow chart of custom image processing MATLAB algorithm.

With this custom measuring tool, it is also possible to measure the orientation of fibers. The angles formed at the intersect points between the reference horizontal lines and linear fit of skeleton were measured. Angles ranged from -90^{o} to 90^{o} with 0^{o} being parallel to the reference line and individual angles were placed into data bins of 5^{o} each in the frequency chart.

The end products of this custom code image processing are diameter, orientation measurement of fibers and the corresponding frequency charts (Fig. 4.7D).

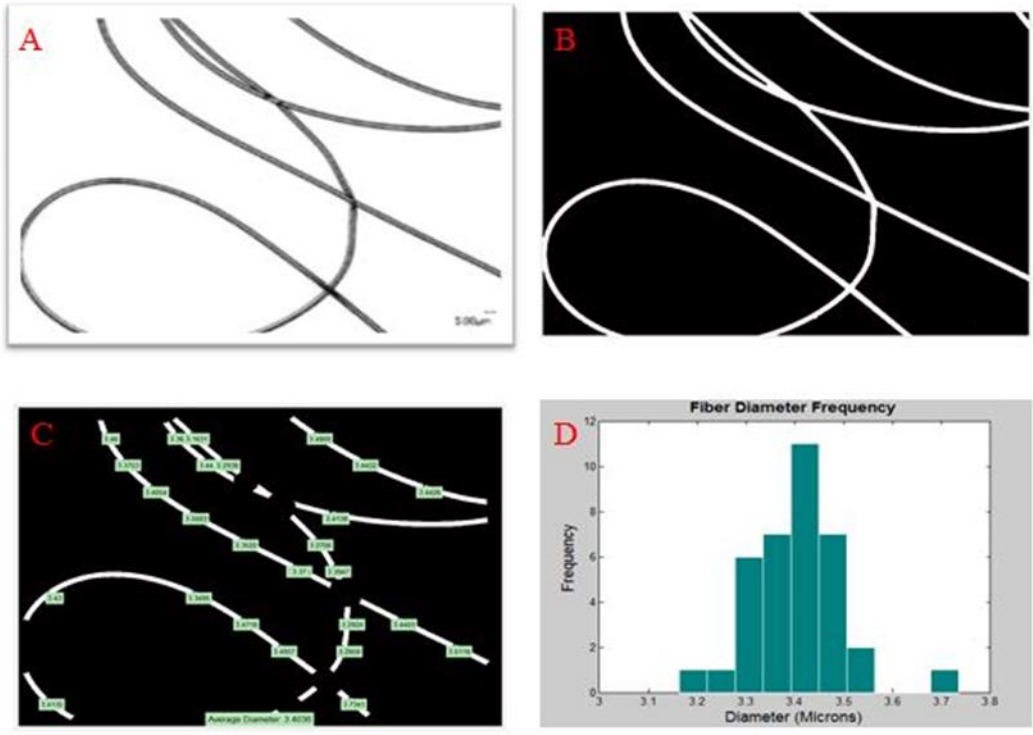

Figure 4.7 Image processing steps: A) binary image, B) reconstructed image, C) measuring averaging fiber diameter, and D) frequency chart of fiber diameter.

Chapter 5 Function of Advanced Electrospinning Method

5.1 Introduction

Polymeric nanofibers produced by simple, and economical electrospinning technique, possess high surface-to-volume ratio, tunable porosity, and desired functional properties [2, 11, 149], which make them a strong candidate for many advanced applications including reinforcement of composite materials, sensors, filtration, drug delivery, and tissue engineering [46, 145, 150, 151]. In recent years, electrospun nanofibers collected in patterned architectures have attracted increased attention due to their usefulness in a broad range of applications such as micro or nano-devices, photonics, microelectronics, and biomedical fields [24, 150, 152]. One of the most simple and effective methods for developing nanofibrous structures is to use a patterned conductive electrode as collector. Zhang and Chang [23] employed an electro-conductive template with woven structure and produced a patterned design similar to the patterned template collector after electrospinning. Electrospun nonwoven patterned meshes of gelatin–polycaprolactone (Gt–PCL), were successfully prepared using several patterned collectors by Zhao et al. [30] and they demonstrated that the surface topography of the collector structures determined the architecture of the pattern generated.

Preparation of ordered and controllable micro or nano-structure is one of the leading challenges because electrospun nanofibers are generally collected as non-woven and randomly oriented structures [153]. Positioning and ordering of individual fibers into the pattering architecture is often needed for tissue regeneration [24] and micro or nano-device fabrications [150]. Various approaches have been described in the literature for positioning the nanofibers in desired directions, for instance; rotating drum [154, 155] or disc [49], pair of parallel electrodes [21, 156], and controlling the electrical field [61, 65]. The most simple and straightforward methods for developing oriented electrospun fibers are the high

speed rotational drum or disk techniques. Nevertheless, directional deposition and developing suitable scaffolds are quite difficult to obtain in these cases. Li and co-workers [27] have suggested that electrospun nanofibers can be prepared as uniaxial aligned arrays by using two parallel conductive collectors separated by air gap. They also demonstrated that multi-layered structures of aligned nanofibers could be produced by changing the configuration of patterned electrodes. Brown and colleagues [83] have shown that highly ordered and complex porous structures can be produced by using melt electrospinning technique. Low production rates compared to solution electrospinning technique and size limits of ultrafine fibers (dia. >1μm) are the main drawbacks in this technique.

However, controlling the fiber deposition in any desired direction and location within the pattern remains challenging, particularly for solution electrospinning. A possible mechanism for achieving this is by concentration of electric field in the desired direction of deposition, and the ability to change this direction when needed. But this is difficult to implement. The reason is that changing the direction of the high voltage potential field, from one set of electrodes to another set, causes sparking in the relay contacts used for this switching, which can destabilize the process.

Moreover, a number of key issues need to be addressed, for instance, how to control the amount of fibers deposited and how to generate variable deposition density in various sections within electrospun patterned architecture. This study presents a versatile electrospinning method for fabricating well-aligned and controllable micro/nanofibrous patterns in which the density can be varied at different locations as needed.

5.2 Material and Experimental Procedure

PVA: PVA is white, odorless, tasteless, and translucent granular powder. It is water soluble, partial soluble in ethanol, and insoluble in all other organic solvents. The melting point of polyvinyl alcohol is around 180 to 190°C. The molecular weight ranges from 26,300 to 300,000 and a degree of hydrolysis is 86.5 to 89%. The chemical formula for PVA structure is $[CH_2CH(OH)]_n$. PVA has huge applications in the food industries, various pharmaceutical, biomedical and textile industries [157, 158]. PVA based

commercial products exhibit low environmental impact due to its biodegradability, aqueous solubility, and high chemical resistance. In food packaging systems, PVA films show outstanding protective properties. In medical devices, PVA can be engaged as a biomaterial because of their excellent properties of biocompatible, nontoxic, swelling, and bio-adhesive.

The schematic sketch of experimental setup is shown in Figure 5.1, where multiple electrodes are used which can be switched by microprocessor control system. A syringe pump (New Era Pump Systems Inc., NE-300, USA) was employed for delivering polymer solution to the needle tip (0.26 mm inner diameter). Polyvinyl alcohol (PVA, Mw ~ 130,000, Aldrich) was dissolved in distilled water to prepare a 8 wt% solution, which was then loaded into the plastic syringe. The flow rate of the polymer solution through the capillary/needle was 100 μL/h. A stable, lab-made direct current (DC) power supply provided the high voltage to the needle tip and the collector electrodes. The applied voltage and the collector distance from the needle tip were 10 KV and 6 cm, respectively. The fibers were collected on a 2 mm thick acrylic sheet through which copper wire electrodes (1.6 mm diameter) protruded so that the sheet plus copper electrodes together acted as fiber collection system. After deposition, the electrodes were carefully removed so that the fibers remained on the acrylic sheet. The microprocessor based control system can switch the potential of electrodes within a few milliseconds. Therefore, charge carrying fibers can be moved from one electrode's location to another within this short duration.

5.3 Electrical Field Analysis

The high voltage, which creates electrical field between needle tip and collector, is one of the important parameters in electrospinning method. The high voltage has significant effect on electrospun fiber morphologies. It induces charges on the solution droplet, and as a result, the jet accelerates faster and draws more materials from the Tylor cone. It also defines the location of electrospun fiber deposition. However, the electrical field can be controlled by adjusting the applied voltage, gap between the needle tip and collector, and shape of the collector.

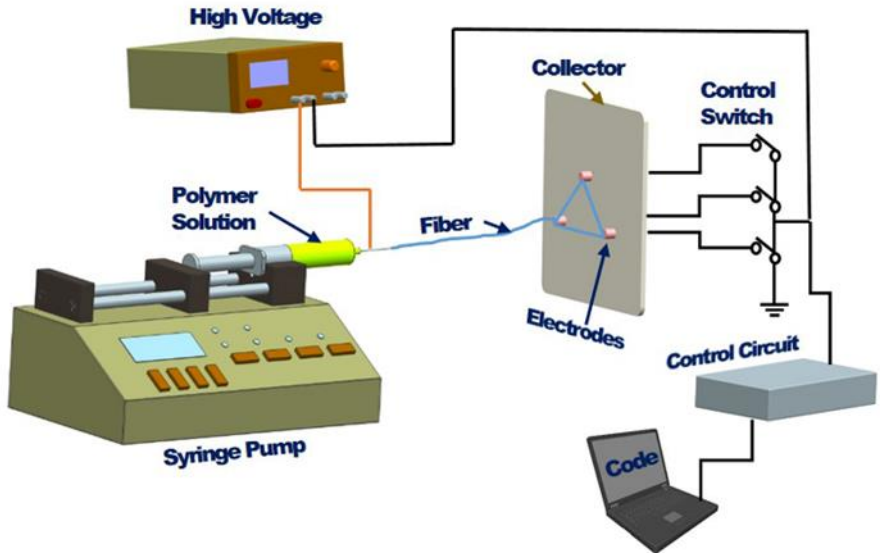

Figure 5.1 Schematic of the experimental setup.

A number of research groups investigated the electric field distribution of electrospinning process to understand and control the electrospun fiber deposition pattern. Zhao et al. [30] simulated the electric field distribution using a grounded Al foil, and a grounded metal grid collectors in electrospinning (as shown in Fig. 5.2). They showed that the electric field lines distributed uniformly near the Al foil, demonstrating that the electrostatic attraction forces on the jets were uniform over the entire Al foil. Therefore, nanofibers could be deposited as randomly oriented non-woven fabric mats. On the other hand, the electrical field lines were concentrated and pointed toward the protrusions in the metal grid as illustrated in Figure 5.2B. This result indicated that the electrical field strength was strong over the metal grids as compared to other areas. Hence, the charged jet could be moved towards the surface of the metal grids due to the concentrated electrical field (Fig. 5.2D).

The electric field distribution of plate-plate type electrospinning was analyzed by Hong-wei and coworkers [159]. They demonstrated that the electric-field vector had axially symmetric distribution (Fig. 5.3A) which was responsible for non-uniform fiber distribution. They reported that the value of field strength decreases with the increases of collector surface area. In Fig. 5.3B shows relation between electric field and collecting distance of plate-plate type electrospinning. The field strength dropped very sharply after a short distance from spinneret pipe orifice.

Li et al. [21] used two parallel conductive silicon strips separated by an air gap (shown in Fig. 5.4A). They calculated the electrical field strength vectors between the needle tip and the ground collector using Student's QuickField program (Fig. 5.4B). They showed that the electrical field vectors near the conductive collectors were split into two fractions and pointed toward opposite edges of the gap.

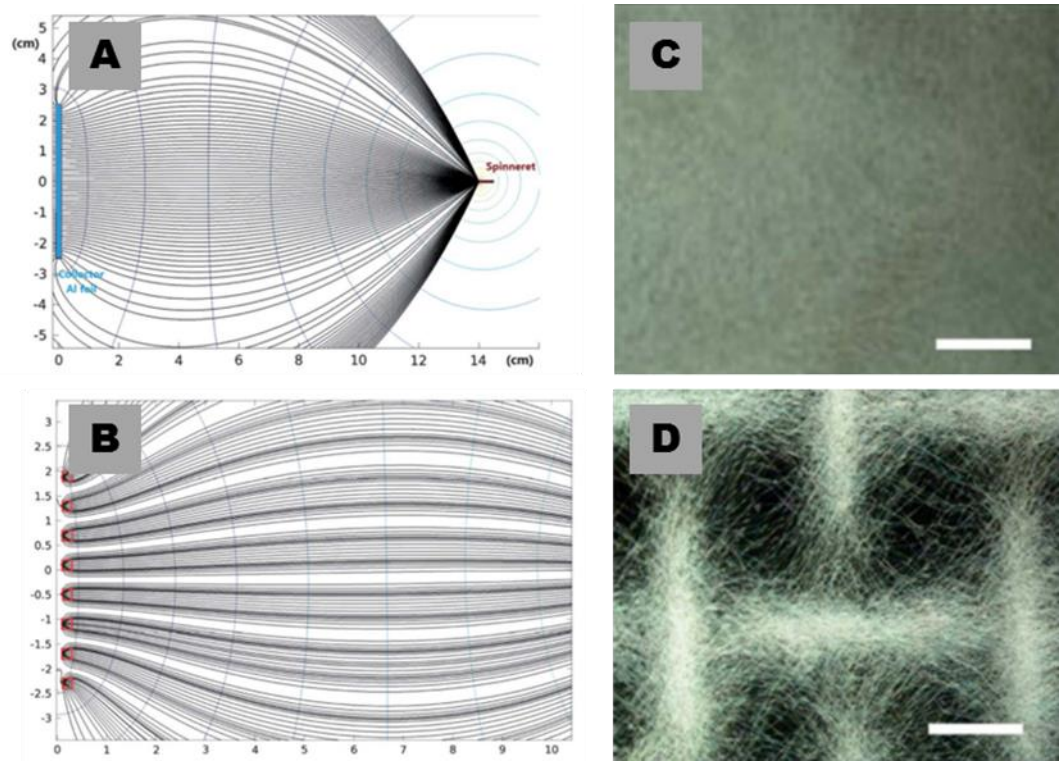

Figure 5.2 Electric field simulations of electrospinning using an Al foil (A), metal grid (B). Tip-to-collector distance was14 cm and supplied voltage to the spinneret was 20 kV. The corresponding optical images of the electrospun mats (C) and (D), respectively [30].

Therefore, finite element method (FEM) is a useful method for simulating electric field strength and field distribution in electrospinning to save cost and improve efficiency. In his study, we employed FEM for analyzing the electrical field distribution due to switching the voltage potential of electrodes and to find a relationship with the system parameters such as distance between adjacent electrodes, and the diameter of electrodes.

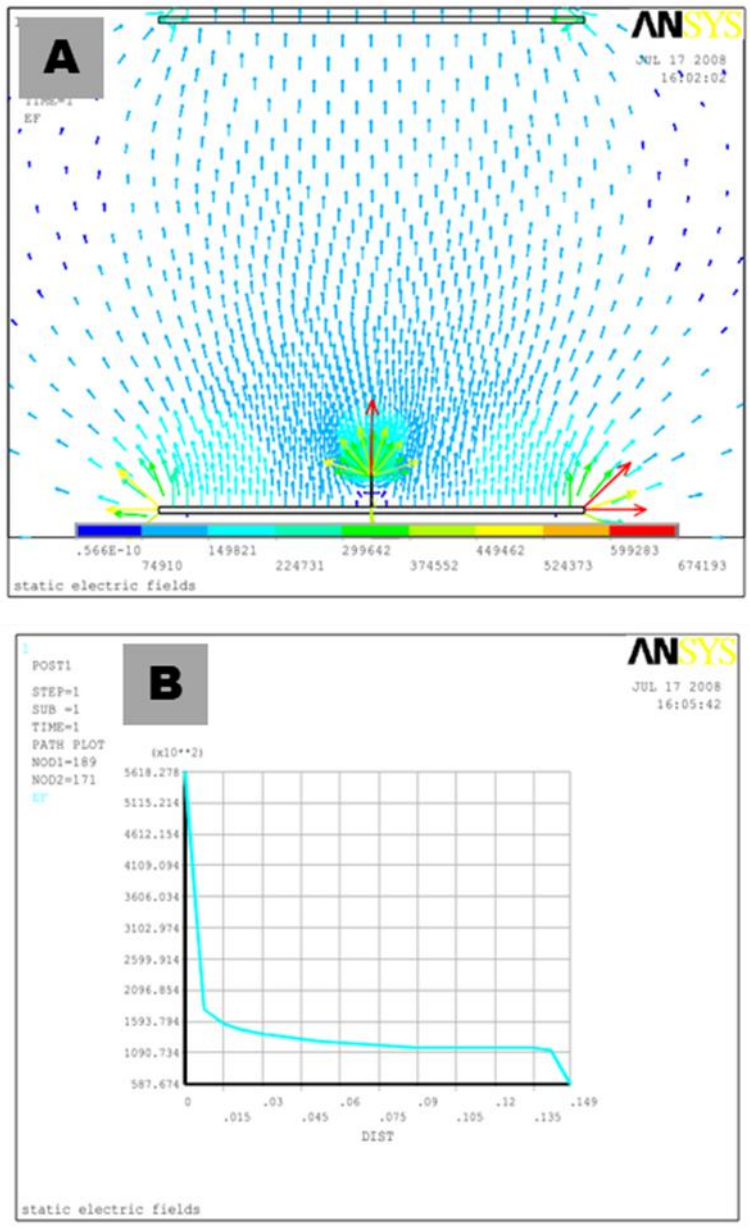

Figure 5.3 Electric field vector distribution of plate-plate type electrospinning (A), and electrical field measured from spinneret to collector (B) [159].

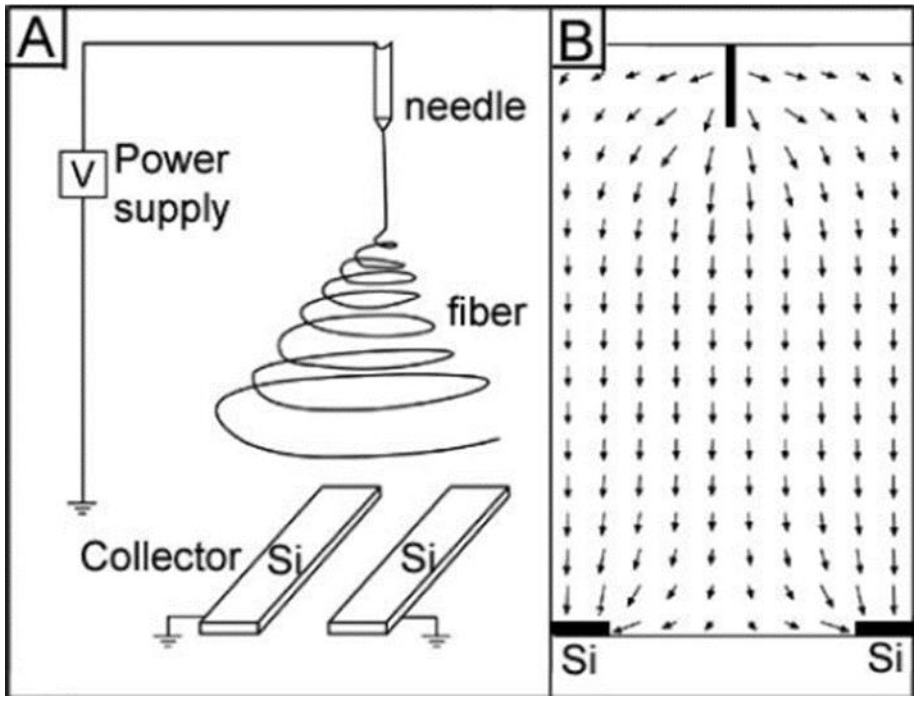

Figure 5.4 Schematic illustration of parallel plate electrospinning setup separated by air gap (A), and measured electrical field strength between the spinneret and the collector (B) [21].

5.3.1 Modeling and FE Analysis

The electric field of our advanced electrospinning system was analyzed using COMSOL Multiphysics® software. This method consist of a 3D geometrical model, meshing by 3D elements, material properties, boundary conditions, and other features that are used to represent the physical system.

Steady-state electrical field modeling with the COMSOL Multiphysics is carried out in either conductive or insulated media. The governing Maxwell's equations in the steady-state electric currents is:

$$\nabla.(-\sigma_2 \nabla V) = 0 \qquad (5.1)$$

Where, σ_2 is the material conductivity and V is the voltage potential

The equation 5.1 is solved for the voltage field, *V*, which is used to compute the electric field,

$$\mathrm{E} = -\nabla V \qquad (5.2)$$

And current,

$$\mathrm{J} = \sigma \mathrm{E} \qquad (5.3)$$

The Maxwell's equations for the electric fields in perfectly insulating media, can be re-written as:

$$\nabla.(-\epsilon \nabla V) = 0 \qquad (5.4)$$

Where, ε is the material permittivity.

A three-dimensional geometry of electrospinning including two parallel electrodes separated by an air gap of 15 mm was developed by using a modeling software NX 10 (shown in Fig. 5.5). The needle inner diameter was 0.26 mm and solid electrode diameter was 1.6 mm. The distance between the needle and collector was 60 mm. A box 100 mm (L) x 55 mm (W) x 55 mm (H) was drawn to model the surrounding environment.

Meshing is an important and fundamental step in FE analysis. The electrical field near the needle and electrodes are crucial in the electrospinning method. Therefore, we generated automatic mesh in the needle with extra fine tetrahedral elements, whereas, electrodes were meshed with fine tetrahedral elements and the rest of the geometry was constructed by normal tetrahedral elements shown in Fig. 5.6 (more details are presented in appendix). The materials of needle, electrodes, and surrounding were stainless steel, copper, and air, respectively. At the needle, a 10 KV positive voltage potential was applied and zero potential to electrodes.

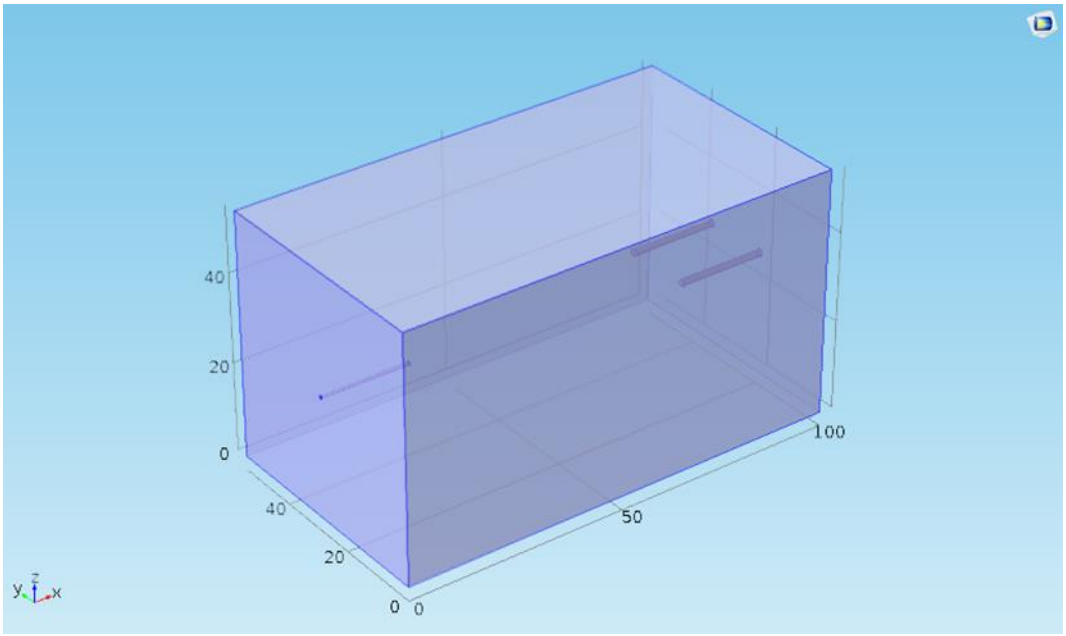

Figure 5.5 Three-dimensional model of our developed electrospinning system.

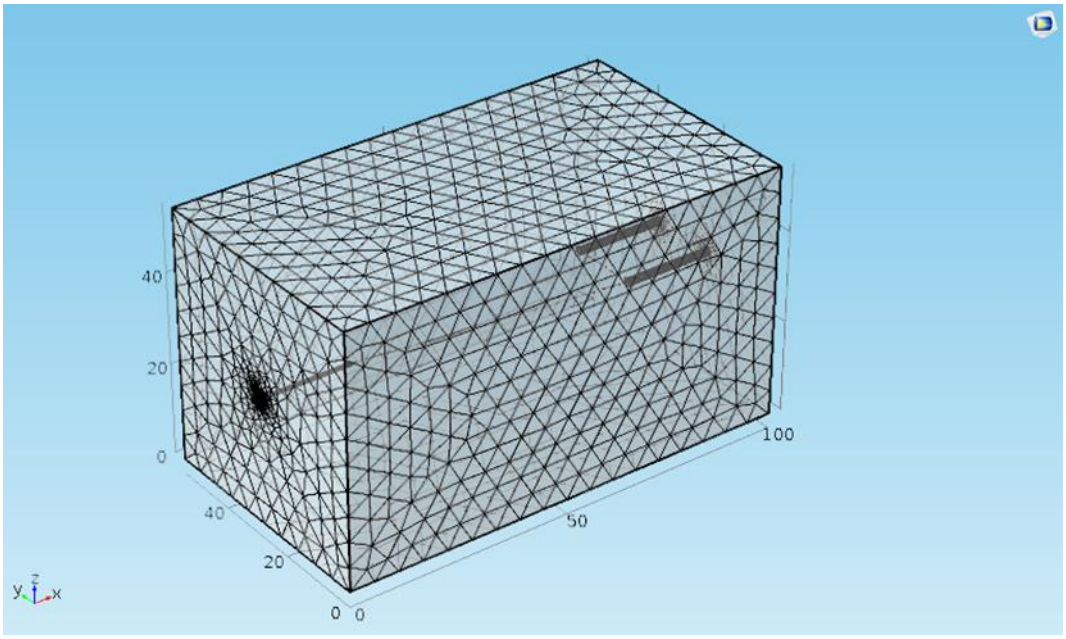

Figure 5.6 Three-dimensional tetrahedral mesh generated for FE analysis.

5.4 Results and Discussion

5.4.1 Nanofibrous Patterns Generation

We demonstrated that it is possible to obtain controlled fiber depositions in the desired patterns with our versatile method in which any number of collector electrodes can be used. One schematic of electrodes configurations is shown in Figure 5. 7a. Four electrodes were placed at the corners of a rectangle 1.5 cm high and 2.6 cm wide with an additional electrode at the center. Figure 5.7b shows the switching times of these electrodes. The voltage potential of electrodes were switched in a pattern which consisted of a 3 ms period in which two electrodes were active concurrently. This is called overlap time (OT). Then the 1st electrode was switched off while only the 2nd remained active for 50 ms called net time (NT) after which the 3rd electrode was activated. 3 ms later the 2nd electrode was deactivated and after another 50 ms, the 4th electrode was activated and the cycle progressed in a clockwise direction following the electrodes switching sequence of 1-2-3-4-5-1. Figure 5.7c shows an image of the pattern obtained after a 30 s deposition of electrospun fibers. It is clearly seen that a number of aligned fibers were deposited in-between 1st and 5th electrodes as these were concurrently activated during part of the cycle. In comparison, there were no fibers deposited in this zone (illustrated in Figure 5.7d) when the voltage potentials altered in a sequence of 1-2-3-4-5-3-1 and at no point the 1st and 5th electrodes were active concurrently. It is seen that charged electrospun fibers generally followed the switching pattern executed by the control program. The electrostatic forces acting on the electrospun fibers attract them toward the active electrodes and by switching them at a very fast pace, the charged fibers can be moved from one location to another, and as a result, electrospun fibers can be deposited on designated areas.

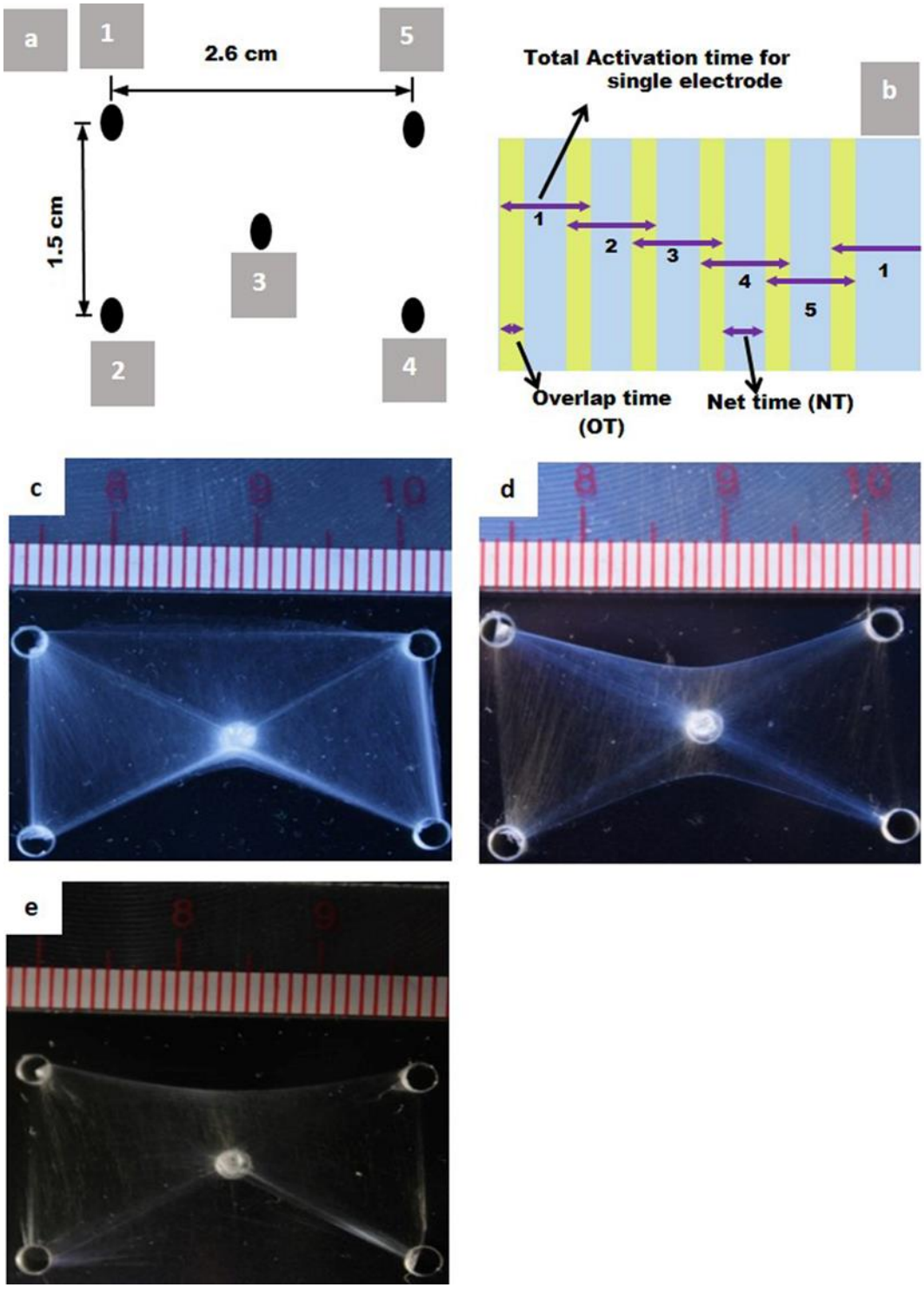

Figure 5.7 a) A schematic illustration of electrodes configurations and b) control timing for driving electrodes to generate designated pattern. Pictorial views of electrospun patterns for active electrode switching sequence of c) 1-2-3-4-5-1, d) 1-2-3-4-5-3-1, and e) when all electrodes are concurrently active.

To better understand the effect of switching activity of the electrodes, another electrospun pattern was obtained using a similar arrangement of electrodes but by activating all the electrodes concurrently for 30 s. and is displayed in Figure 5.7e. Unlike well-controlled depositions obtained earlier, in this case the electrospun fibers were deposited over the entire patterned structure. This is due to the fact that the electrostatic field generated by the high potential difference is distributed equally throughout the electrode arrangements. Therefore, the electrospun fibers spread out all over the areas rather than going to designated regions.

An extensive range of micro/nanofibrous patterned architectures can be produced with our method. Deploying three electrodes in triangular array and activating them in a sequence of 1-2-3-1, a triangular patterned architecture was generated which is displayed in Figure 5.8A. The electrospinning time was 60 s. Figure 5.8B displays a hexagonal array where electrodes were activated in a sequence of 1-2-3-4-5-6-1 and electrospun for 30 s. In a similar fashion, a quadrilateral shape patterned architecture was fabricated using four electrodes (shown in Figure 5.8C).

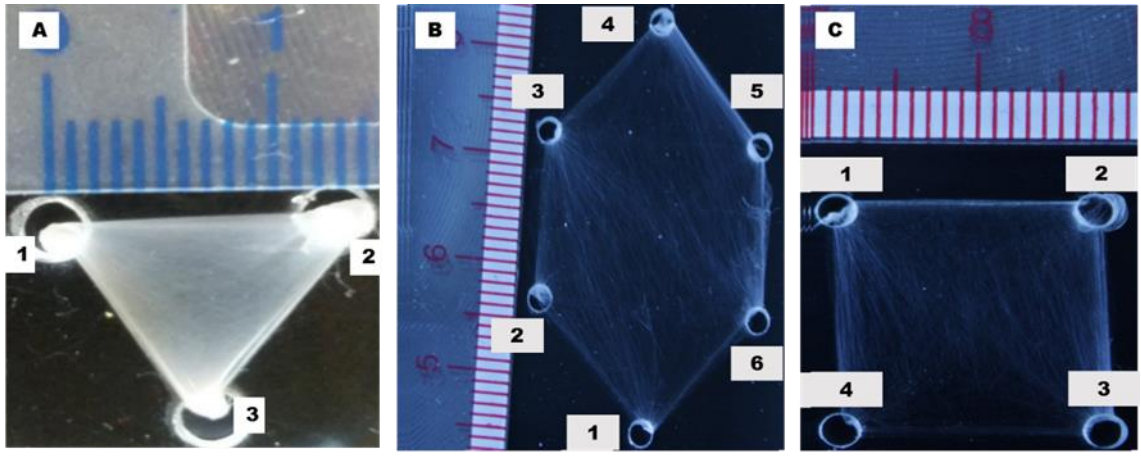

Figure 5.8 Pictorial views showing the electrospun patterned architectures; A) triangular shape, electrospun time was 60 s B) hexagonal shape and C) rectangular shape. In both B and C cases electrospun time was 30 s and the control time of electrodes was 3 ms OT and 50 ms NT.

5.4.2 Internal Structures of Patterns

In order to demonstrate the difference in fiber depositions between the switching electrodes system and the continuously grounded electrodes, we compared the fiber deposition patterns for three cases. Two, three, and four electrodes were used to produce straight, triangular, and rectangular shaped patterns as shown in Figures 5.9a-c, respectively, by switching electrodes with 3 ms OT and 50 ms NT. This was compared with the deposition patterns when electrodes in similar configuration were continuously grounded and shown in Figures 5.9d-f. The inset in each image shows the configuration of electrodes and the location where the image was taken. All the electrodes were 1.5 cm away from each other.

Although it is possible to generate patterned architectures with the fixed ground electrodes, it is obvious from the optical images that the alignment of fibers in the patterns improved significantly when the electrodes' activation was switched from one location to another. This resulted in the concentration of electric field between the active electrodes [30]. In addition, due to the altering potentials between adjacent electrodes in short duration, the charged fibers were forcibly driven from one location to another. As a result, the degree of alignment in that direction was increased. With the continuously grounded electrodes a constant electrical field was allotted equally among the electrodes, and therefore, the charged fibers moved toward the electrodes due to less concentrated and more distributed electrostatic fields and resulted in greater randomness in alignment of fiber deposition.

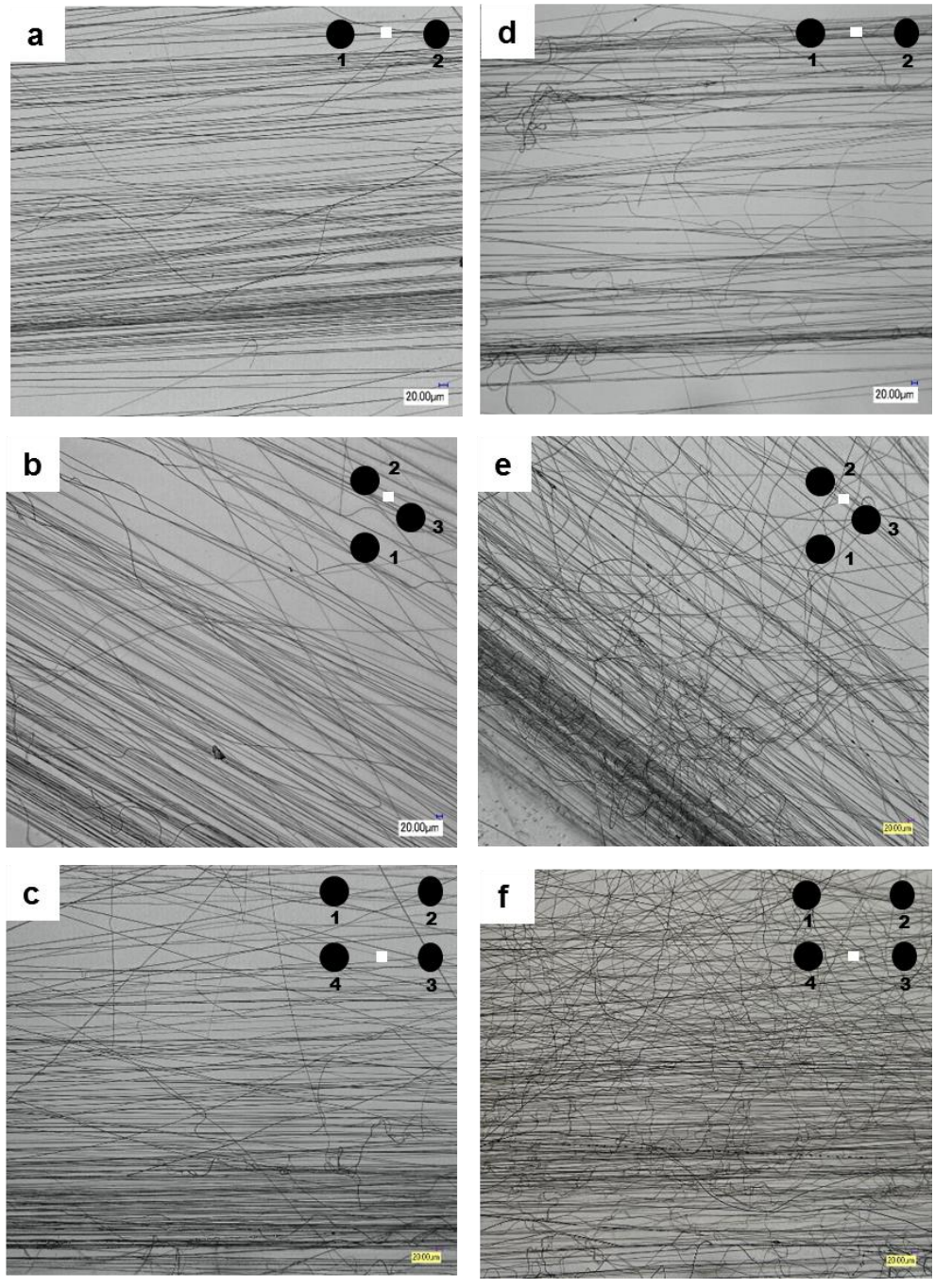

Figure 5.9 Optical images of the electrospun fibers collected with several electrode configurations. In images a, b and c, the electrodes were switched at OT for 3 ms and NT for 50 ms when using two, three, and four electrodes respectively. Images d, e and f show the same cases, but when the electrodes are kept concurrently active. In all arrangements, the electrodes were placed 1.5 cm apart from each other.

5.4.3 Controlling Nanofibrous Patterned Architecture

Although deposition of electrospun fibers into the pattern depends on the acceleration of the ejected stream, feed rate of solution through the needle tip, and the distance between the needle tip and electrodes, the amount of fibers could be controlled either by controlling the deposition time of electrospinning or by regulating the activation time of electrodes. In this study, three electrodes were placed in triangular shape for fiber deposition and optical images were obtained at the centers of each pair of electrodes. We kept acceleration, feed rate, and the distance constant, and studied the effects of varying the activation times of the electrode for four cases, namely, a) all electrodes active simultaneously; or regulating b) OT to 3 ms and NT to 100 ms; c) OT to 3 ms and NT to 50 ms; d) OT to 3 ms and NT to 7 ms. Effort was made to keep the deposition time for each electrospinning experiment as close to 4 s as possible. A camera was used at its high speed setting to compute accurate deposition times so that the results could be normalized to one second for each experiment. Figure 5. 10 displays the OM images of PVA electrospun fibers for control timing of OT 3 ms and NT 50 ms and deposition time of 3.667 s. During the NT, electrospun fibers mostly deposited on the conductive electrodes; or in a random manner; whereas in the OT, the fibers deposited in-between the active electrodes with high alignment. Optical images for all cases were binarized and characterized for deposition density with our custom made MATLAB image processing algorithm and results are shown in Figure 5.11. Total amount of fiber depositions were calculated by summation of all fibers that are seen in the three images taken similarly for each case. After that, they were normalized by their individual deposition times. It is observed that fiber depositions decrease with increase in net time. The deposition density of electrospun fibers was highest for the case ‘d’ when OT was 3 ms and NT was 7 ms as it had the highest OT and the highest number of switching cycles per second. The fiber deposition was reduced by nearly 45 percent when NT increased by 35 percent for the case ‘c’ compared to ‘d’. For the case ’b’, there was a 39 percent increase of NT, and depositions decreased to approximately 70 percent compared to ‘d’. Finally, for case ‘a’ when all the electrodes were active concurrently for the entire duration of experiment, the fiber deposition was reduced to around 77 percent compared to ’d’. The phenomena might be explained with the electrostatic field patterns and strengths. When an insulating air gap is

introduced between the collector electrodes, it modifies the pattern of external electrical field [21, 30]. It is reported that the electrical field strength is equally distributed among the present (active) electrodes and has higher magnitude toward them. Therefore, in this three electrodes case, the electrospun fibers were mostly deposited between the two active electrodes during OT part of the cycle but this deposition was very low during NT part of the cycle. Hence the deposition density decreased as NT increased, or equivalently, OT decreased. Therefore, by regulating NT and OT using the control system, the amount of fibers depositions on the pattern could be controlled. However, when all electrodes were concurrently active, the field strength along the desired region was significantly lower resulting in lower yield as observed.

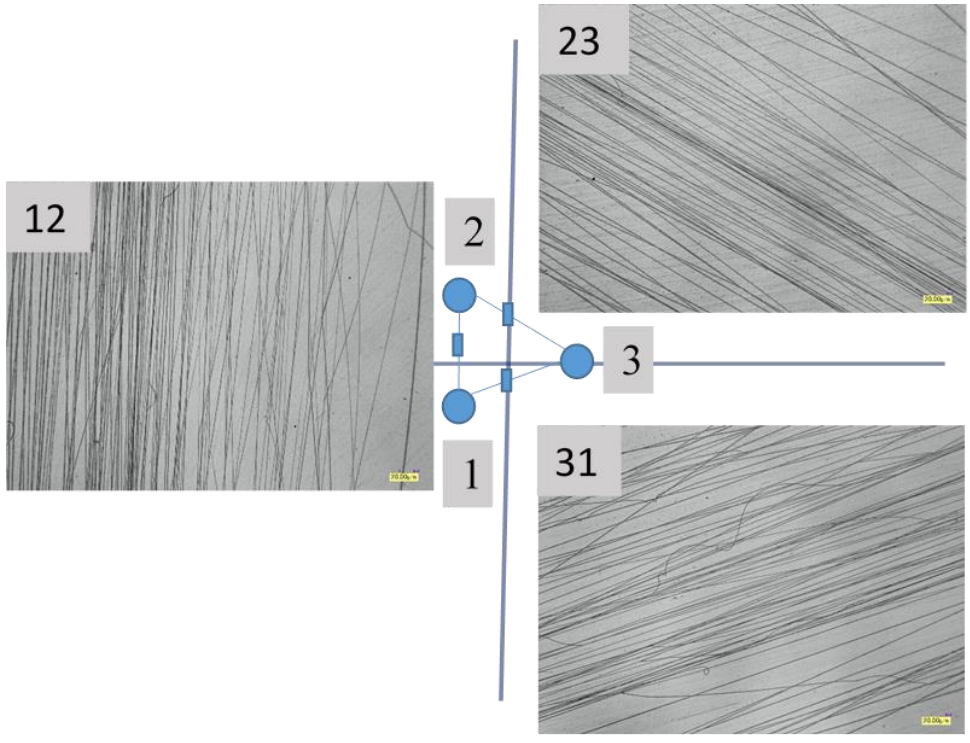

Figure 5.10 Optical micrograph images of PVA electrospun fibers collected at the mid-point between 12) 1 and 2 23) 2 and 3, and 31) 3 and 1, electrodes for 3.667 s deposition.

5.4.4 Alignment of Nanofibrous Electrospun Mat

To see the effects of changing NT for an OT of 3 ms on the alignment of electrospun fibers, we collected fibers using three electrodes placed in triangular shape as described in the preceding experiment. Four values of NT were investigated, namely 0, 7, 50 and 100. Note that NT = 0 implies that all the electrodes are continuously activated. Binary images of the electrospun fibers at the mid-point of two adjacent electrodes (between 2 and 3) for various NT values are shown in Figures 5.12A, C, E, and G. The corresponding results for orientation of fibers with respect to horizontal axis are depicted in Figures 5.12B, D, F, and H. Custom made MATLAB codes were employed for the analysis of the images. Reference lines at 100 pixel intervals were drawn along the horizontal axis of the images and the angles formed between the lines and fibers were measured. Angles ranged from -90^o to 90^o with 0^o being parallel to the reference line and individual angles were placed into data bins of 5^o each. The orientations of fibers in the image for each case were calculated at about 70 to 250 locations depending upon the fiber deposition density.

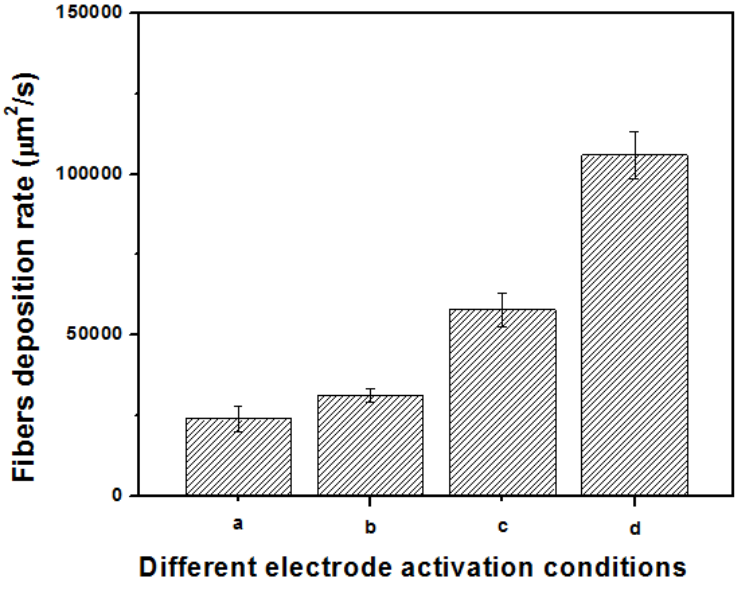

Figure 5.11 Normalized deposition density of electrospun fibers for four cases of electrode control a) all electrodes active, b) OT is 3 ms and NT is 100 ms, c) OT is 3 ms and NT is 50 ms, and d) OT is 3 ms and NT is 7 ms.

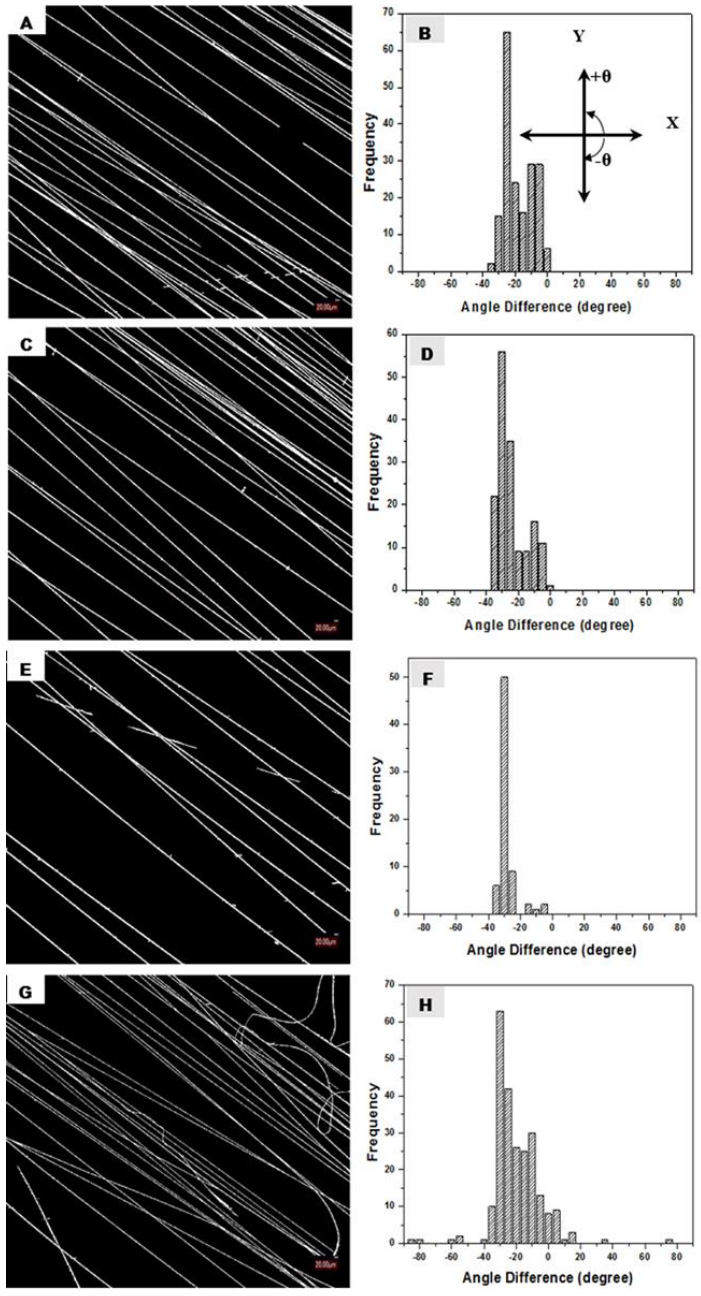

Figure 5.12 Binarized images of electrospun fibers that were collected at the center of two adjacent electrodes (between electrodes 2 and 3 of the triangular pattern) for various control timing: A) OT is 3 ms and NT is 7 ms, C) OT is 3 ms and NT is 50 ms, E) OT is 3 ms and NT is 100 ms, G) all electrodes active. The corresponding statistical analysis for the orientation of fibers with respect to horizontal axis are shown in Figures B, D, F, and H.

Close observation of the deposition pattern and alignment for the four switching cases discussed earlier, and shown in Figures 5.12, reveals highly oriented electrospun fibers for cases when the electrodes are switched i.e when NT is not zero. When all the electrodes were active (Fig. 5.12G, N=0), the randomness of deposited fibers increased. This can also be explained by the less concentrated electrostatic field strength as discussed above. The average diameter of electrospun fibers was around 2.2 μm for all cases.

5.4.5 Controlling the Density of Electrospun Mat

The deposition density of electrospun fibers plays a key role in tissue morphogenesis [160, 161]. Xie et al. [162] revealed neuritis growth could be altered in aligned nanofibers, in addition to some other parameters, by changing the deposition density of nanofibers. In the system that we have developed, the deposition density of the electrospun fibers can be easily controlled and it is possible to deposit different amount of fibers at different locations by changing the overlap time between two electrodes spanning the desired region and by the number of cycles of deposition that a region is subjected to. Figure 5.13 displays optical images showing the differences in deposition density of electrospun fibers at various sections of the triangular pattern. The OT between electrodes 1 and 2 (Fig. 5.13), 2 and 3 (Fig. 5.13B), and 3 and 1 (Fig 5.13C) were 2 ms, 3 ms, and 4 ms, respectively. It is clear from the images that by controlling the deposition time between adjacent electrodes, the density of electrospun fibers can be regulated in desired regions.

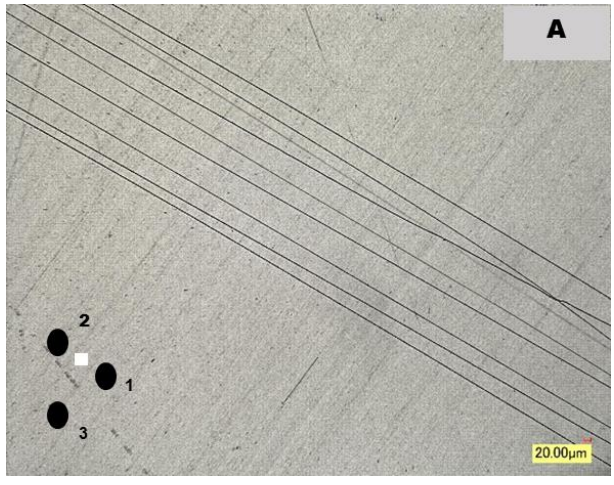

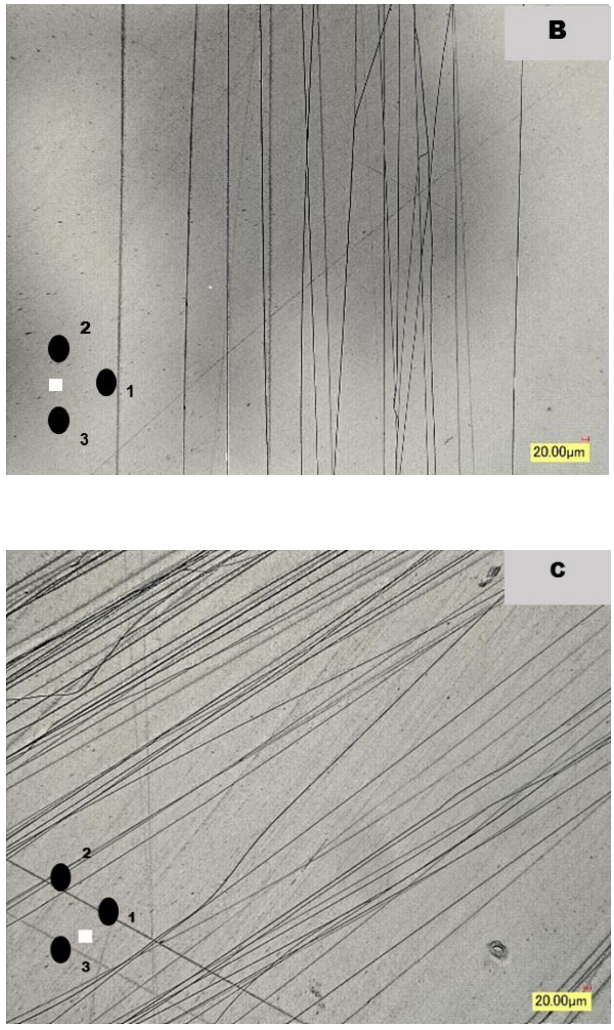

Figure 5.13 Optical images of nanofibers showing differences in deposition density at various sections of triangular shape pattern for various OT A) 2 ms, in-between electrodes 1 and 2, B) 3 ms, in-between electrodes 2 and 3, C) 4 ms, in-between electrodes 3 and 1. The deposition time was around 3 s and NT was 50 ms.

5.4.6 Functionally Graded Deposition

By employing the number of electrodes and by controlling their switching pattern, we elucidated that a great variety of functionally graded architectures can be produced with this versatile technique. One schematic of electrodes configurations is shown in Figure 5.14A where three pairs of electrodes 2 cm apart were placed in a column. The vertical separation between each pair of electrodes was 0.5 cm. The voltage potential of electrodes

were switched with 3 ms OT and 7 ms NT. The cycling ratios between active electrodes 1 & 2, 3 & 4, and 5 & 6 were 10, 5, and 2, respectively. The total electrospinning time was 6.73 s. Optical micrograph images were obtained at the centers of each pair of electrodes as shown in Figure 5.14B-D. It is clear from the images that by controlling the deposition time between adjacent electrodes, a gradient of electrospun fibers can be acquired into the architecture. The average fiber diameter was 1.8 μm.

Figure 5.14E shows functionally graded nanofibers for various electrospun times but for the same cycle ratio of electrodes activation and switching time as described in previous section. Optical micrograph images were obtained at three locations between each pair of electrodes and characterized the deposition density with a MATLAB image processing algorithm developed in house. Data from these images is shown in Figure 5.14E with standard error bar. Images were taken in similar manner for each case. To compute the total deposition time for each electrospinning experiment a camera was used at its high speed setting. It is observed that the ratios of fiber depositions between electrodes 1 & 2, 3 & 4, and 5 & 61 were 4.1:2.2:1 for a spinning time of 6.73 s; 4.5:2.7:1 for spinning time of 5.20 s and 3.5:2.1:1 for spinning time of 4.33 s. Varying the number of cycles in-between the adjacent active electrodes, the duration of electrostatic field strengths are mostly prolonged or condensed on that particular locations. Therefore, the charged electrospun fibers generally follow the switching pattern, resulting in various deposition densities as well as porosity of electrospun fibers in the desired regions.

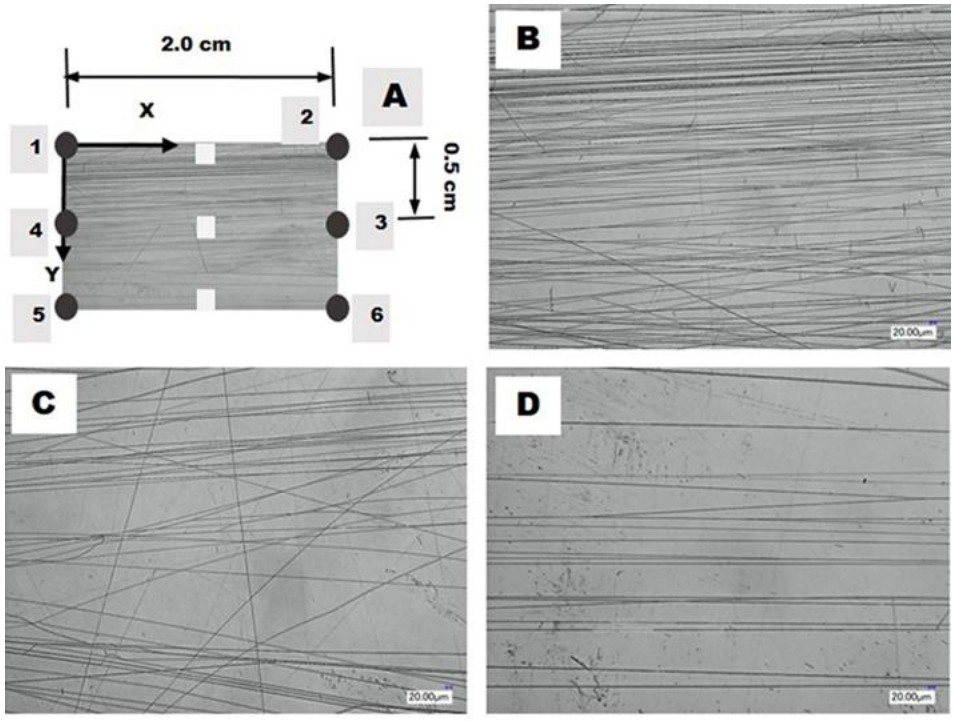
2.0 cm
X
A
1
2
0.5 cm
4
3
Y
5
6
B
C
D

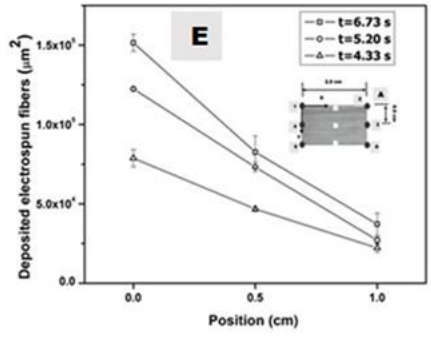
E
t=6.73 s
t=5.20 s
t=4.33 s
Deposited electrospun fibers (μm²)
1.5x10⁵
1.0x10⁵
5.0x10⁴
0.0
0.0
0.5
1.0
Position (cm)

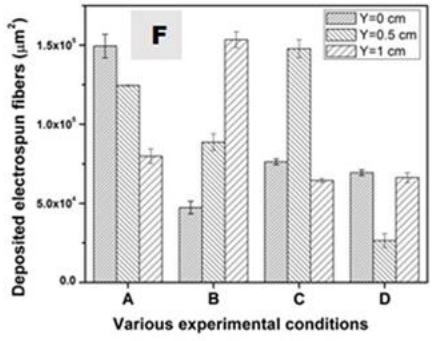
F
Y=0 cm
Y=0.5 cm
Y=1 cm
Deposited electrospun fibers (μm²)
1.5x10⁵
1.0x10⁵
5.0x10⁴
0.0
A
B
C
D
Various experimental conditions

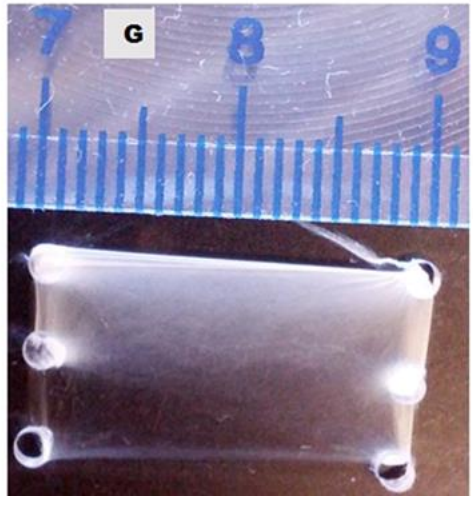
G
7
8
9

Figure 5.14 Optical images showing the packing density of electrospun nanofibers at different locations due to changing activation times of electrode pairs. The activation times are in a ratio of 10:5:2 between electrode pairs 1&2; 3&4, 5&6 and the deposition image in between them are shown in figures B, C, and D, respectively. (E) Functionally graded deposition of nanofibers for different electrospun timing t = 6.73 s, t = 5.2 s, and t = 4.33 s. (F) Effects of changing the activation cycling ratios on deposition densities. The activation times are in a ratio of A) 4:3:2, B) 2:4:8, C) 2:5:2, and D) 5:2:5 between electrode pairs 1&2, 3&4, and 5&6. (G) Pictorial view of functionally graded deposition for 1 minute electrospun.

Figure 5.14F shows four cases of functionally graded nanofibers which were accumulated by controlling the number of cycles between electrode pairs at different locations. In all cases, the electrode activation and switching time were 3 ms OT and 7 ms NT and total electrospinning time was between 4 s to 6 s. The activation cycles among the three pairs of electrodes were controlled to provide deposition time ratios of A) 4:3:2, B) 2:4:8, C) 2:5:2, and D) 5:2:5; between electrodes 1^{st} and 2^{nd}, 3^{rd} and 4^{th}, and 5^{th} and 6^{th}, respectively. The results of deposited fibers are summarized in Table 1. It is seen that the fibers deposition varies at designated locations based on the control of activated electrodes cycle's ratios. In case A, maximum deposition of electrospun fibers was observed at Y=0 cm and minimum at Y=1 cm, whereas for case B, the maximum and minimum deposition of fibers were at Y=1 cm and Y=0 cm, respectively as desired. Similarly, at Y=0.5 cm location, the density of fibers was maximum in case C and it was reversed for case D following the programmed activation cycle ratios of electrodes. Therefore, it is possible to acquire various packing density as well as porosity of fibers into the electrospun mats as desired with this technique.

Figure 5.14G shows an image of functionally graded scaffolds obtained after one minute deposition of electrospun fibers. The operating conditions of electrospinning were exactly same as that were used to produce Figure 5.14A except electrospinning time. It is clear from this image that with longer deposition time of electrospinning it is possible to obtain more dense functionally graded scaffolds. However, for characterization purpose using automated image analysis algorithms we collected fibers for shorter period of time.

5.4.7 Various Patterns of Deposited Electrospun Fibers

We demonstrated that it is possible to accrue electrospun fibers as a random, uniaxial aligned or multi-directional mats into the patterned architectures with our versatile method. When a single conductive electrode was used, the system behaves like a typical electrospinning setup and electrospun fibers were collected as random or nonwoven form (shown in Figure 5.15A). The polymer jet travels toward planar counter electrodes in a complicated three-dimensional ‘‘whipping’’ action caused by bending instability which is composed in literature [39, 163]. For depositing uniaxial aligned fibers displayed in Figure

5.15B, the single electrode is replaced by a pair of electrodes separated by an air gap. Then, the voltage potential of electrodes were switched with 3 ms OT and 50 ms NT. The electrostatic forces acting on the electrospun fibers attract the fibers toward the active electrode and by switching them at a very fast pace, the charged fibers can be moved from one location to another. As a result, highly ordered electrospun fibers can be deposited in designated areas. Applying similar approach and using multiple electrodes, the aligned fibers can be stacked into various directional multilayered mats. Figure 5.15C-E show bi-directional, tri-directional, and tetra-directional meshes of electrospun fibers when four, six, and eight electrodes were employed, respectively. The Figures also show the configuration of electrodes and the locations where the images were taken. For producing bi-directional mats, the high voltage potential was exchanged between two active electrodes with 3 ms OT and 50 ms NT. The cycle of active electrodes progressed in a clockwise direction following the switching sequence of 1-2-3-4-1. Hence, electrospun fibers were deposited at the center of designed outline in a bi-directional pattern following the direction of switching array executed by the control program. Similarly, tri-directional and tetra-directional aligned mats can also be fabricated by arranging the electrodes configuration and controlling the switching sequence of voltage potential of the collection electrodes.

5.4.8 Numerical Simulation Results

In order to simulate the electrical field distribution of our advanced electrospinning system, we broke down the electrodes switching system into two parts to simplify the FE analysis. From Figure 5.7b, it is clear that there are two steps of control timing for driving the electrodes. One is when both electrodes are active called overlap time (OT) and another is only individual electrode is active known as net time (NT). Therefore, we conducted two FE analyses separately for these two different steps of switching system.

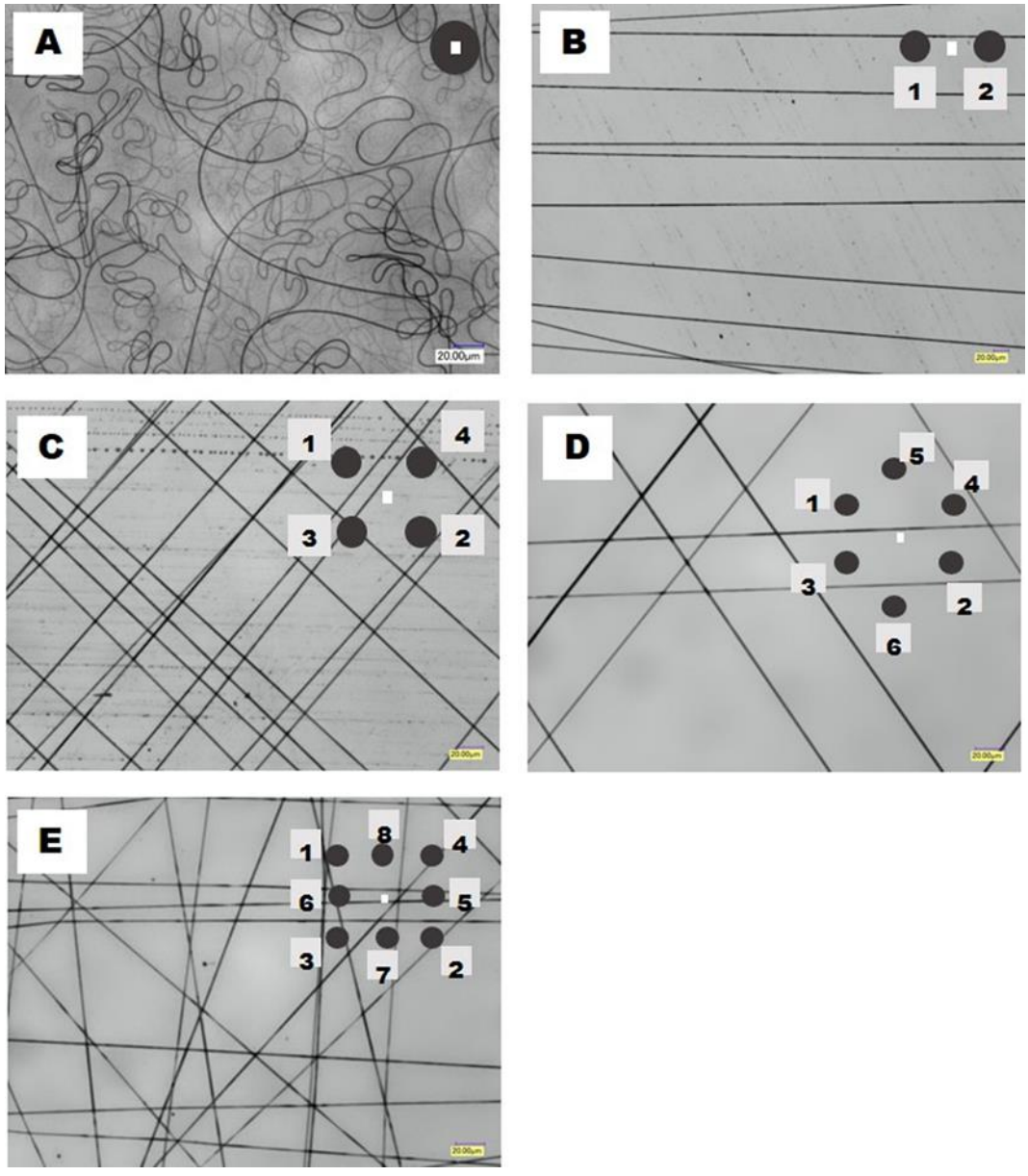

Figure 5.15 Optical images demonstration control of electrospun fiber depositions and alignments A) random, B) uniaxial aligned, C) bi-directional, D) tri-directional, and E) tetra-directional mats using different electrode configurations. The inset in each image shows the configuration of electrodes and the location where the image was taken.

Figure 5.16 shows the electrical fields developed at various locations of electrospinning setup when both electrodes were active during OT. A two-dimensional electrical field strength developed on the front face of electrodes is plotted in Figure 5.16A. It is seen that the electrical field strengths are equally distributed between the electrodes. Three-dimensional electrical field strengths at various positions and field strength stream lines are presented in Figure 5.16B & C. Figure 5.16D displays the electrical field strength alone the path drawn from needle tip to one of the electrodes. The electrical field is much stronger near the needle followed by sharp dropped to almost zero after a short distance. The field strength again increases near the electrodes. Figure 5.16E shows the electrical field strength between two parallel electrodes which were placed 15 cm apart. The higher electrical field strengths towards the electrodes might be beneficial for stretching and orientation of fiber.

During NT of control timing for driving electrodes, only one electrode is active. Therefore, in this simulation we placed zero voltage potential to one electrode keeping other electrode inactive. In this case, electrical field strength moved to the active electrode (shown in Fig. 5.17A). During the NT time, the developed electrical field strength is much higher (Fig. 5.17A) than that of developed on the OT time (Fig. 5.16A). Therefore, it can be hypothesized that fiber may deposit on one electrode face during this NT time. Three-dimensional electrical field strengths at various positions (Fig. 5.17B) and field strength stream lines (Fig. 5.17C) for NT are also comparable with that obtained during OT time. Figure 5.17D & E present the electrical field strength along the path drawn from the needle tip to the active electrode and between two parallel electrodes, respectively. These results also emphasized the previous finding.

Hence, it can be predicted from these FE analyses that electrospun fiber may deposit on one active electrode during NT whereas, during OT, fibers will tend to deposit in-between the electrodes. Therefore, by controlling the electrodes at a very fast pace, fibers could be moved from one location to another. As a result, electrospun fibers can be deposited in designated areas with uniaxial alignment.

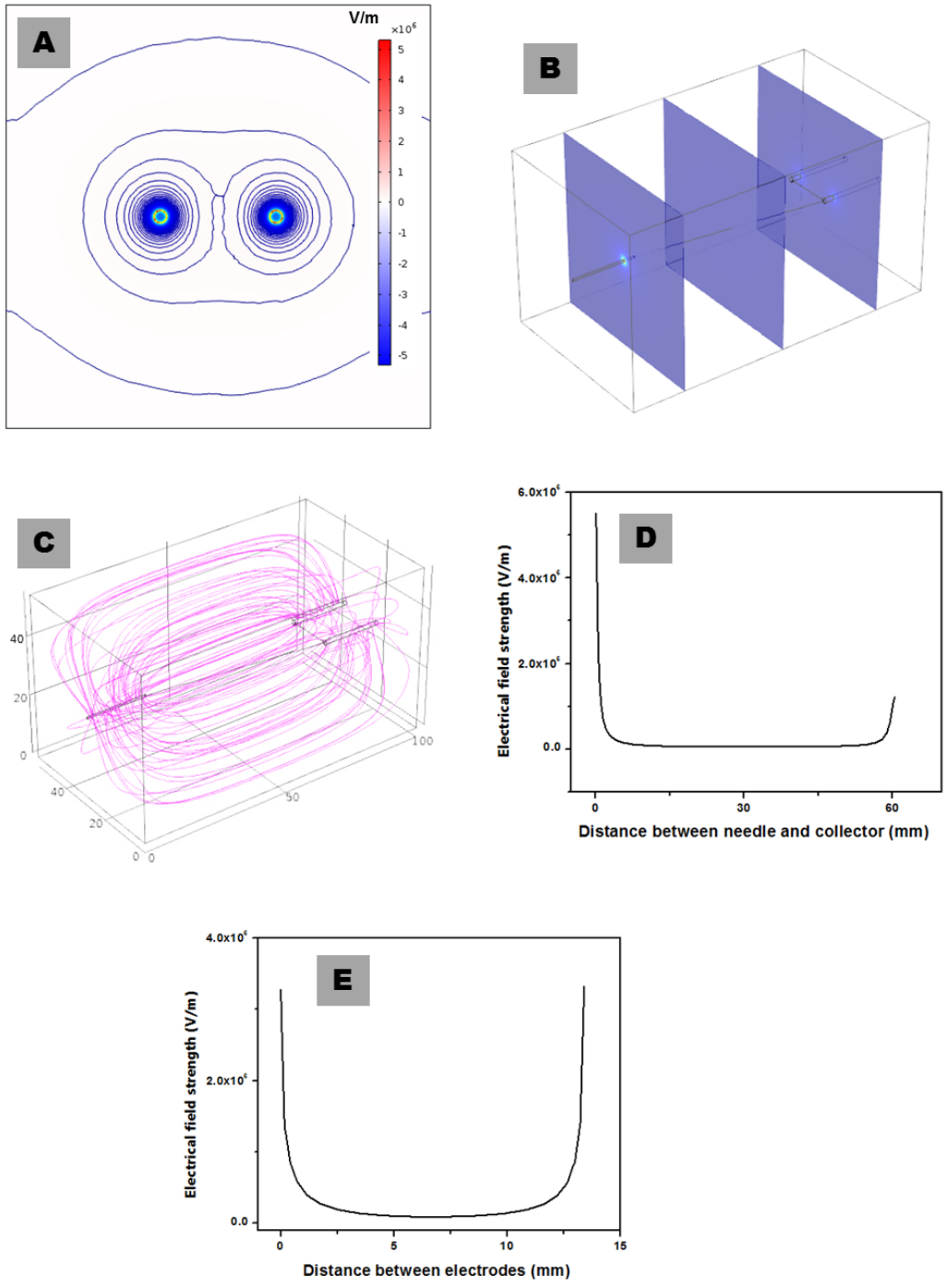

Figure 5.16 (A) 2D plot of electrical field strength on the electrodes face. Electrical field strength showing at three locations (B), electrical field stream lines (C), between needle tip and electrode (D), and between two electrodes.

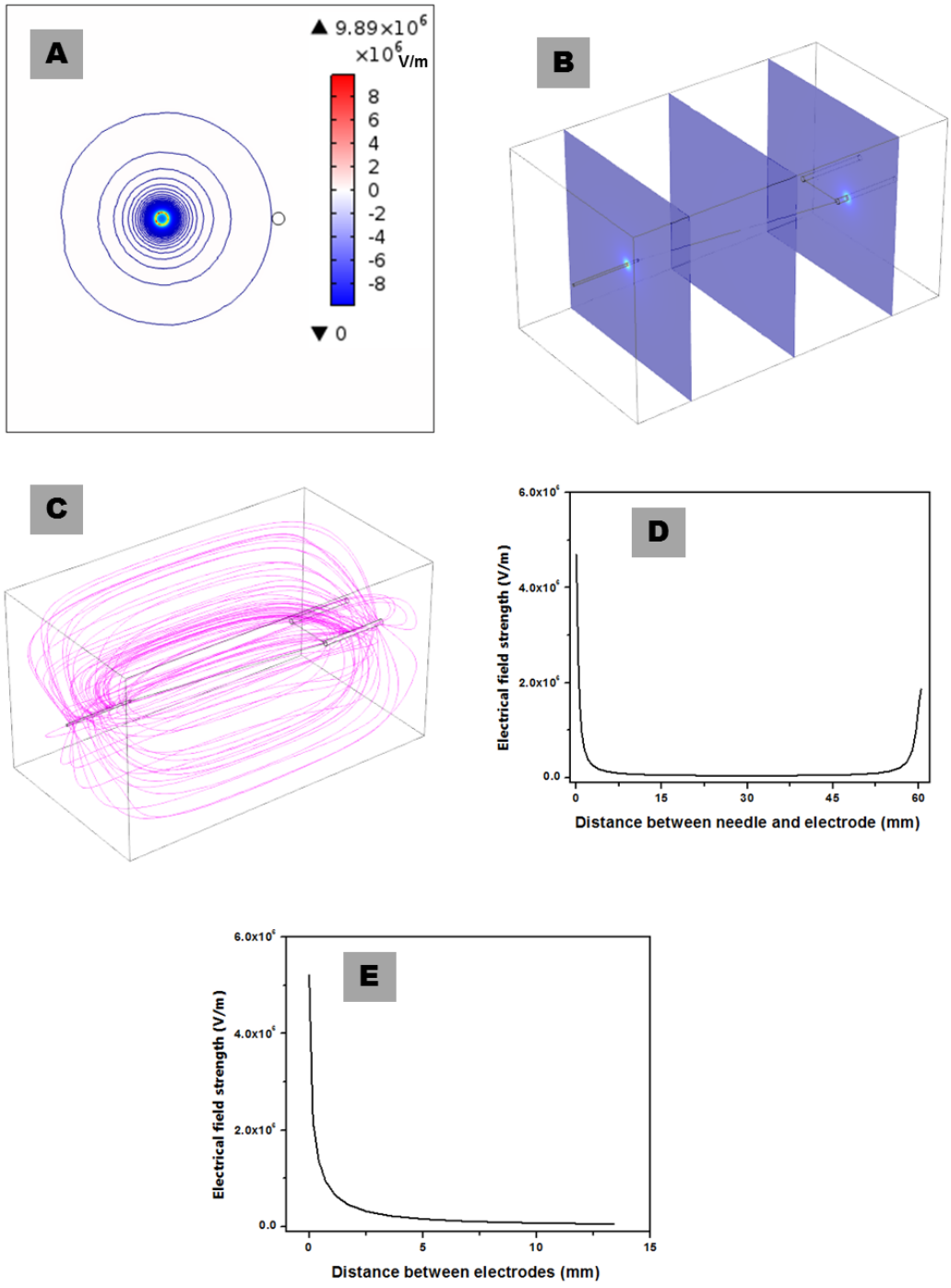

Figure 5.17 (A) 2D plot of electrical field strength on the electrodes face for one electrode active. Electrical field strength showing at three locations (B), electrical field stream lines (C), between needle tip and electrode (D), and between two electrodes.

5.4.9 Effect of Varying Electrode Gap

Several groups have reported that the alignment of the nanofibers improves with the increasing gap size between two grounded parallel plates being used for depositing aligned fibers in electrospinning method [20, 164]. In this study, the effect of varying the gap between two adjacent collector electrodes on the fiber diameter and the alignment of electrospun fiber were investigated. The distance between the electrodes was varied from 1.0 cm to 3.0 cm keeping the needle and the electrode separation constant at 6 cm. The electrode activation and switching time were 3 ms OT and 50 ms NT and total time of electrospinning was around 3 s. The optical micrograph images are shown in Fig. 5.18. It is seen that all the electrospun fibers were aligned with respect to horizontal axis except a slight distortion observed when electrodes were placed at 1 cm apart from each other which is similar to other researcher's finding [164]. At 1 cm electrodes gap, some distortions might occur due to the low electrical field generated, under which the electrostatic repulsive forces were not strong enough to make them completely aligned. The alignment of electrospun PVA fibers are summarized on Table 5.1. The minimum standard deviation was observed at 1.5 cm gap followed by 2.0, 3.0, 2.5, and 1.0 cm electrodes gap. The effects of gap between two adjacent electrodes on the diameter of electrospun PVA fibers are displayed in Fig. 5.19. The diameter of the electrospun fibers initially decreased with increasing gap, reached a minimum at a gap of 2 cm and then increased slightly again. This phenomena can be explained by changes in the electrical field strength acting on the electrodes.

To understand the effect of gap distance between electrodes on electrospun fiber morphology, we conducted electrostatics FE analysis. The input parameters such as materials properties and boundary conditions were similar to experimental works. Figure 5.20 demonstrates the calculated electrical field strength for various gaps between two adjacent electrodes. It is seen that the field strengths were comparatively low up to 1.5 cm electrodes gap followed by the maximum field strength for 2.0 cm electrodes gap. The field strengths for 2.5 and 3.0 cm electrodes gap were slightly lower than 2.0 cm but higher than 1.0 and 1.5 cm. These results correlate well with experimental findings. We found the thinnest fiber diameter for 2.0 cm separation of electrodes where electrical field strength

was maximum. For 1.0 and 1.5 cm electrodes gap distance, the electrical field showed lowest and almost similar magnitude. These behaviors also observed in the experiments for producing thicker electrospun fiber diameters. Similarly, for 2.5 cm and 3.0 cm separation of electrodes, the electrical field strengths were in the moderate ranges, therefore, electrospun fibers were also in the middle range. Higher electrical field favors production of thinner fiber and vice versa when solution and processing parameters of electrospinning kept constant.

The voltage potential is one of the crucial parameters in electrospinning which governs the electrical field strength along with the distance between needle and collector. Lui and Dzenis [164] showed that the electrical field strength increases with increases of gap size between two parallel plates. Because of lower electrical field strength at smaller gap, the electrostatic forces acting on the fiber jet are not strong enough to stretch out the fiber fully which reduces the stretching effect and yields a thicker fiber diameter [93, 165]. In contrast, increasing the gap between the electrodes increases the electrical field strength and induces higher electrostatic forces on the fiber jet which favors the formation of thinner fibers. Further increase in the strength of electrical field increases the material flow leading to thicker fibers [88].

Hence, electrical field strength has a very strong correlation with fiber morphology in electrospinning if all other parameters remain constant.

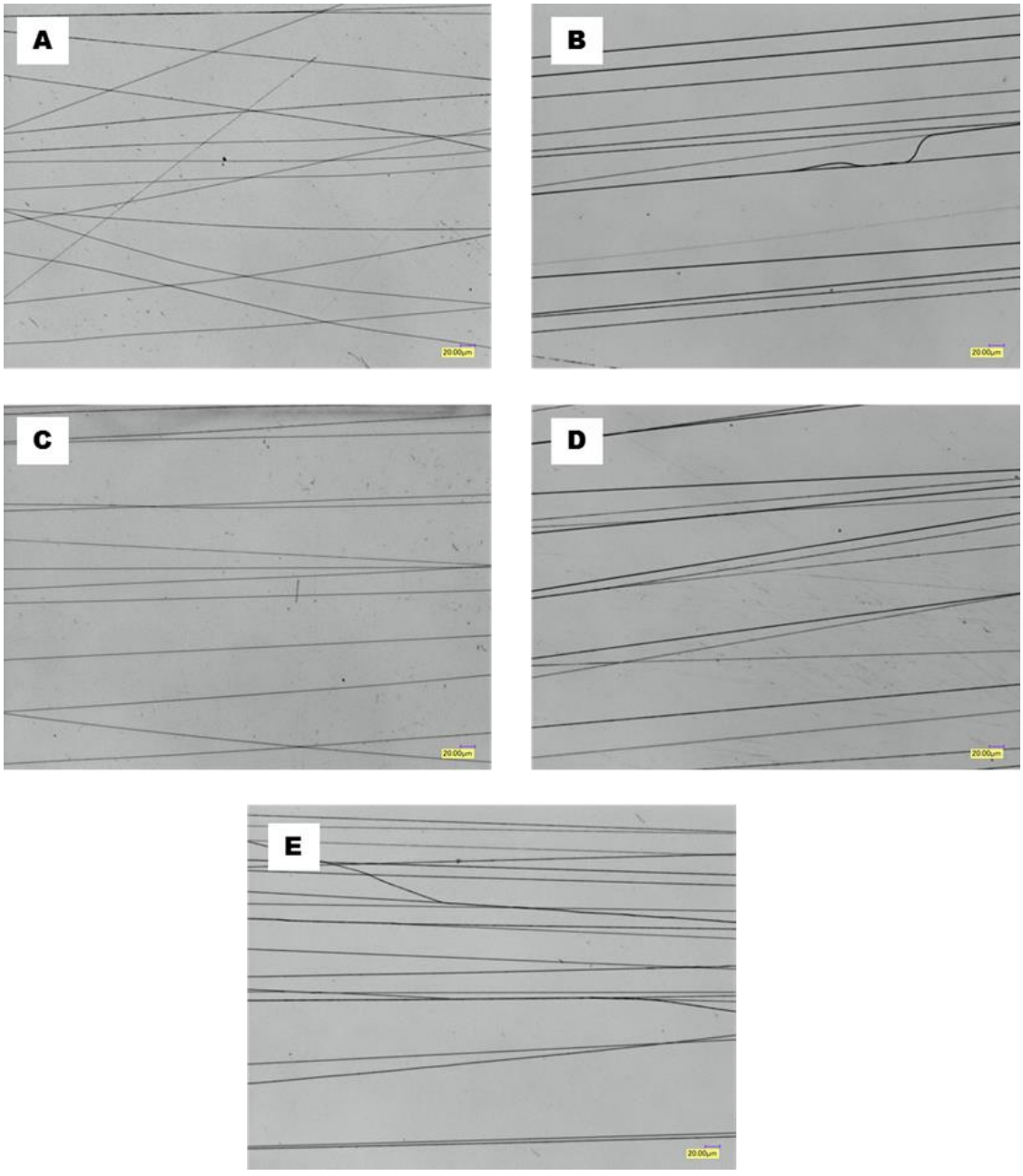

Figure 5.18 Optical micrograph images of electrospun PVA fibers for gap between two adjacent electrodes (A) 1 cm, (B) 1.5 cm, (C) 2.0 cm, (D) 2.5 cm, and (E) 3.0 cm.

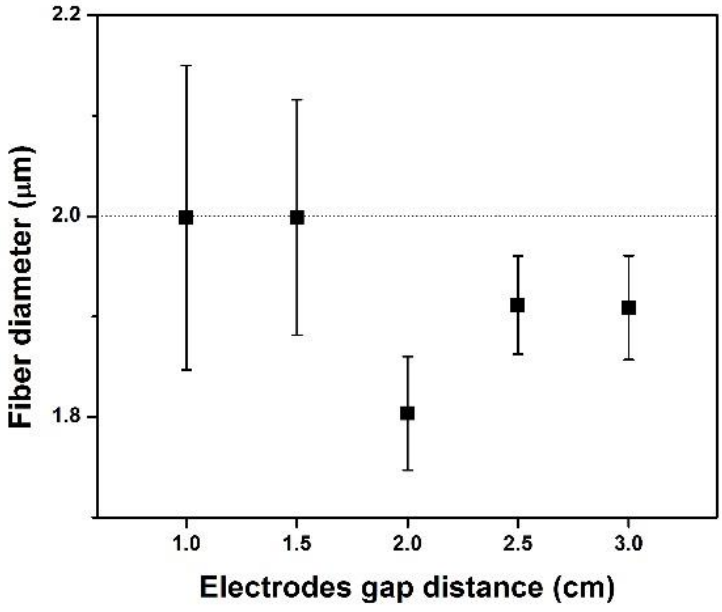

Figure 5.19 Effects of gap between two adjacent electrodes on the diameter of electrospun PVA fibers.

Table 5. 1 Effects of angle due to variation of gap between two adjacent electrodes of electrospun PVA fibers.

Electrodes gap	**Mean angle with respect to horizontal axis**
1.0 cm	-1.29 ± 5.93
1.5 cm	0.82 ± 2.36
2.0 cm	0.93 ± 2.85
2.5 cm	1.85 ± 4.81
3.0 cm	0.52 ± 3.90

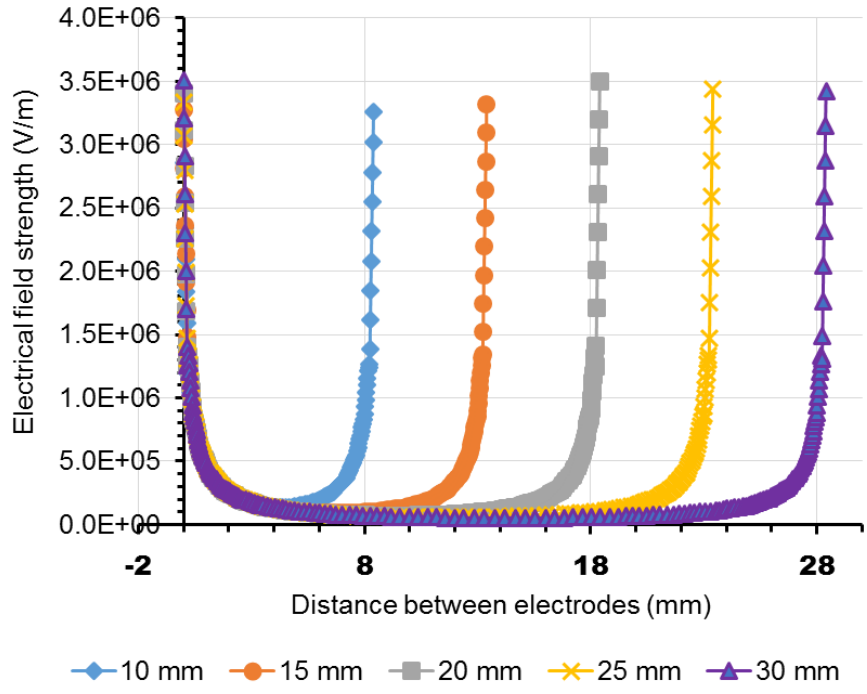

Figure 5. 20 The electrical field strength for various gaps between two adjacent electrodes calculated by FE analysis.

5.4.10 Effect of Electrode Size

The effect of electrodes size was investigated in this study. Three different circular electrodes 0.8 mm, 1.6 mm, and 2.6 mm of diameter were chosen. Two adjacent electrodes were placed horizontally 1.5 cm apart. A 10 KV high voltage was applied at the needle tip of the syringe where 12 wt % PVA solution was extruded at a rate of 200 µL/h. The electrode activation and switching times were 3 ms OT and 50 ms NT and total time of electrospinning was around 3 s. The gap between needle tip and collector electrodes was 8 cm. The optical micrograph images are shown in Figure 5.21A - C. The corresponding fiber diameter distributions are presented in Figure 5.21D-F. The average fiber diameter is found to be 1.8 µm with 0.8 mm diameter of electrodes. The fiber diameter reduced to 1.3 µm when 1.6 mm electrodes were used. Fiber diameter again increased to 1.6 µm with the increase of electrodes diameter to 2.6 mm. The orientation of electrospun fibers is shown in Figure 5.21G – I. It is seen that the alignment of fibers improved with increased

electrode diameter. This phenomena can be explained with the electrical field distribution as shown in Figure 5.22.

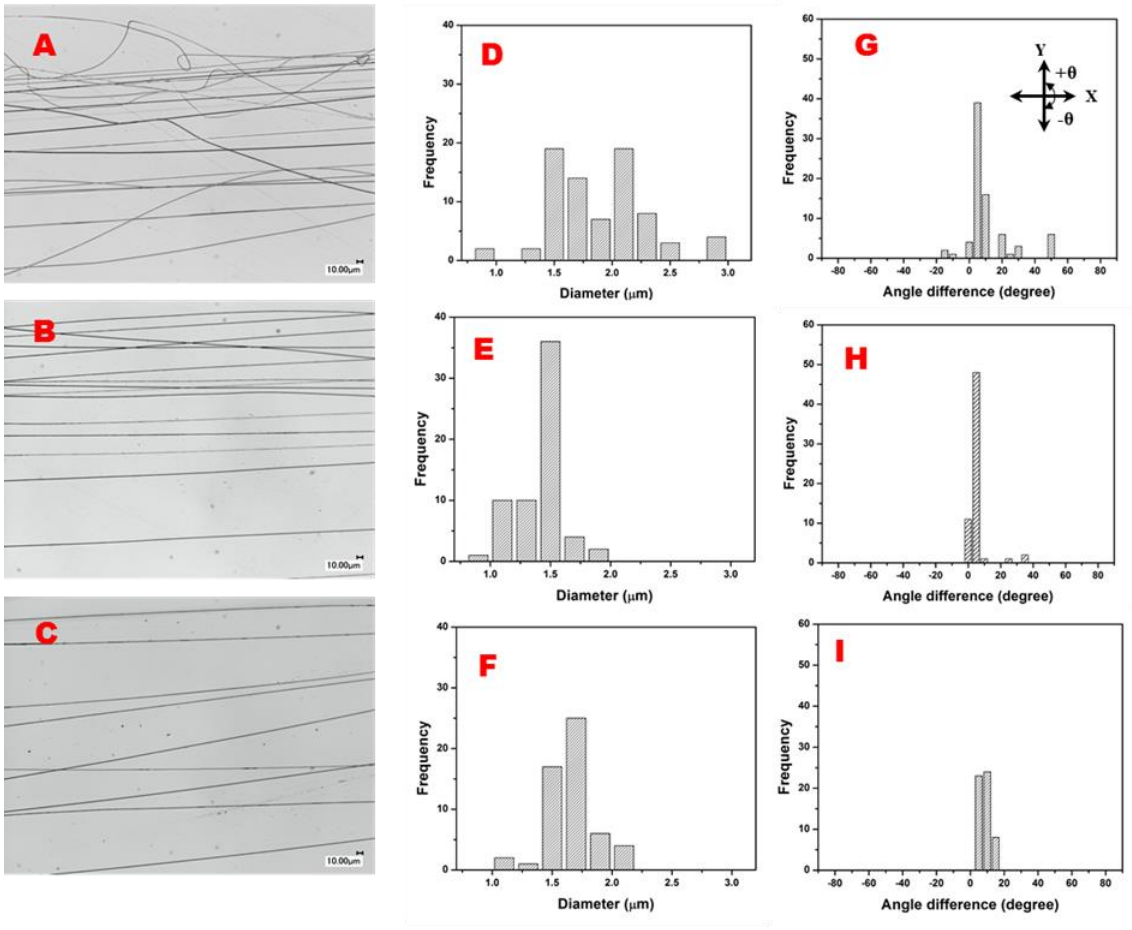

Figure 5.21 Optical micrograph images of electrospun PVA fibers collected on different electrodes diameter (A) 0.8 mm, (B) 1.6 mm, and (C) 2.6 mm. The corresponding fiber diameter distribution (D – F), and fiber orientation (G – I), respectively.

The FE results show that electrical field strength is very high for 0.8 mm diameter of electrodes. Therefore, it can be concluded that the jet from Taylor cone move fast and at the same time it drew more materials when 0.8 mm diameter electrode was used. Hence, the electrospun fiber diameters and the alignment obtained by 0.8 mm diameter of electrodes were not satisfactory. The electrical field strength dropped as the surface area of electrode face increased. For that reason, the electrospun fiber morphology and orientation improved when 1.6 mm and 2.6 mm diameter electrodes were used. However,

insufficient electrical field may causes thicker fiber diameter as they cannot stretch out fully by the deficiency of electrostatic force which is reflected in our experimental results.

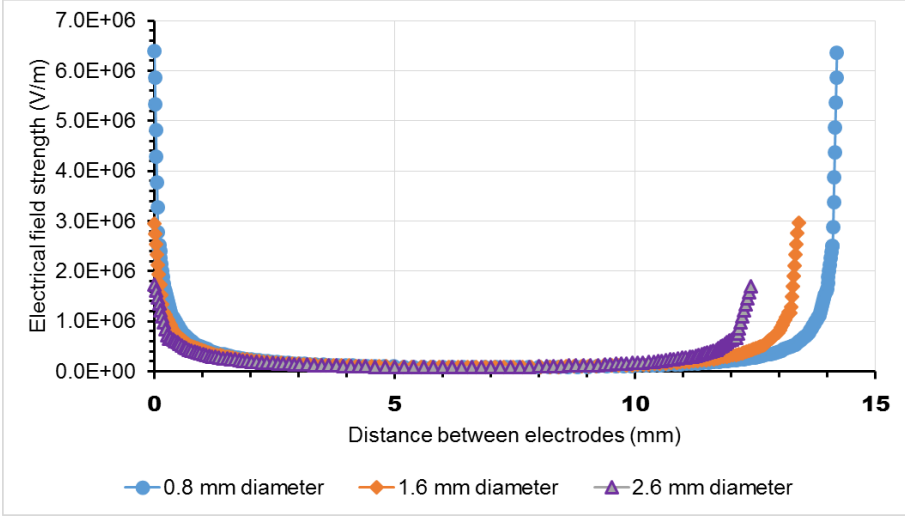

Figure 5. 22 The electrical field strength between two adjacent electrodes for different electrode sizes.

Chapter 6 Nanocomposites

6.1 Introduction

One dimensional nanofibrous structures are found to be of great potential because of their inherent properties such as high surface-to-volume ratio, tunable porosity, and desired functional properties [25, 26, 160, 166]. The functionality and applicability of these structures can be further enhanced by incorporating a secondary phase. Advanced reinforced composites with fillers and with the reduction of their size, from microscale to nanoscale, can exhibit enhanced structural properties including high strength to weight ratios and high modulus. Electrospinning [149, 167], in situ polymerization [168], Solvent casting [169], and melt mixing [170], are important methods for the fabrication of nanocomposites. Electrospinning has been adopted as a simple, versatile, and economical technique that is capable of fabricating ultrafine fibers from a rich variety of materials. With the aid of electrospinning nanocomposite can be developed when nanoadditives such as nanoclays, carbon nanotubes, titanium dioxide, etc, are added to the polymer solution. Polymeric nanocomposites are of significant interest because of their outstanding end use applications. Zhou et al.[171] have studied with electrospun cellulose nanocrystals (CNC) reinforcing maleic anhydride grafted PLA bio-nanocomposite scaffolds and showed that adding 5 wt % CNC improved the tensile strength up to 10 MPa. Similarly, it is reported that inclusion of cellulose nanofibers in PVA improved the mechanical properties as well as thermal properties [172-175]. Zhang and co-workers [176] found that the introduction of TiO_2 into PLA has improved the thermal stability, toughness, and UV resistance of nanocomposites. A number of research groups developed carbon nanotubes polymer nanocomposites and claimed that composites with carbon nanotubes carried higher mechanical strength and stiffness and higher electrical and thermal conductive properties [177-180].

Wollastonite is considered as a promising reinforcement for thermoplastic composites because of their high aspect ratio and excellent inherent properties. A large number of

studies have been carried out using wollastonite fillers by conventional methods such as compression molding and injection molding [181-183]. The mechanical properties [184], thermal properties [185], and rheological behavior [184] were investigated.

Wood flour have also been used as effective reinforcement material as it carries various advantages including low cost, availability in abundance, low abrasiveness, high specific strength & stiffness, biodegradability and relatively low density [186, 187]. Mechanical properties of PLA composites filled with a mixture of softwood or hardwood floor have been focused in the literature [188, 189]. Thermal and mechanical characteristics of poly(vinyl alcohol) modified by phthalic anhydride (PA) compounded with the wood flour in hot press have been studied by Ozaki et al [190].

In many applications, for example filtration, it is required to have high mechanical strength on the electrospun nanofiber membranes [191]. The agglomeration of nano-additives which prevents good filler dispersion in the matrix, is the biggest barrier in order to develop the high potential applicable advanced nanocomposite. Although a number of research groups have investigated the improvement in the functional properties of nanoadditive based composite [1, 10, 172, 192]. The performance of electrospun fibrous nanocomposite needs to be investigated further. Therefore, in this study, we focus on introducing various micro/nano additives such as wollastonite, and wood flour in electrospun PVA nanofibers. Fibrous PVA nanocomposites consisting of wollastonite or wood flour were fabricated using electrospinning method. Morphological, mechanical, and thermal properties of nanocomposite scaffolds were investigated.

6.2 Experimental

6.2.1 Materials

Wollastonite: Wollastonite is a white calcium silicate ($CaSiO_3$) mineral product of various inorganic components. The main two components of wollastonite are calcium (Ca) and silicon dioxide (SiO_2). Pure wollastonite is bright white but it can be gray, brown, green or red based on amount of impurities in it. Needle shaped wollastonites are prepared in industries by crushing them from a big chunk. The chemical compositions of wollastonite

520U supplied by Fibertec, USA, are listed in Table 6.1. The average diameter, aspect ratio, and specific gravity of wollastonite used in this study is 5 microns, 20, and 2.9, respectively.

The amount of volatile material (gas) that is removed from wollastonite by heating at 1,000°C is called Loss on Ignition (LOI). The lower value of LOI reduces problems of gas bubble entrapment and gas scattering during the firing of ceramics resulting in lowered firing costs, and reduces firing time.

Reinforced wollastonite can improve the mechanical properties (tensile, flexural, impact), minimize distortion at elevated temperatures, improve dimensional stability, and provide low moisture absorption of the composite materials [184].

Table 6.1 Chemical compositions of wollastonite 520U

Component	**CaO**	**SiO_2**	**Fe_2O_3**	**Al_2O_3**	**MgO**	**L.O.I***
Weight %	45.7	52.2	0.15	0.25	0.20	0.50

*Losing percent of quantity after burning

Wood flour: Wood flour also referred as wood fiber is a finely ground wood cellulose produced from dry wood waste by various types of grinders. All high grade (high durability and high strength) wood flour is produced from hardwoods and low grade wood flour comes from softwoods. Wood pulverization method can be divided into two types, such as wet and dry pulverization. Dry pulverization is suitable for industrial applications where the size of wood floors are more than 100 µm. In wet pulverization, the wood floors are less than 100 µm in size. Moreover, wood can be pulverized along the direction of fiber in higher water content media, leading to a fibrous wood floor [193]. The size and shape of the wood flour greatly affects the performance of the composite materials [194].

The wood floor that was used in this study was purchased from the American wood fibers company (USA).

6.2.2 Fabrication of Nanofibrous Composite Mats

PVA was dissolved in distilled water by continuous magnetic stirring for four hours using a hot plate at 70 ^{o}C. After that, wollastonite were added to the aqueous PVA solution in order to produce composites with 5, 10, 15, and 20 wt % wollastonite. Prior to that, wollastonite was filtered with 106 µm standard test sieve (Gilson company, Inc., USA) to remove agglomeration. The total concentration of PVA/wollastonite was fixed at 12 wt %. Stirring was continued for three hours at room temperature. Then, aqueous composite solution was immediately loaded into the plastic syringe which was pumped through the needle tip (0.51 mm inner diameter) with the flow rate of 500 μL/h. A 20 KV high voltage was applied to the needle tip and the collector electrodes which were kept a 10 cm apart. The electrospun fibers were collected on a rotating drum with 1000 rpm. The electrospun fibrous scaffolds were dried at 40 ^{o}C for 12 h. PVA/wood flour nanocomposites were also prepared following the same steps as described for PVA/wollastonite nanocomposites

6.2.3 Characterization

Scanning Electron Microscopy (SEM)

The surface morphologies of electrospun fibers were examined using an SEM (JSM 6060) operated at 5 kV. Prior to examination, all the samples were sputter-coated with a thin layer of platinum.

Digital Optical Microscope (DOM)

Digital optical microscopy (DOM) (VHX – 1000E, Keyence) was employed to determine surface morphologies, fiber diameter, and thickness of electrospun mats. Custom MATLAB image processing algorithm was developed to calculate the fiber diameter from DOM image.

X-ray Computed Tomography (XCT)

X-ray computed tomography (XCT), a nondestructive method, computes 3D information of inner structure of tested sample. PVA and PVA/Wollastonite nanofibrous composite were scanned using high resolution x-ray micro computed tomography (Skyscan 1172, Brucker) with a resolution of 2.5 µm. The voltage and current at the micro-focus tube were 20 kV and 104 µA, respectively. The specimen was rotated at 0.2 degree on a rotary stage

between the x-ray tube and the matrix detector where an average of six projection images were taken at each angular position. A 3D image was mathematically reconstructed from these projection images.

Fourier Transform Infrared Spectroscopy (FTIR)

The presence of chemical composition of wollastonite into the PVA/wollastonite nanofibrous composite was confirmed by using a Bruker FTIR spectrometer. All spectra were acquired with a resolution of 2 cm^{-1} after 64 continuous scans.

Rheology

Dynamic viscoelastic properties of PVA and its composites solution were evaluated on an ARES rheometer (TA instruments). A dynamic frequency sweep (stain control) test was carried out by running a sinusoidal shear strain profile $\gamma = \gamma_o \sin(\omega t)$ at an amplitude γ_o of 0.001 and an angular frequency ω, ranged from 0.01 to 100 rad/s. All experiments were performed using 25 mm parallel plate with gap of 1 mm at 25 ^oC temperature.

Dynamic Mechanical Analysis (DMA)

Tensile strength tests of nanofibrous mats were performed using dynamic mechanical analysis (DMA) Q800 (TA instruments) at 25 ^oC with a force ramp of 0.5 N min^{-1}. Samples were cut using razor blade with a width of 6.5 mm; thickness were measured under optical microscope and gauge lengths of the sample were evaluated by the instrument directly. The average thickness measured for all the electrospun scaffolds was in the range of 40 to 60 µm. As the samples were soft and flexible, therefore, both ends of tested sample were covered with the scotch tape to distribute the load uniformly along the sample. The sample was then loaded to the film tension clamp where the maximum force was set at 18 N with an initial preload force of 0.05 N. The data reported are the average of five observations. From the test results, Young's modulus (E), tensile strength (σ_t), and elongation at break (ε_b) were evaluated.

Differential Scanning Calorimeters (DSC)

The thermal properties of nanofibrous mats were investigated with the help of differential scanning calorimeters Q20 (TA instruments). The specimens were heated from room temperature to 200 ^oC at a heating rate of 10 ^oC min^{-1} and held for 5 minutes to remove

any prior thermal history. Then, the specimens cooled at a rate of 10 ^{o}C min^{-1} up to 40 ^{o}C. Finally, the thermal data was collected reheating the sample from 40 ^{o}C to 200 ^{o}C at 10 ^{o}C min^{-1}.

Thermogravimetric Analyzer (TGA)

The thermal stability of electrospun nanofibrous mats was evaluated by thermogravimetric analyzer Q50 (TA instruments) from room temperature to 600 ^{o}C at a heating rate of 10 ^{o}C min^{-1} under nitrogen atmosphere. Approximately 3.5 mg of nanofibrous scaffolds were used for each test.

6.3 Results and Discussion

6.3.1 PVA/Wollastonite Fibrous Nanocomposite

6.3.1.1 Surface Morphology

Raw wollastonite and the dispersion of wollastonite in the polymer solution are displayed in Figure 6.1. Figure 6.2 present the surface morphology of PVA and PVA/Wollastonite fibrous nanocomposites. The DOM and SEM micrographs provide significant information about the distribution of fillers into the matrix. Examining these images, it is clearly seen that reinforced wollastonite were embedded in the PVA matrix. Wollastonite particles which were smaller than electrospun fibers, were completely enclosed within the fibers whereas larger particles were adhered to the matrix. Most of the wollastonite rods were laid along the fiber direction. The reason for this is when composite solution was extruded through a very narrow needle during electrospinning, the wollastonite rods acquired alignment because of tremendous high shear forces developed between the inner surface of the needle and the solution. In addition, it is obvious from SEM images (Fig. 6.2b and 6.2c) that electrospun fibers of PVA were more uniform and smooth compared to PVA/wollastonite composite. Adding wollastonite to the PVA solution reduced the viscosity of the solution which is shown in the rheology section. Both viscosity and surface tension between reinforced and matrix materials might be the reason of producing this non-uniform fibers.

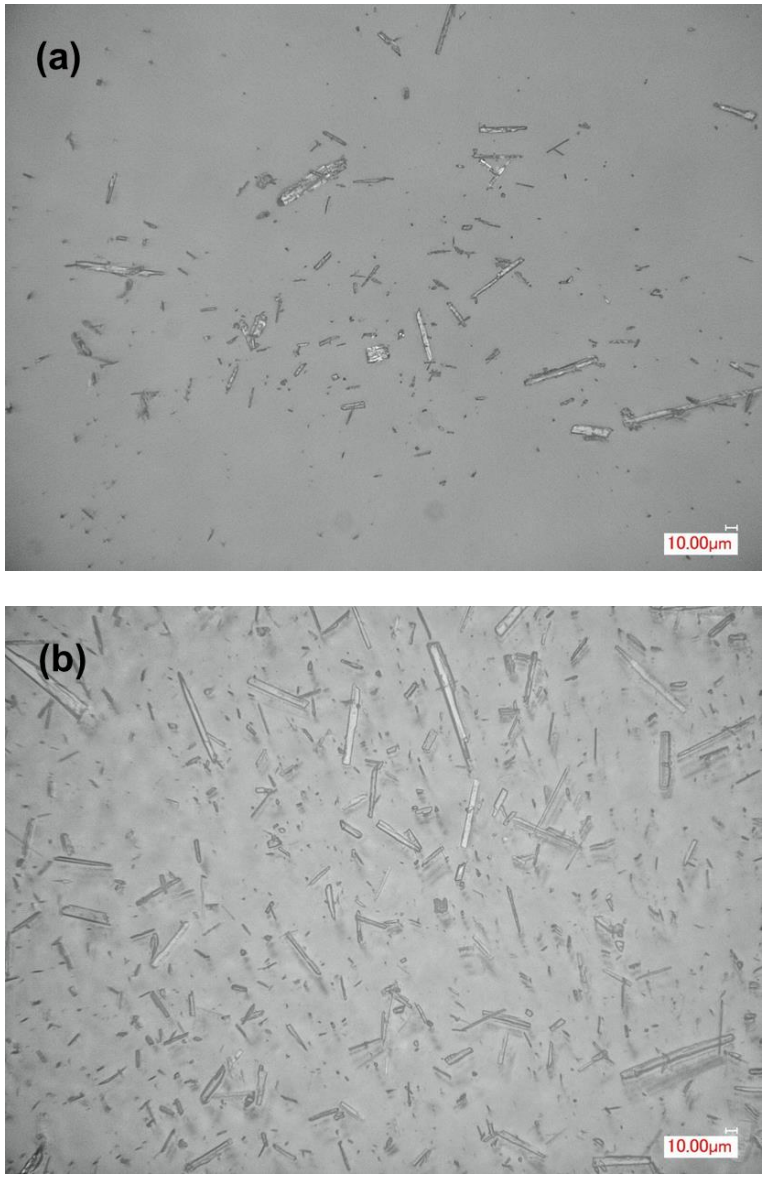

Figure 6.1 DOM micrographs of dry wollastonite (a), and dispersion of wollastonite in PVA aqueous solution (b).

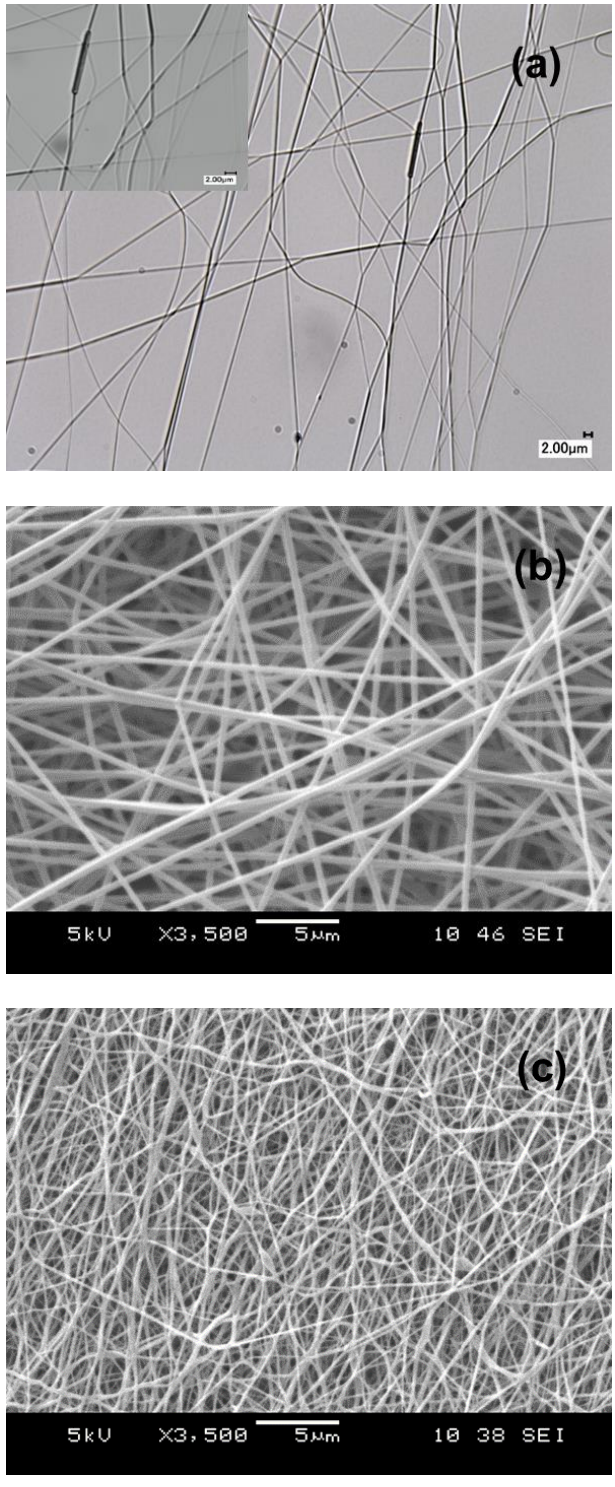

Figure 6.2 (a) DOM micrograph of PVA nanocomposite with 15 wt% wollastonite and SEM images of (b) pure PVA, (c) 15 wt % wollastonite nanocomposite.

Two-dimensional shadow projection image (SPI) and 3D maximum projection images (MPI) are shown in Figure 6.3 in order to differentiate PVA and PVA/Wollastonite fibrous nanocomposite. High resolution XCT was able to distinguish wollastonite particle-reinforced PVA composite because of their density difference. Moreover, by using quite low x-ray voltage of 20 kV and the performance of the XCT device, contrast and spatial resolutions, it was possible to segregate features of PVA and wollastonite particles. From SPI (Fig. 6.3a), it is clear that the reinforced wollastonite particles are evenly distributed in the matrix without making any agglomeration. Also the PVA nanofibrous mat appears very neat and smooth (Fig. 6.3b). Similar findings were observed in the 3D MPI (shown in Fig. 6.3 c and d) where particles of wollastonite are seen to be adhered together in the matrix materials.

FTIR spectra of nanofibrous PVA and PVA/Wollastonite (20 wt%) composite are illustrated in Figure 6.4. Compared with PVA nanofibrous mat, the PVA/wollastonite nanofibrous composite shows few additional absorbance peaks in the spectrum at 900, 643, 568, 505, and 450 cm^{-1}, which could be attributed OH deformation linked to $2Al^{3-}$, Si-O-Si bond bending, Fe-O stretching, O-Si-O bending, and Ca-O stretching, respectively [184, 195]. These results clearly pointed to the presence of wollastonite on the electrospun nanocomposite fibers.

6.3.1.2 Fiber Diameter

Fiber diameter of PVA and its composites was characterized by using custom made MATLAB algorithm. The average fiber diameter with standard deviation is summarized in Table 6.2. The fiber diameter of PVA is slightly higher as compared to PVA/Wollastonite composite fibers. The thinnest fiber diameter was observed for loading 5 wt% of wollastonite into the composite materials followed by 20, 10 and 15 wt% of wollastonite. Since all the processing parameters of electrospinning remained same except solution viscosity, it is emphasized that the solution viscosity plays an important role in the formation of fiber morphology.

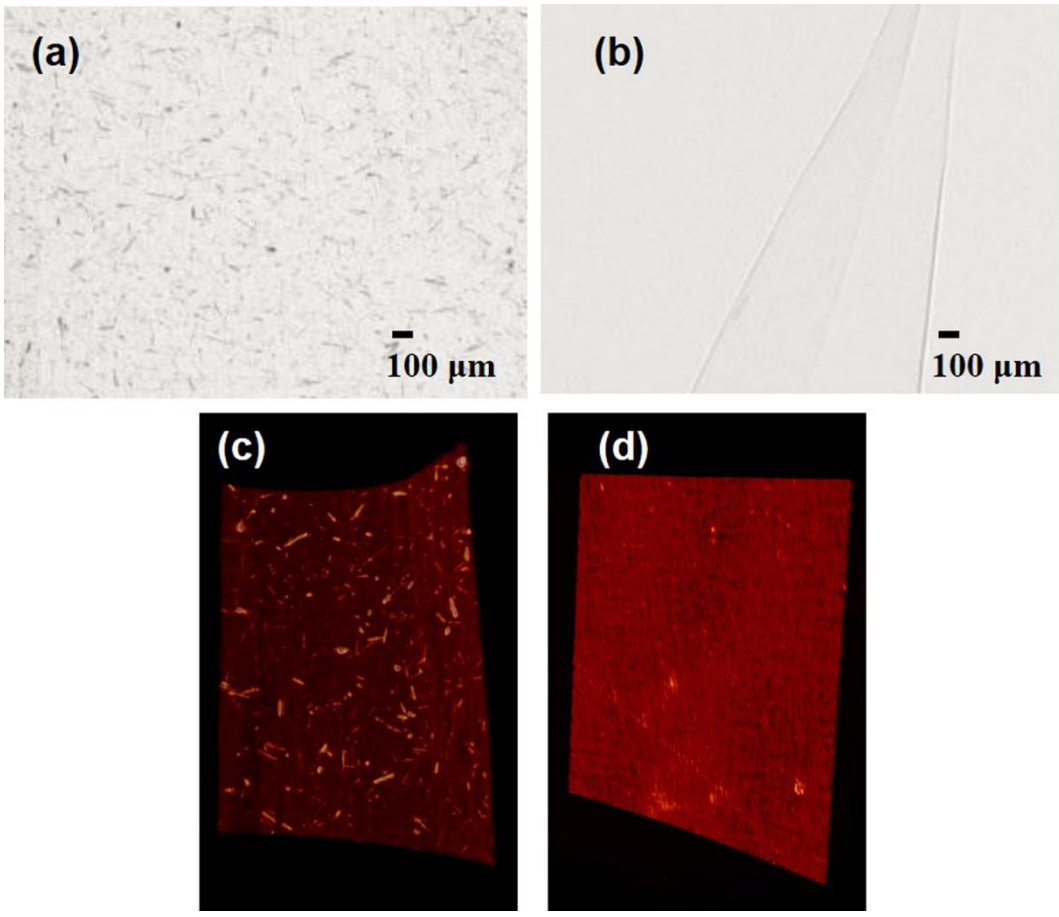

Figure 6.3 SP images of PVA/wollastonite nanocomposite (a), PVA mat (b), and 3D MPI images of PVA/wollastonite (c), PVA mat (d).

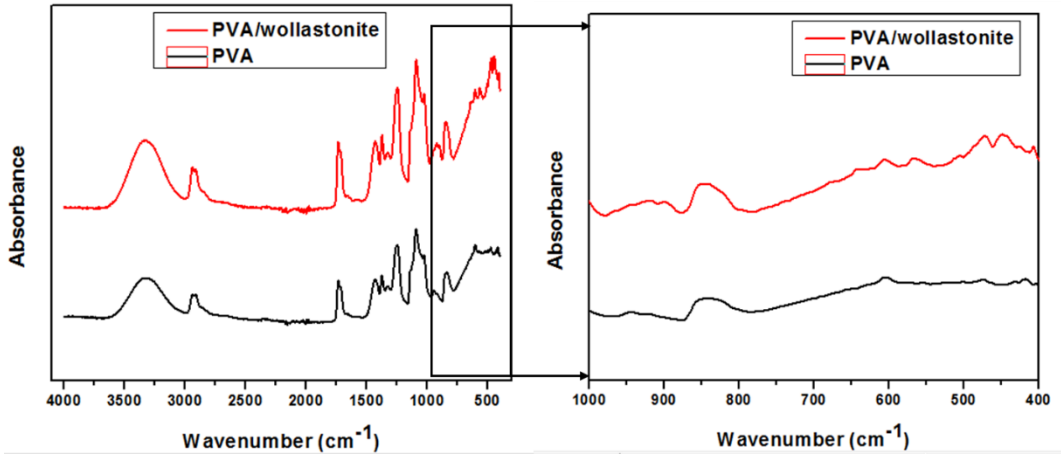

Figure 6.4 FTIR spectrum of PVA and PVA/Wollastonite nanocomposites

6.3.1.3 Rheology

Figure 6.5 shows the rheological properties of PVA solution comprising various amount of wollastonite. It is noted that all of the samples showed similar rheological behaviors. The dynamic viscosity decreased linearly with increased frequency indicating non-Newtonian flow behavior and distinct shear thinning over the range of frequencies. The dynamic viscosity for pure PVA solution is higher than the samples with wollastonite reinforced composites at all frequencies. We kept the overall solution concentration of pure PVA and PVA/wollastonite composite at 12 wt%. Therefore, the moleculer chains of PVA were quantitively higher in PVA solution resulted higher viscosity compared to composite solution. PVA solution having 5 wt % wollastonite has the lowest viscosity as it contained the smallest amount of reinforcement materials followed by 10, 15, and 20 wt % of wollastonite composites which is very common phenomena for short fiber reinforced composites [196]. Shear viscocity increased with the addition of fillers showing the constraint exerted by of the wollastonite particles on the motions of PVA molecular chains.

Table 6.2 Fiber diameter of PVA and PVA/Wollastonite nanocomposites with different weight fractions.

Materials	**Diameter (μm)**
Pure PVA	1.186 ± 0.21
PVA + 5 % Wollastonite	0.891 ± 0.16
PVA + 10% Wollastonite	1.06 ± 0.28
PVA + 15% Wollastonite	1.09 ± 0.16
PVA + 20% Wollastonite	0.943 ± 0.16

6.3.1.4 Mechanical Properties

Tensile Tests

A typical stress-strain curve of nanofibrous PVA and its composites is illustrated in Figure 6.6 and the summary of tensile characteristics of the samples under tensile tests are depicted in Table 6.3.

It is shown that the tensile strength increased significantly after adding small amount (5 wt %) of wollastonite in PVA_5 wollastonite sample. Tensile strength of PVA and PVA_5 wollastonite were 3.92 and 5.12 MPa, respectively, shows 31 % improvement over PVA mat. Likewise, 85 %, 183 %, and 206 % increment of tensile strengths were observed in PVA_10 wollastonite (7.25 MPa), PVA_15 wollastonite (11.09 MPa), and PVA_20 wollastonite (11.99 MPa) sample, respectively, compared to PVA. These improvements indicate good dispersion of particles in the matrix as well as strong adhesion between matrix and fillers which leads to superior load transfer from the matrix to reinforcement.

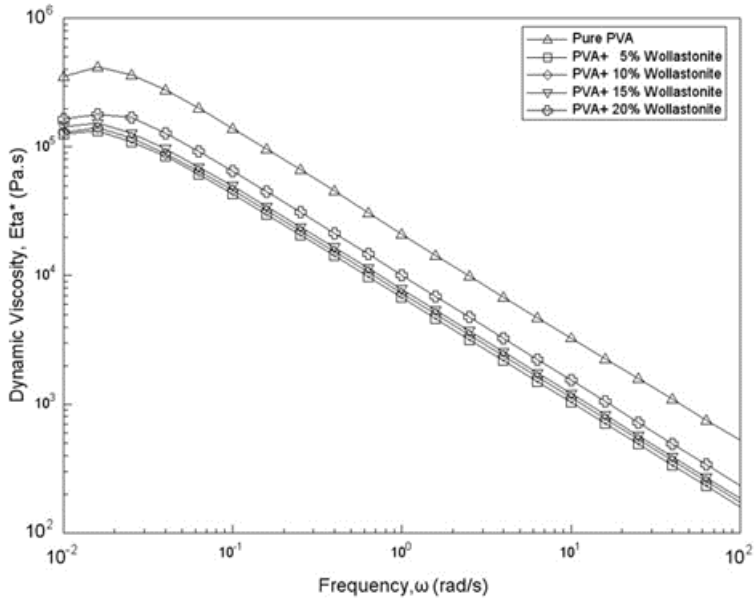

Figure 6.5 Dynamic viscosity curves of PVA and PVA/wollastonite composites solution

Similar trend was noticed in the tensile modulus of PVA/Wollastonite samples. The addition of wollastonite in the matrix yielded stiffer composite than that of PVA sample. PVA_20 wollastonite exhibited the highest tensile modulus (198 MPa) as it composed

maximum amount of reinforcement (20 wt %). In this case, tensile modulus improved by 138 % as compared to PVA (83.27 MPa). Similarly, for PVA_5 wollastonite, PVA_10 wollastonite, and PVA_15 wollastonite composites, progress of stiffness were 17 %, 48 %, and 134 %, respectively.

On the other hand, the elongation at break of nanofibrous PVA/Wollastonite composite reduced significantly compared to PVA scaffolds showing good adhesion and dispersion of reinforcement to the matrix. Nanofibrous PVA mat showed elongation at break of 59 %, whereas, adding 5 wt % reinforcement resulted 43 % of elongation. Further increasing the concentration of reinforcement to the matrix led to even more decrease in deformation to as low as 19 % for 20 wt % reinforced PVA composite.

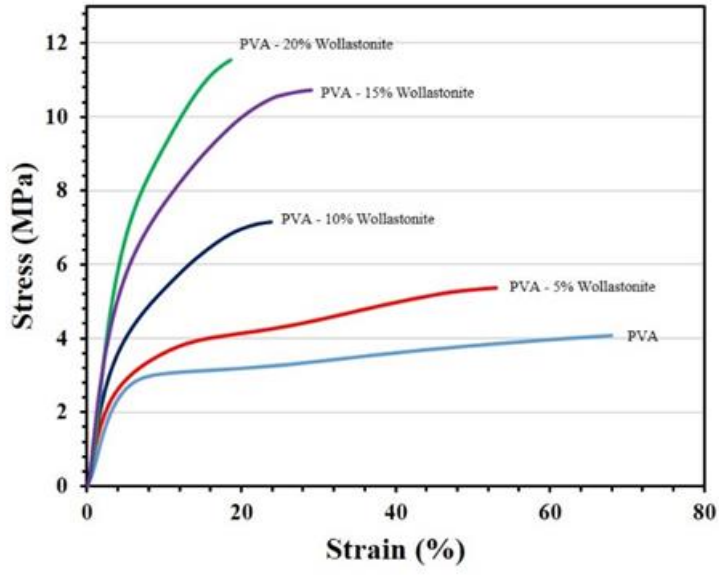

Figure 6.6 Typical tensile stress-strain curve of PVA scaffolds and its composites

6.3.1.5 Thermal Properties

Thermal properties of electrospun PVA/Wollastonite nanofibrous composites were investigated using TGA and DSC and a comparison was made with PVA nanofibers. Figure 6.7 depicts the TGA and DTGA curves of PVA/Wollastonite nanocomposites containing 0, 5, 10, 15, and 20 wt % of wollastonite. The summery of these results are exhibited in Table 6.4. It is shown that the shape of the curves are almost similar showing

more or less same decomposition and onset temperature. Therefore, incorporation of wollastonite particles does not alter the degradation mechanism as well as thermal stability of PVA. It is also seen that the residue of PVA/wollastonite composites gradually increased with increased wollastonite content, indicating homogeneous distribution of wollastonite in the composite.

Table 6.3 Tensile properties of PVA scaffolds and its composites

Materials	**Tensile Strength (MPa)**	**Young's Modulus (MPa)**	**Elongation at break (%)**
PVA	3.92 ± 0.39	83.27 ± 9.60	58.59 ± 21.88
PVA + 5 % Wollastonite	5.12 ± 0.67	97.59 ± 27.21	42.79 ± 8.51
PVA + 10 % Wollastonite	7.25 ± 0.59	122.95 ± 65.04	37.24 ± 4.78
PVA + 15 % Wollastonite	11.09 ± 1.08	194.72 ± 25.04	27.6 ± 2.12
PVA + 20 % Wollastonite	11.99 ± 0.97	198.58 ± 31.87	19.34 ± 5.35

DSC measurements of PVA nanofibrous composites with different loading amounts of wollastonite particles are displayed in Figure 6.8 and Table 6.5. It is seen that there were no obvious changes in the glass transition temperature (T_g) with increased wollastonite contents to the PVA/Wollastonite composites. The melting temperature (T_m) of the samples was calculated from the maximum peaks of exothermic DSC thermographs. A slight decrease was observed in T_m, from 167.4 ^oC for pure PVA nanofibers to 162.7, 162.4, 160.7, and 162.1 ^oC for nanofibrous composites having 5, 10, 15, and 20 wt % of wollastonite, respectively. This phenomena might have occurred because inclusion of wollastonite particles may act as nucleates for PVA crystallization which accelerate the

number of crystal into the nanocomposites and consequently lowering the melting point [184, 197].

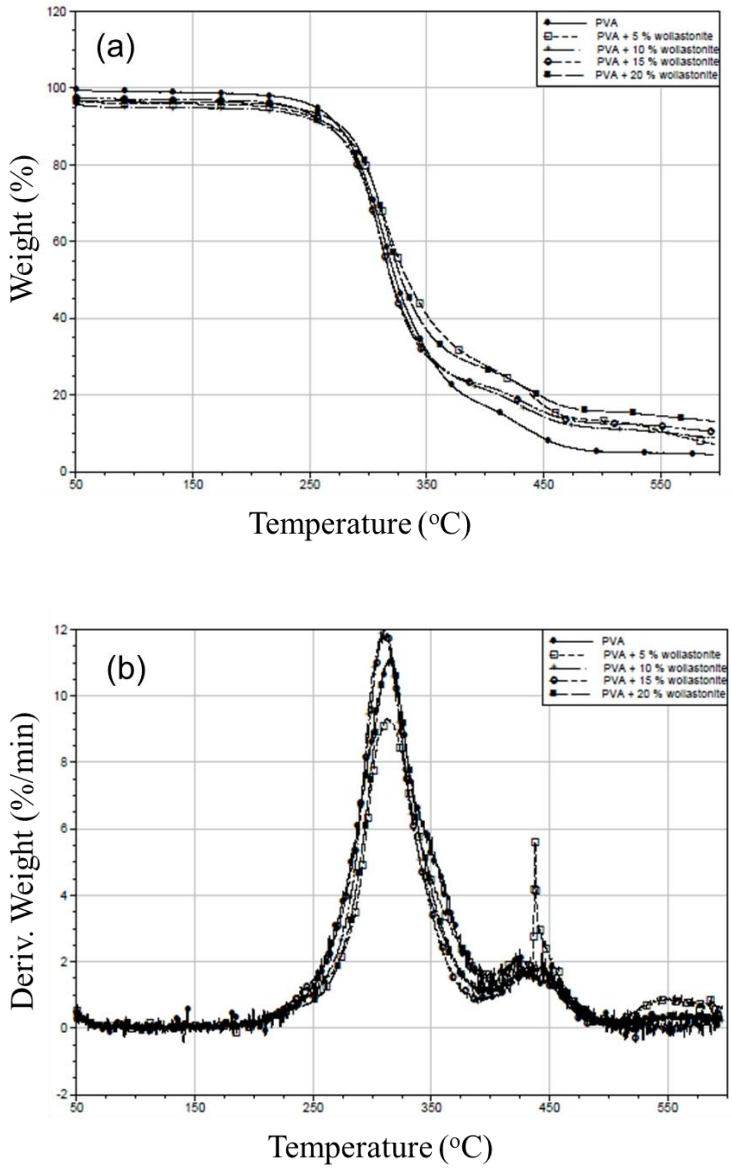

Figure 6.7 TGA (a), DTGA (b), profiles of PVA and PVA/Wollastonite composites.

Table 6.4. Summary of TGA results of PVA and PVA/Wollastonite composites.

Materials	On-set temperature (ºC)	Residue (%)	Degradation rate (°C)
PVA	281.31	4.47	315.30
PVA + 5 % Wollastonite	282.88	7.33	312.30
PVA + 10 % Wollastonite	282.22	8.78	307.32
PVA + 15 % Wollastonite	276.22	10.48	310.25
PVA + 20 % Wollastonite	286.07	13.18	314.81

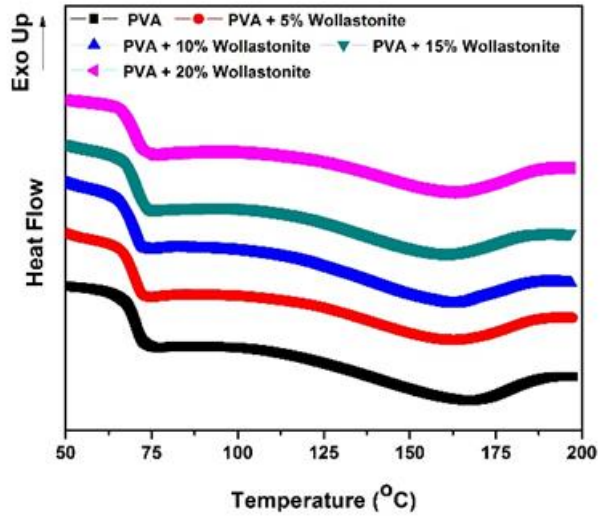

Figure 6.8 DSC thermograms of the second heating for PVA and its nanocomposites with wollastonite

Table 6.5 Summary of DSC results of PVA and its nanocomposites with wollastonite

Materials	**T_g (°C)**	**T_m (°C)**
Pure PVA	70.64	167.4
PVA + 5 % Wollastonite	70.21	162.70
PVA + 10% Wollastonite	70.82	162.39
PVA + 15% Wollastonite	70.57	160.74
PVA + 20% Wollastonite	70.61	162.11

6.3.2 PVA/Wood Flour Fibrous Nanocomposite

6.3.2.1 Surface Morphology

Raw wood flour and aqueous composite solution reinforced with wood flour are shown in Figure 6.9. The optical image (Fig. 6.9B) demonstrates that the wood flour dispersed homogeneously throughout the aqueous PVA solution without agglomeration.

Surface morphology of pure PVA and PVA/Wood flour nanocomposite is presented in Figure 6.10. Both the DOM and SEM image show the filler distribution in the PVA matrix. Majority of the wood flour are fully embedded by the PVA materials whereas, the large wood fillers compared to fiber diameter are also adhered to the polymers making beads on the fiber surface. These results indicate that nanofibrous composites are possible to be developed by electrospinning method even with larger particle filler materials compared to fiber diameter.

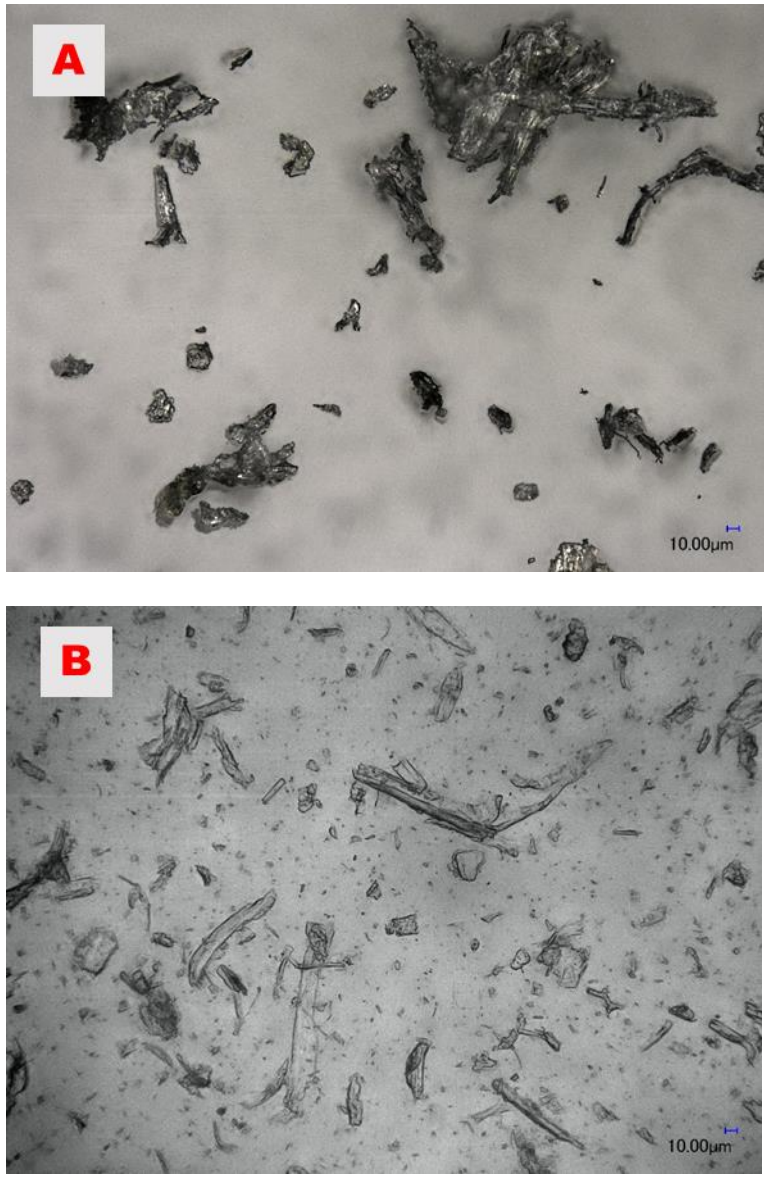

Figure 6.9 Optical micrographs of raw wood (A), and dispersion of wood flour in PVA aqueous solution (B).

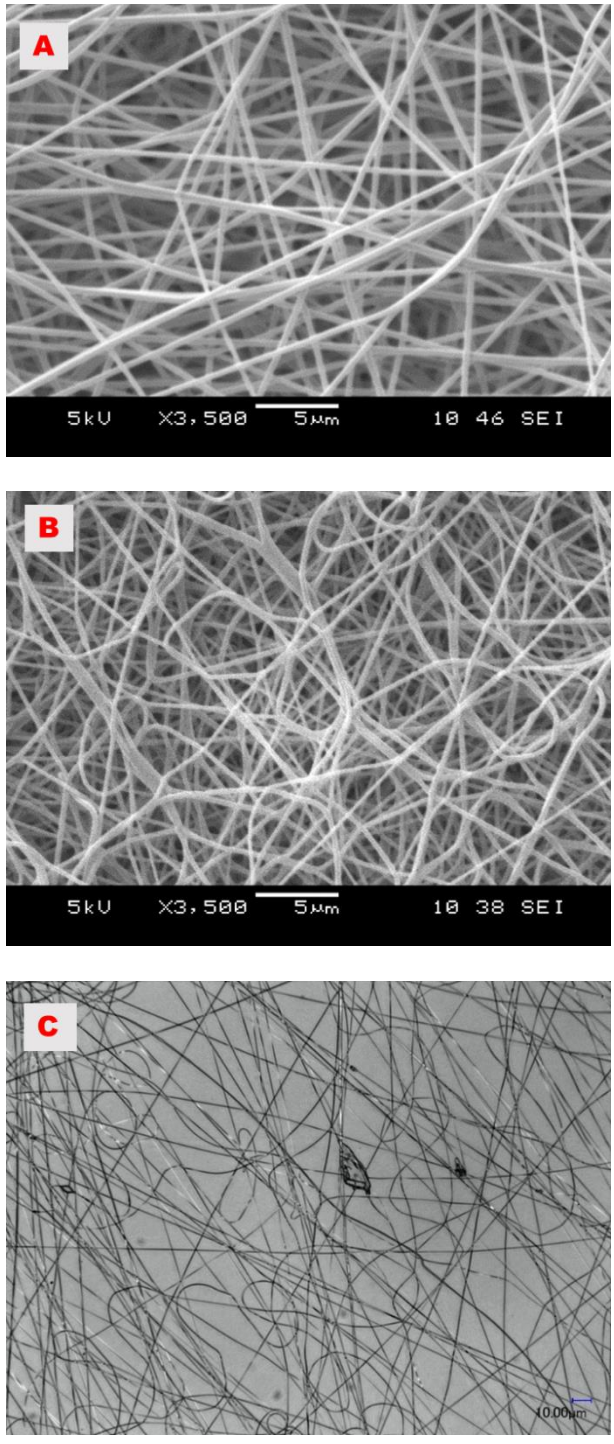

Figure 6.10 SEM image of pure PVA nanofiber (A), and PVA/Wood flour (15 wt%) nanocomposite (B).

Fiber Diameter

Fiber diameters of PVA and PVA/Wood flour nanocomposites were calculated using custom made MATLAB algorithm from optical micrograph images. The optical image of electrospun pure PVA nanofibers and its frequency chart of diameter are presented in Figure 6.11A & F, respectively. Figure 6.11B-E depict optical images of 5, 10 15, and 20 wt% of wood flour reinforced PVA nanocomposites and their corresponding fiber diameter distribution charts are displayed in Fig. 6.11G-J, respectively. The average fiber diameter of different nanocomposites are summarized in Table 6.6. The addition of the wood flour increased the average fiber diameter as compared to the pure PVA nanofiber although they lie in the error ranges of PVA nanofibers.

Table 6.6 Fiber diameter of PVA and PVA/wood flour nanocomposites.

Materials	**Diameter (µm)**
Pure PVA	1.186
PVA + 5 % Wood flour	1.167
PVA + 10% Wood flour	1.258
PVA + 15% Wood flour	1.291
PVA + 20% Wood flour	1.096

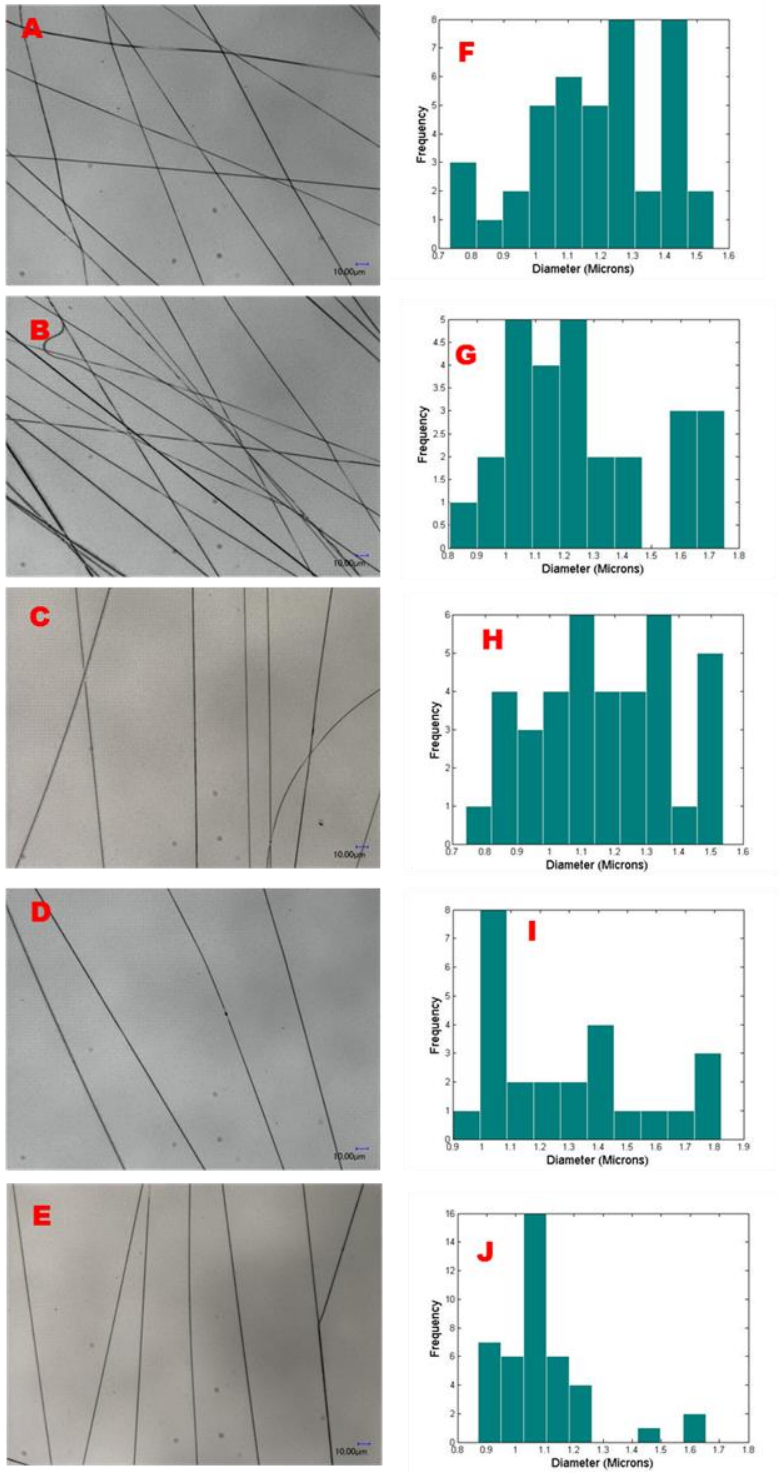

Figure 6.11 Optical micrograph images of pure PVA nanofiber (A), and 5 wt% (B), 10 wt% (C), 15 wt% (D), 20 wt% (E), of wood flour reinforced PVA nanocomposites. Their corresponding fiber diameter distribution chats (from F to J) are shown, respectively.

6.3.2.2 Mechanical Properties

Tensile Tests

Figure 6.12 shows the stress-strain curves of pure PVA and PVA/Wood flour fibrous nanocomposite. The tensile strength, Young's modulus and elongation at break are listed in the Table 6.7. As compared to the tensile strength of pure PVA (3.92 MPa), 5 wt % addition of wood flour increased the tensile strength by 45 % to 5.69 MPa. The tensile strength for PVA + 10 % and PVA + 15 % wood flour nanocomposites show 67 % and 86 % improvement respectively. A significant improvement is observed in the tensile strength of PVA + 20 % wood flour nanocomposite (228 %) as compared to pure PVA. The improvement of tensile strength of the PVA/wood nanocomposites indicate the presence of wood flour in the composites and the superior ability to transfer load from matrix to filler materials.

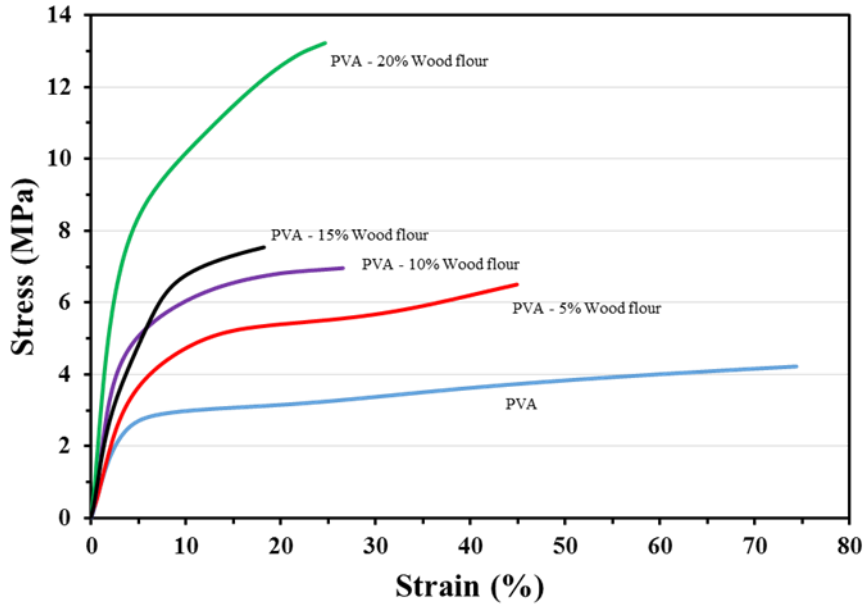

Figure 6.12 Typical tensile stress-strain curve of PVA scaffolds and PVA/Wood flour composites

Table 6.7 Tensile properties of PVA scaffolds and its composites

Materials	**Tensile Strength (MPa)**	**Young's Modulus (MPa)**	**Elongation at break (%)**
PVA	3.92 ± 0.39	83.27 ± 9.60	58.59 ± 21.88
PVA + 5 % Wood	5.69 ± 1.09	100.96 ± 30.60	46.89 ± 7.86
PVA + 10 % Wood	6.55 ± 0.57	157.87 ± 10.92	23.10 ± 4.88
PVA + 15 % Wood	7.3 ± 0.21	153.4 ± 9.84	25.65 ± 11.92
PVA + 20 % Wood	12.87 ± 1.73	214.13 ± 42.12	15.41 ± 8.35

A significant improvement in Young's modulus thus stiffer nanofibers were observed from the steeper slopes of all the PVA/wood flour nanocomposite as compared to pure PVA nanofibers. Similar trend is also observed in tensile strength of composite materials. 21 %, 90 %, 84 %, and 157 % improvements were achieved in Young's modulus when PVA nanofibers were reinforced with 5 %, 10 %, 15 %, and 20 % wood flour, as compared to PVA scaffolds. These results further emphasized the uniform distribution of filler materials and exchange of load from matrix to reinforcement materials.

In contrast, a decreasing trend was observed in the elongation at break of PVA/wood flour nanocomposite as compared to pure PVA mat. The remarkable decrease in the elongation at break observed as 58.59 % for pure PVA to 15.41 % for PVA + 20 % wood flour nanocomposite. The large aspect ratio of wood flour and the interaction between the wood flour and PVA which restricts the polymer chain's movement thus limits mechanical deformation can be considered as the main reasons for reduced ductility.

6.3.2.3 Thermal Properties

The TGA and the differential TG (DTG) curves are depicted in the Figures 6.13 (a) & 6.13 (b), respectively, in order to investigate the thermal properties of PVA/Wood flour nanocomposites. Onset temperature, maximum thermal decomposition temperature and char yield is shown in Table 6.8. A single step decomposition observed in PVA scaffold as well as its composite materials pointing there were no chemical bonds created with the addition of wood. Only strong adhesion is occurred between the PVA matrix materials and wood flour reinforcement materials. The onset and degradation temperatures of all the nanocomposite slightly dropped as compared to the value for the neat PVA. Therefore, the thermal stability of nanocomposites did not undergo any noticeable change with the addition of wood floor.

DSC measurements of PVA nanofibrous composites containing 0, 5, 10, 15, and 20 wt % of wood flour are displayed in Figure 6.14 and Table 6.9. It is seen that there were no obvious changes in the glass transition temperature (T_g) with addition of wood flour to the PVA/wood composites. The melting temperature (T_m) of the samples was calculated from the maximum peaks of exothermic DSC thermographs. A higher melting temperature was observed in nanofibrous composites promoting higher thermal resistance.

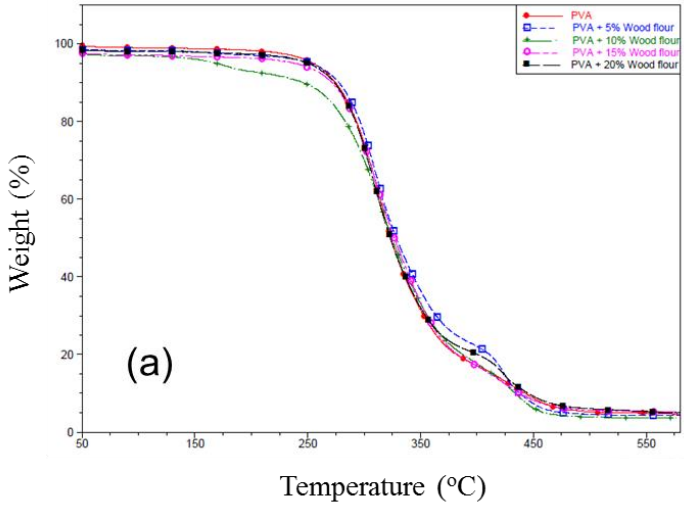

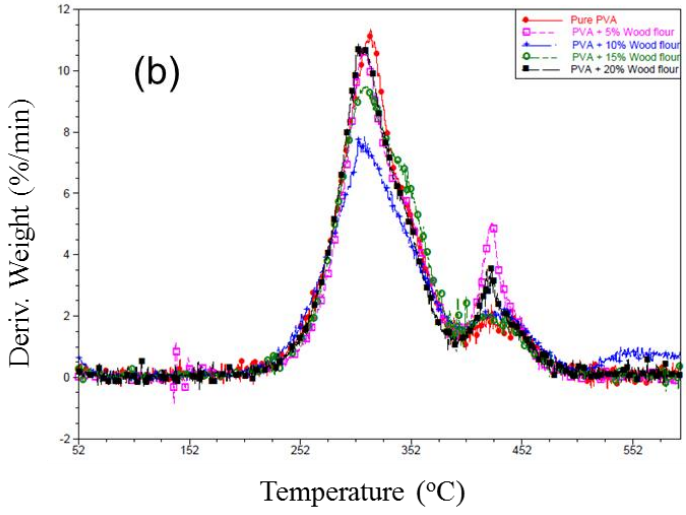

Figure 6.13 TGA (a), DTGA (b), profiles of PVA and PVA/Wood flour nanocomposites.

Table 6.8 Summary of TGA results of PVA and PVA/Wood nanocomposites.

Materials	**On-set temperature (ºC)**	**Degradation rate (°C)**	**Residue (%)**
PVA	281.31	315.30	4.47
PVA + 5 % Wood flour	282.85	310.28	4.30
PVA + 10 % Wood flour	271.74	310.07	5.01
PVA + 15 % Wood flour	277.89	311.08	5.15
PVA + 20 % Wood flour	278.84	304.46	4.75

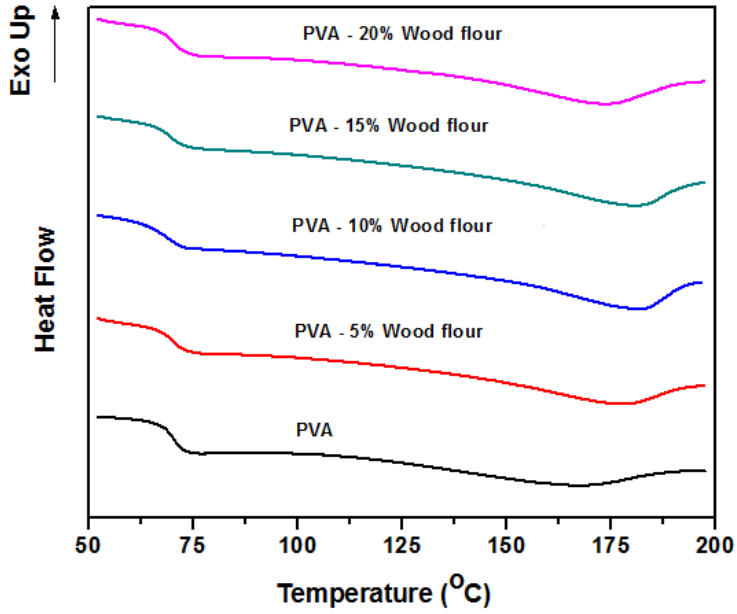

Figure 6.14 DSC thermograms of the second heating for PVA and its nanocomposites with wood floor.

Table 6.9 Summary of DSC results of PVA and its nanocomposites with wood flour

Materials	**T_g (°C)**	**T_m (°C)**
Pure PVA	70.64	167.4
PVA + 5 % Wood flour	69.46	177.84
PVA + 10% Wood flour	69.69	182.31
PVA + 15% Wood flour	69.15	180.74
PVA + 20% Wood flour	70.31	173.74

Chapter 7 Conclusions, Contributions, and Recommendations

7.1 Conclusions

In the preliminary phase of this research, we developed a stable high voltage direct current (DC) power supply in the laboratory with maximum capacity of 30 KV. The main parts of high voltage power supply system are: high voltage flyback transformer, a PWM circuit, and a feedback circuit. The output of high voltage can be adjusted by changing the duty cycle and frequency of the PWM signal and a feedback circuit is used to regulate a stable voltage.

In order to design a dynamic electrostatic potential system, we replaced a single conductive electrode, typically used in an electrospinning process, with multiple electrodes. The voltage potential of these electrodes are altered with the help of microprocessor based control system. Switching the voltage potential of electrodes is the critical to generating various shapes of nanofibrous patterns. We demonstrated using finite element method that the distribution of high voltage electrical fields change with the electrodes switching patterns. Therefore, electrospun charged fibers could be moved from one location to another location. By switching the electrodes at a very fast pace, the electrospun fibers can be deposited in designated areas. Based on the required deposition patterns, a number of conductive electrodes may be needed and can be arranged in desired location. For each setup, separate ARDUINO codes need to be uploaded to the microprocessor. We interface the high voltage control system to the personal computer via HyperTerminal.

We have disclosed that using our new advanced technique of controlling the activeness of electrodes with a microprocessor based system, various kinds of nanofibrous patterns can be fabricated. By increasing the number of electrodes and by controlling their switching pattern, a great variety of architectures can be obtained. The amount of electrospun fibers could be controlled either by controlling the deposition time of electrospinning or by

regulating the activation time of electrodes. The OT and the switching frequency between the adjacent electrodes are the main factors which control the amount of depositions in the architectures. By contrast, it is observed that when all electrodes were concurrently active (constant ground system), the field strength along the desired region was significantly lower resulting in lower yield.

We have demonstrated that various kinds of functionally graded nanofibrous architectures can be constructed by changing the electrospun time in-between the active pair of electrodes. Electrode's activation cycle durations, controlled by microprocessor system play a key role in regulating electrospun fibers deposition in the architecture. It has also been shown that the fibers can be deposited as randomly oriented nonwoven, uniaxial aligned or multi-directional mat by employing a number of electrodes and activating them in desired patterns. This is possible as the electrostatic forces can be altered by switching the potentials of electrodes, thereby, controlling the deposition and orientation of the fibers. The results clearly indicate that the packing density or the porosity and the orientation of electrospun fibers can be regulated within the architectures.

We have investigated the effect of varying the gap between two adjacent collector electrodes on the fiber diameter and the alignment of electrospun fiber. It is found that the diameter of electrospun fibers initially decreased with increasing gap, reached a minimum and then increased slightly again. The degree of alignment of electrospun fibers with respect to horizontal axis improved by increasing the separation gap of electrodes except when electrodes were placed very close to each other. FE analysis elucidated that the electrical field strength was comparatively lower at smaller gap, therefore, electrostatic forces acting on the fiber jet are not strong enough to stretch out the fibers fully, and yields a thicker fiber diameter. Increasing the gap between the electrodes increases the electrical field strength and induces higher electrostatic forces on the fiber jet which favors the formation of thinner fibers. Further increase in the strength of electrical field increases the material flow leading to thicker fibers.

The effect of electrodes size was also investigated. It is found that the alignment of fibers improves but the diameter of fibers reduces with increased electrode diameter. The results from FE analysis explained these phenomena. Very high electrical field strength develops

for small diameter of electrodes, and results in thicker and random fibers. Excessive electrical field draws more materials from the Taylor cone and the jet also travels very fast. The electrical field strength decreases as the surface area of electrode face increases. Thus, the electrospun fiber morphology and orientation improves.

It is anticipated that this simple and versatile advanced method of electrospinning based on microprocessor control of electrodes will have great potential for the fabrication of a wide variety of nanofibrous patterned architectures and will have significant impact on future developments of electrospinning process. This will lead to widespread applications both in health sciences and the industry.

Nanofibrous PVA scaffolds, PVA/Wollastonite and PVA/Wood flour composites were successfully prepared via electrospinning. Morphological results exhibited that the reinforced wollastonite and wood flour were well distributed into the PVA matrix. In addition, x-ray computed tomography and Fourier transform infrared spectroscopy confirmed the existence of wollastonite particles in the nanofibrous composites. The mechanical properties such as tensile strength and tensile modulus improved significantly with the addition of reinforcements indicating good adhesion and dispersion of filler materials into the matrix. PVA_20 wollastonite nanofibrous composite showed the maximum tensile strength, and tensile modulus but minimum elongation at break when it was reinforced by 20 wt % of wollastonite. Similar trend has been observed in PVA/Wood flour fibrous nanocomposites. Thermal results show that the introduction of wollastonite and wood flour had no distinct change in the thermal stability of composites. In short, the developed nanofibrous PVA/Wollastonite and PVA/Wood flour composites could be of potential use for many applications where high mechanical strength and thermal stability are needed, for instance, filtration and bone tissue engineering.

7.2 Contributions

- We developed a versatile advanced electrospinning method where a single conductive electrode, typically used in an electrospinning process, was replaced with multiple electrodes.

- Controlling the activeness of electrodes with a microprocessor based system, various kinds of nanofibrous patterns can be fabricated.
- The amount of electrospun fibers could be controlled either by controlling the deposition time of electrospinning or by regulating the activation time of electrodes.
- The voltage potential of these electrodes are altered with the help of microprocessor based control system. Therefore, electrospun charged fibers could be moved from one location to another location. By switching the electrodes at a very fast pace, the electrospun fibers can be deposited in designated areas.
- A great variety of functionally graded nanofibrous architectures can be constructed by changing the electrospun time in-between the active pair of electrodes.
- Electrospun nanofibers can be deposited as randomly oriented nonwoven, uniaxial aligned or multi-directional mat by employing a number of electrodes and activating them in desired patterns.
- Nanofibrous PVA scaffolds, PVA/Wollastonite and PVA/Wood flour composites were successfully prepared using rotating drum electrospinning technique.

7.3 Recommendations

We have demonstrated that our advanced electrospinning method can be used for developing various patterned architectures, controlled amount of deposition in the electrospun scaffolds, fabricating different types of functionally graded scaffolds, uniaxial aligned mats and to produce aligned multidirectional nanofibers. Although we have worked on many possibilities of generating various types of nanofibrous scaffolds with our versatile setup, further improvements/modifications can be carried out for specific potential applications. Therefore, following is recommended for future work:

- We have collected electrospun fibers on acrylic sheet through which copper wire electrodes protruded so that the sheet plus copper electrodes together acted as fiber collection system. We have protruded the copper rods so that the electrical field is not disturbed. An extensive experimental works can be carried out in order to direct deposition of electrospun fibers on the substrate materials.

- We have developed ordered and functionally graded nanofibrous architectures which can be useful for many advanced applications i.e, tissue engineering scaffolds, and electronics devices. Therefore, the work can be extended by implementing our improved method to the medical science and industrial applications.
- We have employed FEM to investigate the behaviors of electrical field with the control switching patterns. A mathematical model can be developed to determine quantitatively the electrospinning process.
- Other polymeric materials can be researched.
- Some parametric studies have been investigated with our developed setup which are shown in chapter 5. To make an empirical model of this system a number of other parametric studies need to be carried out that can be correlate with FE analysis.

References

[1] Z.-M. Huang, Y. Z. Zhang, M. Kotaki, and S. Ramakrishna, "A review on polymer nanofibers by electrospinning and their applications in nanocomposites," *Composites Science and Technology*, vol. 63, pp. 2223-2253, 2003.

[2] S. Agarwal, A. Greiner, and J. H. Wendorff, "Functional materials by electrospinning of polymers," *Progress in Polymer Science*, vol. 38, pp. 963-991, 2013.

[3] J. Fang, H. Niu, T. Lin, and X. Wang, "Applications of electrospun nanofibers," *Chinese Science Bulletin*, vol. 53, pp. 2265-2286, 2008.

[4] W. Lu, J. Sun, and X. Jiang, "Recent advances in electrospinning technology and biomedical applications of electrospun fibers," *Journal of Materials Chemistry B*, vol. 2, p. 2369, 2014.

[5] C. Mit-uppatham, M. Nithitanakul, and P. Supaphol, "Ultrafine electrospun polyamide-6 fibers: effect of solution conditions on morphology and average fiber diameter," *Macromolecular Chemistry and Physics*, vol. 205, pp. 2327-2338, 2004.

[6] R. Nayak, R. Padhye, I. L. Kyratzis, Y. B. Truong, and L. Arnold, "Recent advances in nanofibre fabrication techniques," *Textile Research Journal*, vol. 82, pp. 129-147, January 1, 2012 2012.

[7] X. Xing, Y. Wang, and B. Li, "Nanofibers drawing and nanodevices assembly in poly (trimethylene terephthalate)," *Optics express*, vol. 16, pp. 10815-10822, 2008.

[8] R. Dersch, T. Liu, A. Schaper, A. Greiner, and J. Wendorff, "Electrospun nanofibers: Internal structure and intrinsic orientation," *Journal of Polymer Science Part A: Polymer Chemistry*, vol. 41, pp. 545-553, 2003.

[9] J. R. Capadona, O. Van Den Berg, L. A. Capadona, M. Schroeter, S. J. Rowan, D. J. Tyler, *et al.*, "A versatile approach for the processing of polymer nanocomposites with self-assembled nanofibre templates," *Nature Nanotechnology*, vol. 2, pp. 765-769, 2007.

[10] I. S. Chronakis, "Novel nanocomposites and nanoceramics based on polymer nanofibers using electrospinning process—A review," *Journal of Materials Processing Technology*, vol. 167, pp. 283-293, 2005.

[11] A. Greiner and J. H. Wendorff, "Electrospinning: a fascinating method for the preparation of ultrathin fibers," *Angew Chem Int Ed Engl*, vol. 46, pp. 5670-703, 2007.

[12] S. Ramakrishna, "An Introduction to Electrospinning and Nanofibers " 2005.

[13] F. Anton, "Process and apparatus for preparing artificial threads," ed: Google Patents, 1934.

[14] F. Anton, "Method and apparatus for spinning," ed: Google Patents, 1944.

[15] G. Taylor, "Disintegration of Water Drops in an Electric Field," *Proceedings of the Royal Society A: Mathematical, Physical and Engineering Sciences*, vol. 280, pp. 383-397, 1964.

[16] H. L. Simons, "Process and apparatus for producing patterned non-woven fabrics," ed: Google Patents, 1966.
[17] P. K. Baumgarten, "Electrostatic spinning of acrylic microfibers," *Journal of Colloid and Interface Science,* vol. 36, pp. 71-79, 1971/05/01 1971.
[18] I. Hayati, A. I. Bailey, and T. F. Tadros, "Investigations into the mechanisms of electrohydrodynamic spraying of liquids: I. Effect of electric field and the environment on pendant drops and factors affecting the formation of stable jets and atomization," *Journal of Colloid and Interface Science,* vol. 117, pp. 205-221, 5// 1987.
[19] A. Varesano, R. A. Carletto, and G. Mazzuchetti, "Experimental investigations on the multi-jet electrospinning process," *Journal of Materials Processing Technology,* vol. 209, pp. 5178-5185, 2009.
[20] M. B. Bazbouz and G. K. Stylios, "Alignment and optimization of nylon 6 nanofibers by electrospinning," *Journal of Applied Polymer Science,* vol. 107, pp. 3023-3032, 2008.
[21] D. Li, Y. Wang, and Y. Xia, "Electrospinning of Polymeric and Ceramic Nanofibers as Uniaxially Aligned Arrays," *Nano Letters,* vol. 3, pp. 1167-1171, 2003/08/01 2003.
[22] H. B. Wang, M. E. Mullins, J. M. Cregg, A. Hurtado, M. Oudega, M. T. Trombley, *et al.*, "Creation of highly aligned electrospun poly-L-lactic acid fibers for nerve regeneration applications," *J Neural Eng,* vol. 6, p. 016001, Feb 2009.
[23] D. Zhang and J. Chang, "Patterning of Electrospun Fibers Using Electroconductive Templates," *Advanced Materials,* vol. 19, pp. 3664-3667, 2007.
[24] Y. Wang, G. Wang, L. Chen, H. Li, T. Yin, B. Wang, *et al.*, "Electrospun nanofiber meshes with tailored architectures and patterns as potential tissue-engineering scaffolds," *Biofabrication,* vol. 1, p. 015001, Mar 2009.
[25] Z. Qi, H. Yu, Y. Chen, and M. Zhu, "Highly porous fibers prepared by electrospinning a ternary system of nonsolvent/solvent/poly(l-lactic acid)," *Materials Letters,* vol. 63, pp. 415-418, 2009.
[26] L. Natarajan, J. New, A. Dasari, S. Yu, and M. A. Manan, "Surface morphology of electrospun PLA fibers: mechanisms of pore formation," *RSC Adv.,* vol. 4, pp. 44082-44088, 2014.
[27] D. Li, Y. Wang, and Y. Xia, "Electrospinning Nanofibers as Uniaxially Aligned Arrays and Layer-by-Layer Stacked Films," *Advanced Materials,* vol. 16, pp. 361-366, 2004.
[28] W. E. Teo and S. Ramakrishna, "A review on electrospinning design and nanofibre assemblies," *Nanotechnology,* vol. 17, pp. R89-R106, Jul 28 2006.
[29] L. M. Bellan and H. G. Craighead, "Control of an electrospinning jet using electric focusing and jet-steering fields," *Journal of Vacuum Science & Technology B: Microelectronics and Nanometer Structures,* vol. 24, p. 3179, 2006.
[30] S. Zhao, Q. Zhou, Y. Z. Long, G. H. Sun, and Y. Zhang, "Nanofibrous patterns by direct electrospinning of nanofibers onto topographically structured non-conductive substrates," *Nanoscale,* vol. 5, pp. 4993-5000, Jun 7 2013.
[31] J. Doshi and D. H. Reneker, "Electrospinning process and applications of electrospun fibers," in *Industry Applications Society Annual Meeting, 1993., Conference Record of the 1993 IEEE,* 1993, pp. 1698-1703 vol.3.

[32] U. Sharma, Q. Pham, and J. Marini, "Electrospinning process for fiber manufacture," ed: Google Patents, 2015.
[33] A. L. Yarin, S. Koombhongse, and D. H. Reneker, "Taylor cone and jetting from liquid droplets in electrospinning of nanofibers," *Journal of Applied Physics,* vol. 90, pp. 4836-4846, 2001.
[34] D. H. Reneker, A. L. Yarin, H. Fong, and S. Koombhongse, "Bending instability of electrically charged liquid jets of polymer solutions in electrospinning," *Journal of Applied physics,* vol. 87, pp. 4531-4547, 2000.
[35] T. Subbiah, G. Bhat, R. Tock, S. Parameswaran, and S. Ramkumar, "Electrospinning of nanofibers," *Journal of Applied Polymer Science,* vol. 96, pp. 557-569, 2005.
[36] T. Han, D. H. Reneker, and A. L. Yarin, "Buckling of jets in electrospinning," *Polymer,* vol. 48, pp. 6064-6076, 9/21/ 2007.
[37] D. H. Reneker, A. L. Yarin, H. Fong, and S. Koombhongse, "Bending instability of electrically charged liquid jets of polymer solutions in electrospinning," *Journal of Applied Physics,* vol. 87, p. 4531, 2000.
[38] J.-H. He, Y. Wu, and W.-W. Zuo, "Critical length of straight jet in electrospinning," *Polymer,* vol. 46, pp. 12637-12640, 2005.
[39] D. H. Reneker and A. L. Yarin, "Electrospinning jets and polymer nanofibers," *Polymer,* vol. 49, pp. 2387-2425, 5/13/ 2008.
[40] M. M. Hohman, M. Shin, G. Rutledge, and M. P. Brenner, "Electrospinning and electrically forced jets. I. Stability theory," *Physics of Fluids,* vol. 13, pp. 2201-2220, 2001.
[41] M. M. Hohman, M. Shin, G. Rutledge, and M. P. Brenner, "Electrospinning and electrically forced jets. II. Applications," *Physics of Fluids,* vol. 13, pp. 2221-2236, 2001.
[42] Y. M. Shin, M. M. Hohman, M. P. Brenner, and G. C. Rutledge, "Electrospinning: A whipping fluid jet generates submicron polymer fibers," *Applied Physics Letters,* vol. 78, pp. 1149-1151, 2001.
[43] J. Xie, S. M. Willerth, X. Li, M. R. Macewan, A. Rader, S. E. Sakiyama-Elbert, *et al.*, "The differentiation of embryonic stem cells seeded on electrospun nanofibers into neural lineages," *Biomaterials,* vol. 30, pp. 354-362, 1// 2009.
[44] S. A. Theron, E. Zussman, and A. L. Yarin, "Experimental investigation of the governing parameters in the electrospinning of polymer solutions," *Polymer,* vol. 45, pp. 2017-2030, 2004.
[45] A. Frenot and I. S. Chronakis, "Polymer nanofibers assembled by electrospinning," *Current Opinion in Colloid & Interface Science,* vol. 8, pp. 64-75, 2003.
[46] H. Liu, X. Ding, G. Zhou, P. Li, X. Wei, and Y. Fan, "Electrospinning of Nanofibers for Tissue Engineering Applications," *Journal of Nanomaterials,* vol. 2013, pp. 1-11, 2013.
[47] J. Liu, G. Chen, H. Gao, L. Zhang, S. Ma, J. Liang, *et al.*, "Structure and thermo-chemical properties of continuous bundles of aligned and stretched electrospun polyacrylonitrile precursor nanofibers collected in a flowing water bath," *Carbon,* vol. 50, pp. 1262-1270, 2012.
[48] M. C. Beilke, J. W. Zewe, J. E. Clark, and S. V. Olesik, "Aligned electrospun nanofibers for ultra-thin layer chromatography," *Analytica chimica acta,* vol. 761, pp. 201-208, 2013.

[49] W. S. Khan, R. Asmatulu, M. Ceylan, and A. Jabbarnia, "Recent progress on conventional and non-conventional electrospinning processes," *Fibers and Polymers,* vol. 14, pp. 1235-1247, 2013.
[50] W.-A. Yee, "Morphologies, structures and properties of electrospun poly (vinylidene difluoride)-based materials," 2012.
[51] D. Yang, B. Lu, Y. Zhao, and X. Jiang, "Fabrication of Aligned Fibrous Arrays by Magnetic Electrospinning," *Advanced Materials,* vol. 19, pp. 3702-3706, 2007.
[52] X. Ji, W. Yang, T. Wang, C. Mao, L. Guo, J. Xiao, *et al.*, "Coaxially electrospun core/shell structured poly (L-lactide) acid/chitosan nanofibers for potential drug carrier in tissue engineering," *Journal of biomedical nanotechnology,* vol. 9, pp. 1672-1678, 2013.
[53] J. E. Díaz, A. Barrero, M. Márquez, and I. G. Loscertales, "Controlled Encapsulation of Hydrophobic Liquids in Hydrophilic Polymer Nanofibers by Co-electrospinning," *Advanced Functional Materials,* vol. 16, pp. 2110-2116, 2006.
[54] Z. Sun, E. Zussman, A. L. Yarin, J. H. Wendorff, and A. Greiner, "Compound Core–Shell Polymer Nanofibers by Co-Electrospinning," *Advanced Materials,* vol. 15, pp. 1929-1932, 2003.
[55] O. O. Dosunmu, G. G. Chase, W. Kataphinan, and D. H. Reneker, "Electrospinning of polymer nanofibres from multiple jets on a porous tubular surface," *Nanotechnology,* vol. 17, p. 1123, 2006.
[56] I. C. Um, D. Fang, B. S. Hsiao, A. Okamoto, and B. Chu, "Electro-Spinning and Electro-Blowing of Hyaluronic Acid," *Biomacromolecules,* vol. 5, pp. 1428-1436, 2004/07/01 2004.
[57] A. L. Yarin and E. Zussman, "Upward needleless electrospinning of multiple nanofibers," *Polymer,* vol. 45, pp. 2977-2980, 4// 2004.
[58] S. Kidoaki, I. K. Kwon, and T. Matsuda, "Mesoscopic spatial designs of nano- and microfiber meshes for tissue-engineering matrix and scaffold based on newly devised multilayering and mixing electrospinning techniques," *Biomaterials,* vol. 26, pp. 37-46, 1// 2005.
[59] T. A. Telemeco, C. Ayres, G. L. Bowlin, G. E. Wnek, E. D. Boland, N. Cohen, *et al.*, "Regulation of cellular infiltration into tissue engineering scaffolds composed of submicron diameter fibrils produced by electrospinning," *Acta Biomaterialia,* vol. 1, pp. 377-385, 7// 2005.
[60] T. Vinoy, Z. Xing, A. C. Shane, and K. V. Yogesh, "Functionally graded electrospun scaffolds with tunable mechanical properties for vascular tissue regeneration," *Biomedical Materials,* vol. 2, p. 224, 2007.
[61] M. M. L. Arras, C. Grasl, H. Bergmeister, and H. Schima, "Electrospinning of aligned fibers with adjustable orientation using auxiliary electrodes," *Science and Technology of Advanced Materials,* vol. 13, p. 035008, 2012.
[62] Y. Yang, Z. Jia, J. Liu, Q. Li, L. Hou, L. Wang, *et al.*, "Effect of electric field distribution uniformity on electrospinning," *Journal of Applied Physics,* vol. 103, p. 104307, 2008.
[63] L. M. Bellan and H. G. Craighead, "Control of an electrospinning jet using electric focusing and jet-steering fields," *Journal of Vacuum Science & Technology B,* vol. 24, pp. 3179-3183, 2006.

[64] J. M. Deitzel, J. D. Kleinmeyer, J. K. Hirvonen, and N. C. Beck Tan, "Controlled deposition of electrospun poly(ethylene oxide) fibers," *Polymer,* vol. 42, pp. 8163-8170, 9// 2001.
[65] G. H. Kim, "Electrospun PCL nanofibers with anisotropic mechanical properties as a biomedical scaffold," *Biomed Mater,* vol. 3, p. 025010, Jun 2008.
[66] X.-y. Ye, Y.-n. Jin, X.-j. Huang, L. Luo, and Z.-k. Xu, "Simulation of electrical field for the formation mechanism of Bird's Nest patterned structures by electrospinning," *Chinese Journal of Polymer Science,* vol. 31, pp. 514-520, 2012.
[67] R. Casasola, N. L. Thomas, A. Trybala, and S. Georgiadou, "Electrospun poly lactic acid (PLA) fibres: Effect of different solvent systems on fibre morphology and diameter," *Polymer,* vol. 55, pp. 4728-4737, 9/2/ 2014.
[68] T. A. Kowalewski, S. Barral, and T. Kowalczyk, "Modeling electrospinning of nanofibers," in *IUTAM symposium on modelling nanomaterials and nanosystems*, 2009, pp. 279-292.
[69] A. A. Vetcher, R. Gearheart, and V. N. Morozov, "Polyacrylamide-based material for electrospun humidity-resistant, water-soluble nanofilters," *Polymers for Advanced Technologies,* vol. 19, pp. 1276-1285, 2008.
[70] R. Deliu, I. Sandu, R. Butnaru, I. G. Sandu, and D. Lukas, "Study of the Influence of Electrospinning Parameters on the Structure and Morphology of Polyvinyl Alcohol Nanofibers," *Re vista de Chimie*, vol. 6, pp. 603-611, 2012.
[71] S. C. Baker, N. Atkin, P. A. Gunning, N. Granville, K. Wilson, D. Wilson, *et al.*, "Characterisation of electrospun polystyrene scaffolds for three-dimensional in vitro biological studies," *Biomaterials,* vol. 27, pp. 3136-3146, 2006.
[72] I. Savva, G. Krekos, A. Taculescu, O. Marinica, L. Vekas, and T. Krasia-Christoforou, "Fabrication and characterization of magnetoresponsive electrospun nanocomposite membranes based on methacrylic random copolymers and magnetite nanoparticles," *Journal of Nanomaterials,* vol. 2012, p. 18, 2012.
[73] H. R. Pant, M. P. Bajgai, C. Yi, R. Nirmala, K. T. Nam, W.-i. Baek, *et al.*, "Effect of successive electrospinning and the strength of hydrogen bond on the morphology of electrospun nylon-6 nanofibers," *Colloids and Surfaces A: Physicochemical and Engineering Aspects,* vol. 370, pp. 87-94, 11/5/ 2010.
[74] H. Liu and Y.-L. Hsieh, "Ultrafine fibrous cellulose membranes from electrospinning of cellulose acetate," *Journal of Polymer Science Part B: Polymer Physics,* vol. 40, pp. 2119-2129, 2002.
[75] J. Ayutsede, M. Gandhi, S. Sukigara, H. Ye, C.-m. Hsu, Y. Gogotsi, *et al.*, "Carbon nanotube reinforced Bombyx mori silk nanofibers by the electrospinning process," *Biomacromolecules,* vol. 7, pp. 208-214, 2006.
[76] D. I. Zeugolis, S. T. Khew, E. S. Yew, A. K. Ekaputra, Y. W. Tong, L.-Y. L. Yung, *et al.*, "Electro-spinning of pure collagen nano-fibres–just an expensive way to make gelatin?," *Biomaterials,* vol. 29, pp. 2293-2305, 2008.
[77] R. Nirmala, H. Panth, C. Yi, K. Nam, S.-J. Park, H. Kim, *et al.*, "Effect of solvents on high aspect ratio polyamide-6 nanofibers via electrospinning," *Macromolecular Research,* vol. 18, pp. 759-765, 2010/08/01 2010.
[78] J. Hao, G. Lei, Z. Li, L. Wu, Q. Xiao, and L. Wang, "A novel polyethylene terephthalate nonwoven separator based on electrospinning technique for lithium ion battery," *Journal of Membrane Science,* vol. 428, pp. 11-16, 2/1/ 2013.

[79] K. H. Lee, H. Y. Kim, Y. M. La, D. R. Lee, and N. H. Sung, "Influence of a mixing solvent with tetrahydrofuran and N,N-dimethylformamide on electrospun poly(vinyl chloride) nonwoven mats," *Journal of Polymer Science Part B: Polymer Physics,* vol. 40, pp. 2259-2268, 2002.
[80] Z. G. Chen, B. Wei, X. M. Mo, and F. Z. Cui, "Diameter control of electrospun chitosan-collagen fibers," *Journal of Polymer Science Part B: Polymer Physics,* vol. 47, pp. 1949-1955, 2009.
[81] M. Sethupathy, S. Ravichandran, and P. Manisankar, "Preparation of PVdF-PAN-V2O5 hybrid composite membrane by electrospinning and fabrication of dye-sensitized solar cells," *International Journal of Electrochemical Science,* vol. 9, pp. 3166-3180, 2014.
[82] X. Zhang, Y. Wang, D. Guo, and Y. Wang, "The Morphology of the Hollow PAN Fibers through Electrospinning," *AASRI Procedia,* vol. 3, pp. 236-241, // 2012.
[83] T. D. Brown, P. D. Dalton, and D. W. Hutmacher, "Direct writing by way of melt electrospinning," *Adv Mater,* vol. 23, pp. 5651-7, Dec 15 2011.
[84] D. W. Hutmacher and P. D. Dalton, "Melt electrospinning," *Chem Asian J,* vol. 6, pp. 44-56, Jan 3 2011.
[85] H. Fong, I. Chun, and D. H. Reneker, "Beaded nanofibers formed during electrospinning," *Polymer,* vol. 40, pp. 4585-4592, 7// 1999.
[86] J. Deitzel, J. Kleinmeyer, D. Harris, and N. B. Tan, "The effect of processing variables on the morphology of electrospun nanofibers and textiles," *Polymer,* vol. 42, pp. 261-272, 2001.
[87] X. Geng, O.-H. Kwon, and J. Jang, "Electrospinning of chitosan dissolved in concentrated acetic acid solution," *Biomaterials,* vol. 26, pp. 5427-5432, 2005.
[88] P. Heikkilä and A. Harlin, "Parameter study of electrospinning of polyamide-6," *European Polymer Journal,* vol. 44, pp. 3067-3079, 10// 2008.
[89] S. H. Tan, R. Inai, M. Kotaki, and S. Ramakrishna, "Systematic parameter study for ultra-fine fiber fabrication via electrospinning process," *Polymer,* vol. 46, pp. 6128-6134, 7/25/ 2005.
[90] K. H. Lee, H. Y. Kim, H. J. Bang, Y. H. Jung, and S. G. Lee, "The change of bead morphology formed on electrospun polystyrene fibers," *Polymer,* vol. 44, pp. 4029-4034, 6// 2003.
[91] A. Koski, K. Yim, and S. Shivkumar, "Effect of molecular weight on fibrous PVA produced by electrospinning," *Materials Letters,* vol. 58, pp. 493-497, 1// 2004.
[92] V. Beachley and X. Wen, "Effect of electrospinning parameters on the nanofiber diameter and length," *Materials science & engineering. C, Materials for biological applications,* vol. 29, pp. 663-668, 2009.
[93] C. Zhang, X. Yuan, L. Wu, Y. Han, and J. Sheng, "Study on morphology of electrospun poly(vinyl alcohol) mats," *European Polymer Journal,* vol. 41, pp. 423-432, 2005.
[94] C. Mit-uppatham, M. Nithitanakul, and P. Supaphol, "Ultrafine Electrospun Polyamide-6 Fibers: Effect of Solution Conditions on Morphology and Average Fiber Diameter," *Macromolecular Chemistry and Physics,* vol. 205, pp. 2327-2338, 2004.
[95] W. K. Son, J. H. Youk, T. S. Lee, and W. H. Park, "The effects of solution properties and polyelectrolyte on electrospinning of ultrafine poly(ethylene oxide) fibers," *Polymer,* vol. 45, pp. 2959-2966, 4// 2004.

[96] Y. Ying, J. Zhidong, L. Qiang, and G. Zhicheng, "Experimental investigation of the governing parameters in the electrospinning of polyethylene oxide solution," *Dielectrics and Electrical Insulation, IEEE Transactions on,* vol. 13, pp. 580-585, 2006.
[97] W.-E. Teo, R. Inai, and S. Ramakrishna, "Technological advances in electrospinning of nanofibers," *Science and Technology of Advanced Materials,* vol. 12, p. 013002, 2011.
[98] C. L. Casper, J. S. Stephens, N. G. Tassi, D. B. Chase, and J. F. Rabolt, "Controlling Surface Morphology of Electrospun Polystyrene Fibers: Effect of Humidity and Molecular Weight in the Electrospinning Process," *Macromolecules,* vol. 37, pp. 573-578, 2004/01/01 2004.
[99] M. Bognitzki, W. Czado, T. Frese, A. Schaper, M. Hellwig, M. Steinhart, *et al.*, "Nanostructured Fibers via Electrospinning," *Advanced Materials,* vol. 13, pp. 70-72, 2001.
[100] Z. Qi, H. Yu, Y. Chen, and M. Zhu, "Highly porous fibers prepared by electrospinning a ternary system of nonsolvent/solvent/poly(l-lactic acid)," *Materials Letters,* vol. 63, pp. 415-418, 2/15/ 2009.
[101] Y. You, J. H. Youk, S. W. Lee, B.-M. Min, S. J. Lee, and W. H. Park, "Preparation of porous ultrafine PGA fibers via selective dissolution of electrospun PGA / PLA blend fibers," *Materials Letters,* vol. 60, pp. 757-760, 3// 2006.
[102] J. T. McCann, M. Marquez, and Y. Xia, "Highly Porous Fibers by Electrospinning into a Cryogenic Liquid," *Journal of the American Chemical Society,* vol. 128, pp. 1436-1437, 2006/02/01 2006.
[103] I. Donmez, F. Kayaci, C. Ozgit-Akgun, T. Uyar, and N. Biyikli, "Fabrication of hafnia hollow nanofibers by atomic layer deposition using electrospun nanofiber templates," *Journal of Alloys and Compounds,* vol. 559, pp. 146-151, 5/15/ 2013.
[104] D. Li and Y. Xia, "Direct Fabrication of Composite and Ceramic Hollow Nanofibers by Electrospinning," *Nano Letters,* vol. 4, pp. 933-938, 2004/05/01 2004.
[105] J. T. McCann, D. Li, and Y. Xia, "Electrospinning of nanofibers with core-sheath, hollow, or porous structures," *Journal of Materials Chemistry,* vol. 15, pp. 735-738, 2005.
[106] S.-H. Park, B.-K. Kim, and W.-J. Lee, "Electrospun activated carbon nanofibers with hollow core/highly mesoporous shell structure as counter electrodes for dye-sensitized solar cells," *Journal of Power Sources,* vol. 239, pp. 122-127, 10/1/ 2013.
[107] L. Cheng, X. Zhou, H. Zhong, X. Deng, Q. Cai, and X. Yang, "NaF-loaded core–shell PAN–PMMA nanofibers as reinforcements for Bis-GMA/TEGDMA restorative resins," *Materials Science and Engineering: C,* vol. 34, pp. 262-269, 1/1/ 2014.
[108] Y. Li, F. Chen, J. Nie, and D. Yang, "Electrospun poly(lactic acid)/chitosan core–shell structure nanofibers from homogeneous solution," *Carbohydrate Polymers,* vol. 90, pp. 1445-1451, 11/6/ 2012.
[109] B.-S. Lee, S.-B. Son, K.-M. Park, J.-H. Seo, S.-H. Lee, I.-S. Choi, *et al.*, "Fabrication of Si core/C shell nanofibers and their electrochemical performances as a lithium-ion battery anode," *Journal of Power Sources,* vol. 206, pp. 267-273, 5/15/ 2012.

[110] G. Yan, J. Yu, Y. Qiu, X. Yi, J. Lu, X. Zhou, *et al.*, "Self-Assembly of Electrospun Polymer Nanofibers: A General Phenomenon Generating Honeycomb-Patterned Nanofibrous Structures," *Langmuir*, vol. 27, pp. 4285-4289, 2011/04/19 2011.
[111] D. Zhang and J. Chang, "Electrospinning of Three-Dimensional Nanofibrous Tubes with Controllable Architectures," *Nano Letters*, vol. 8, pp. 3283-3287, 2008/10/08 2008.
[112] W. Wang, S. Itoh, K. Konno, T. Kikkawa, S. Ichinose, K. Sakai, *et al.*, "Effects of Schwann cell alignment along the oriented electrospun chitosan nanofibers on nerve regeneration," *Journal of Biomedical Materials Research Part A*, vol. 91A, pp. 994-1005, 2009.
[113] I. K. Shim, M. R. Jung, K. H. Kim, Y. J. Seol, Y. J. Park, W. H. Park, *et al.*, "Novel three-dimensional scaffolds of poly(L-lactic acid) microfibers using electrospinning and mechanical expansion: Fabrication and bone regeneration," *Journal of Biomedical Materials Research Part B: Applied Biomaterials*, vol. 95B, pp. 150-160, 2010.
[114] L. H. Leung, S. Fan, and H. E. Naguib, "Fabrication of 3D electrospun structures from poly (lactide-co-glycolide acid)–nano-hydroxyapatite composites," *Journal of Polymer Science Part B: Polymer Physics*, vol. 50, pp. 242-249, 2012.
[115] X.-H. Qin and S.-Y. Wang, "Filtration properties of electrospinning nanofibers," *Journal of Applied Polymer Science*, vol. 102, pp. 1285-1290, 2006.
[116] R. Asmatulu, H. Muppalla, Z. Veisi, W. S. Khan, A. Asaduzzaman, and N. Nuraje, "Study of Hydrophilic Electrospun Nanofiber Membranes for Filtration of Micro and Nanosize Suspended Particles," *Membranes*, vol. 3, pp. 375-388, 11/14 07/24/received 10/18/revised 10/21/accepted 2013.
[117] M. Faccini, C. Vaquero, and D. Amantia, "Development of Protective Clothing against Nanoparticle Based on Electrospun Nanofibers," *Journal of Nanomaterials*, vol. 2012, p. 9, 2012.
[118] C. Tang and H. Liu, "Cellulose nanofiber reinforced poly(vinyl alcohol) composite film with high visible light transmittance," *Composites Part A: Applied Science and Manufacturing*, vol. 39, pp. 1638-1643, 10// 2008.
[119] S. Ramakrishna, J. Mayer, E. Wintermantel, and K. W. Leong, "Biomedical applications of polymer-composite materials: a review," *Composites Science and Technology*, vol. 61, pp. 1189-1224, 2001.
[120] Y. Zhou, H. Yang, X. Liu, J. Mao, S. Gu, and W. Xu, "Electrospinning of carboxyethyl chitosan/poly(vinyl alcohol)/silk fibroin nanoparticles for wound dressings," *International Journal of Biological Macromolecules*, vol. 53, pp. 88-92, 2// 2013.
[121] S. Bose, M. Roy, and A. Bandyopadhyay, "Recent advances in bone tissue engineering scaffolds," *Trends in Biotechnology*, vol. 30, pp. 546-554, 10// 2012.
[122] H. Yoshimoto, Y. M. Shin, H. Terai, and J. P. Vacanti, "A biodegradable nanofiber scaffold by electrospinning and its potential for bone tissue engineering," *Biomaterials*, vol. 24, pp. 2077-2082, 5// 2003.
[123] Y. Zhang, J. R. Venugopal, A. El-Turki, S. Ramakrishna, B. Su, and C. T. Lim, "Electrospun biomimetic nanocomposite nanofibers of hydroxyapatite/chitosan for bone tissue engineering," *Biomaterials*, vol. 29, pp. 4314-4322, 11// 2008.
[124] C. Li, C. Vepari, H.-J. Jin, H. J. Kim, and D. L. Kaplan, "Electrospun silk-BMP-2 scaffolds for bone tissue engineering," *Biomaterials*, vol. 27, pp. 3115-3124, 2006.

[125] J.-H. Jang, O. Castano, and H.-W. Kim, "Electrospun materials as potential platforms for bone tissue engineering," *Advanced Drug Delivery Reviews,* vol. 61, pp. 1065-1083, 10/5/ 2009.
[126] C. M. Vaz, S. van Tuijl, C. V. C. Bouten, and F. P. T. Baaijens, "Design of scaffolds for blood vessel tissue engineering using a multi-layering electrospinning technique," *Acta Biomaterialia,* vol. 1, pp. 575-582, 9// 2005.
[127] L. Soletti, Y. Hong, J. Guan, J. J. Stankus, M. S. El-Kurdi, W. R. Wagner, *et al.*, "A bilayered elastomeric scaffold for tissue engineering of small diameter vascular grafts," *Acta Biomaterialia,* vol. 6, pp. 110-122, 1// 2010.
[128] M. G. Kang, K. M. Kim, K. S. Ryu, S. H. Chang, N.-G. Park, J. S. Hong, *et al.*, "Dye-Sensitized TiO2 Solar Cells Using Polymer Gel Electrolytes Based on PVdF-HFP," *Journal of The Electrochemical Society,* vol. 151, pp. E257-E260, July 1, 2004 2004.
[129] B. H. Lee, M. Y. Song, S.-Y. Jang, S. M. Jo, S.-Y. Kwak, and D. Y. Kim, "Charge Transport Characteristics of High Efficiency Dye-Sensitized Solar Cells Based on Electrospun TiO2 Nanorod Photoelectrodes," *The Journal of Physical Chemistry C,* vol. 113, pp. 21453-21457, 2009/12/24 2009.
[130] T. Cao, Y. Li, C. Wang, C. Shao, and Y. Liu, "A Facile in Situ Hydrothermal Method to SrTiO3/TiO2 Nanofiber Heterostructures with High Photocatalytic Activity," *Langmuir,* vol. 27, pp. 2946-2952, 2011/03/15 2011.
[131] H. J. Kim, Y. S. Kim, M. H. Seo, S. M. Choi, and W. B. Kim, "Pt and PtRh nanowire electrocatalysts for cyclohexane-fueled polymer electrolyte membrane fuel cell," *Electrochemistry Communications,* vol. 11, pp. 446-449, 2// 2009.
[132] M. Li, G. Han, and B. Yang, "Fabrication of the catalytic electrodes for methanol oxidation on electrospinning-derived carbon fibrous mats," *Electrochemistry Communications,* vol. 10, pp. 880-883, 6// 2008.
[133] J. S. Im, S.-J. Park, T. Kim, and Y.-S. Lee, "Hydrogen storage evaluation based on investigations of the catalytic properties of metal/metal oxides in electrospun carbon fibers," *International Journal of Hydrogen Energy,* vol. 34, pp. 3382-3388, 5// 2009.
[134] S. E. Hong, D.-K. Kim, S. M. Jo, D. Y. Kim, B. D. Chin, and D. W. Lee, "Graphite nanofibers prepared from catalytic graphitization of electrospun poly(vinylidene fluoride) nanofibers and their hydrogen storage capacity," *Catalysis Today,* vol. 120, pp. 413-419, 2/28/ 2007.
[135] G. Wee, H. Z. Soh, Y. L. Cheah, S. G. Mhaisalkar, and M. Srinivasan, "Synthesis and electrochemical properties of electrospun V2O5 nanofibers as supercapacitor electrodes," *Journal of Materials Chemistry,* vol. 20, pp. 6720-6725, 2010.
[136] B.-H. Kim, K. S. Yang, H.-G. Woo, and K. Oshida, "Supercapacitor performance of porous carbon nanofiber composites prepared by electrospinning polymethylhydrosiloxane (PMHS)/polyacrylonitrile (PAN) blend solutions," *Synthetic Metals,* vol. 161, pp. 1211-1216, 7// 2011.
[137] E. Formo, E. Lee, D. Campbell, and Y. Xia, "Functionalization of Electrospun TiO2 Nanofibers with Pt Nanoparticles and Nanowires for Catalytic Applications," *Nano Letters,* vol. 8, pp. 668-672, 2008/02/01 2008.
[138] P. Gouma, "Nanostructured polymorphic oxides for advanced chemosensors," *Rev. Adv. Mater. Sci,* vol. 5, p. 122, 2003.

[139] A. Babel, D. Li, Y. Xia, and S. A. Jenekhe, "Electrospun Nanofibers of Blends of Conjugated Polymers: Morphology, Optical Properties, and Field-Effect Transistors," *Macromolecules,* vol. 38, pp. 4705-4711, 2005/05/01 2005.
[140] N. J. Pinto, A. T. Johnson, A. G. MacDiarmid, C. H. Mueller, N. Theofylaktos, D. C. Robinson, *et al.*, "Electrospun polyaniline/polyethylene oxide nanofiber field-effect transistor," *Applied Physics Letters,* vol. 83, pp. 4244-4246, 2003.
[141] M. Bognitzki, H. Hou, M. Ishaque, T. Frese, M. Hellwig, C. Schwarte, *et al.*, "Polymer, Metal, and Hybrid Nano- and Mesotubes by Coating Degradable Polymer Template Fibers (TUFT Process)," *Advanced Materials,* vol. 12, pp. 637-640, 2000.
[142] Y.-Z. Long, M.-M. Li, C. Gu, M. Wan, J.-L. Duvail, Z. Liu, *et al.*, "Recent advances in synthesis, physical properties and applications of conducting polymer nanotubes and nanofibers," *Progress in Polymer Science,* vol. 36, pp. 1415-1442, 10// 2011.
[143] H. Liu, D. Wang, N. Zhao, J. Ma, J. Gong, S. Yang, *et al.*, "Application of electrospinning fibres on sound absorption in low and medium frequency range," *Materials Research Innovations,* vol. 18, pp. S4-888-S4-891, 2014.
[144] V. Thavasi, G. Singh, and S. Ramakrishna, "Electrospun nanofibers in energy and environmental applications," *Energy & Environmental Science,* vol. 1, p. 205, 2008.
[145] J. Chang, M. Dommer, C. Chang, and L. Lin, "Piezoelectric nanofibers for energy scavenging applications," *Nano Energy,* vol. 1, pp. 356-371, 2012.
[146] S. Basu, A. K. Agrawal, and M. Jassal, "Concept of minimum electrospinning voltage in electrospinning of polyacrylonitrile N,N-dimethylformamide system," *Journal of Applied Polymer Science,* vol. 122, pp. 856-866, 2011.
[147] http://www.eetimes.com/document.asp?doc_id=1273089, "Flyback transformer tutorial: function and design," 2006.
[148] S. Park, K. Park, H. Yoon, J. Son, T. Min, and G. Kim, "Apparatus for preparing electrospun nanofibers: designing an electrospinning process for nanofiber fabrication," *Polymer International,* vol. 56, pp. 1361-1366, 2007.
[149] X. Wang, B. Ding, G. Sun, M. Wang, and J. Yu, "Electro-spinning/netting: A strategy for the fabrication of three-dimensional polymer nano-fiber/nets," *Progress in Materials Science,* vol. 58, pp. 1173-1243, 2013.
[150] X. Chen, S. Xu, N. Yao, and Y. Shi, "1.6 V nanogenerator for mechanical energy harvesting using PZT nanofibers," *Nano Lett,* vol. 10, pp. 2133-7, Jun 9 2010.
[151] Y. Dai, W. Liu, E. Formo, Y. Sun, and Y. Xia, "Ceramic nanofibers fabricated by electrospinning and their applications in catalysis, environmental science, and energy technology," *Polymers for Advanced Technologies,* vol. 22, pp. 326-338, 2011.
[152] G. S. Bisht, G. Canton, A. Mirsepassi, L. Kulinsky, S. Oh, D. Dunn-Rankin, *et al.*, "Controlled Continuous Patterning of Polymeric Nanofibers on Three-Dimensional Substrates Using Low-Voltage Near-Field Electrospinning," *Nano Letters,* vol. 11, pp. 1831-1837, 2011.
[153] W. E. Teo, M. Kotaki, X. M. Mo, and S. Ramakrishna, "Porous tubular structures with controlled fibre orientation using a modified electrospinning method," *Nanotechnology,* vol. 16, pp. 918-924, 2005.

[154] C. Huang, R. Chen, Q. Ke, Y. Morsi, K. Zhang, and X. Mo, "Electrospun collagen–chitosan–TPU nanofibrous scaffolds for tissue engineered tubular grafts," *Colloids and Surfaces B: Biointerfaces,* vol. 82, pp. 307-315, 2/1/ 2011.
[155] C.-Y. Wang, K.-H. Zhang, C.-Y. Fan, X.-M. Mo, H.-J. Ruan, and F.-F. Li, "Aligned natural–synthetic polyblend nanofibers for peripheral nerve regeneration," *Acta Biomaterialia,* vol. 7, pp. 634-643, 2// 2011.
[156] V. Beachley and X. Wen, "Effect of electrospinning parameters on the nanofiber diameter and length," *Mater Sci Eng C Mater Biol Appl,* vol. 29, pp. 663-668, Apr 30 2009.
[157] D. Yang, Y. Li, and J. Nie, "Preparation of gelatin/PVA nanofibers and their potential application in controlled release of drugs," *Carbohydrate Polymers,* vol. 69, pp. 538-543, 2007.
[158] S. Wu, F. Li, H. Wang, L. Fu, B. Zhang, and G. Li, "Effects of poly (vinyl alcohol)(PVA) content on preparation of novel thiol-functionalized mesoporous PVA/SiO 2 composite nanofiber membranes and their application for adsorption of heavy metal ions from aqueous solution," *Polymer,* vol. 51, pp. 6203-6211, 2010.
[159] H.-w. Duan, J.-g. Jiang, B.-y. Li, B. Li, and T.-h. He, "Electric Field Finite Element Analysis and Experimentation of PlatePlate Type Electrospinning Machine," *International Journal of Control and Automation,* vol. 7, pp. 179-190, 2014.
[160] H. M. Powell and S. T. Boyce, "Fiber density of electrospun gelatin scaffolds regulates morphogenesis of dermal–epidermal skin substitutes," *Journal of Biomedical Materials Research Part A,* vol. 84A, pp. 1078-1086, 2008.
[161] D.-H. Kim, C.-H. Seo, K. Han, K. W. Kwon, A. Levchenko, and K.-Y. Suh, "Cell Migration: Guided Cell Migration on Microtextured Substrates with Variable Local Density and Anisotropy (Adv. Funct. Mater. 10/2009)," *Advanced Functional Materials,* vol. 19, pp. 1579-1586, 2009.
[162] J. Xie, W. Liu, M. R. MacEwan, P. C. Bridgman, and Y. Xia, "Neurite Outgrowth on Electrospun Nanofibers with Uniaxial Alignment: The Effects of Fiber Density, Surface Coating, and Supporting Substrate," *ACS Nano,* vol. 8, pp. 1878-1885, 2014/02/25 2014.
[163] G. C. Rutledge and S. V. Fridrikh, "Formation of fibers by electrospinning," *Adv Drug Deliv Rev,* vol. 59, pp. 1384-91, Dec 10 2007.
[164] L. Liu and Y. A. Dzenis, "Analysis of the effects of the residual charge and gap size on electrospun nanofiber alignment in a gap method," *Nanotechnology,* vol. 19, p. 355307, Sep 3 2008.
[165] V. Pornsopone, P. Supaphol, R. Rangkupan, and S. Tantayanon, "Electrospinning of methacrylate-based copolymers: Effects of solution concentration and applied electrical potential on morphological appearance of as-spun fibers," *Polymer Engineering & Science,* vol. 45, pp. 1073-1080, 2005.
[166] M. C. Phipps, W. C. Clem, J. M. Grunda, G. A. Clines, and S. L. Bellis, "Increasing the pore sizes of bone-mimetic electrospun scaffolds comprised of polycaprolactone, collagen I and hydroxyapatite to enhance cell infiltration," *Biomaterials,* vol. 33, pp. 524-534, 1// 2012.
[167] B. Sun, Y. Z. Long, H. D. Zhang, M. M. Li, J. L. Duvail, X. Y. Jiang, *et al.*, "Advances in three-dimensional nanofibrous macrostructures via electrospinning," *Progress in Polymer Science,* vol. 39, pp. 862-890, 2014.

[168] Y. Ou, F. Yang, and Z.-Z. Yu, "A new conception on the toughness of nylon 6/silica nanocomposite prepared via in situ polymerization," *Journal of Polymer Science Part B: Polymer Physics*, vol. 36, pp. 789-795, 1998.
[169] B. K. Kuila and A. K. Nandi, "Physical, Mechanical, and Conductivity Properties of Poly(3-hexylthiophene)−Montmorillonite Clay Nanocomposites Produced by the Solvent Casting Method," *Macromolecules*, vol. 37, pp. 8577-8584, 2004/11/01 2004.
[170] R. K. Shah and D. R. Paul, "Nylon 6 nanocomposites prepared by a melt mixing masterbatch process," *Polymer*, vol. 45, pp. 2991-3000, 4// 2004.
[171] C. Zhou, Q. Shi, W. Guo, L. Terrell, A. T. Qureshi, D. J. Hayes, *et al.*, "Electrospun bio-nanocomposite scaffolds for bone tissue engineering by cellulose nanocrystals reinforcing maleic anhydride grafted PLA," *ACS Appl Mater Interfaces*, vol. 5, pp. 3847-54, May 2013.
[172] A. Ramezani Kakroodi, S. Cheng, M. Sain, and A. Asiri, "Mechanical, Thermal, and Morphological Properties of Nanocomposites Based on Polyvinyl Alcohol and Cellulose Nanofiber fromAloe veraRind," *Journal of Nanomaterials*, vol. 2014, pp. 1-7, 2014.
[173] Y. Srithep, L.-S. Turng, R. Sabo, and C. Clemons, "Nanofibrillated cellulose (NFC) reinforced polyvinyl alcohol (PVOH) nanocomposites: properties, solubility of carbon dioxide, and foaming," *Cellulose*, vol. 19, pp. 1209-1223, 2012.
[174] M. S. Peresin, Y. Habibi, J. O. Zoppe, J. J. Pawlak, and O. J. Rojas, "Nanofiber Composites of Polyvinyl Alcohol and Cellulose Nanocrystals: Manufacture and Characterization," *Biomacromolecules*, vol. 11, pp. 674–681, 2010.
[175] W. Li, J. Yue, and S. Liu, "Preparation of nanocrystalline cellulose via ultrasound and its reinforcement capability for poly(vinyl alcohol) composites," *Ultrason Sonochem*, vol. 19, pp. 479-85, May 2012.
[176] H. Zhang, J. Huang, L. Yang, R. Chen, W. Zou, X. Lin, *et al.*, "Preparation, characterization and properties of PLA/TiO2nanocomposites based on a novel vane extruder," *RSC Adv.*, vol. 5, pp. 4639-4647, 2015.
[177] S. Mazinani, A. Ajji, and C. Dubois, "Morphology, structure and properties of conductive PS/CNT nanocomposite electrospun mat," *Polymer*, vol. 50, pp. 3329-3342, 7/3/ 2009.
[178] N. G. Sahoo, S. Rana, J. W. Cho, L. Li, and S. H. Chan, "Polymer nanocomposites based on functionalized carbon nanotubes," *Progress in Polymer Science*, vol. 35, pp. 837-867, 7// 2010.
[179] B. Sundaray, V. Subramanian, T. S. Natarajan, and K. Krishnamurthy, "Electrical conductivity of a single electrospun fiber of poly(methyl methacrylate) and multiwalled carbon nanotube nanocomposite," *Applied Physics Letters*, vol. 88, p. 143114, 2006.
[180] Q. Wang, J. Dai, W. Li, Z. Wei, and J. Jiang, "The effects of CNT alignment on electrical conductivity and mechanical properties of SWNT/epoxy nanocomposites," *Composites Science and Technology*, vol. 68, pp. 1644-1648, 6// 2008.
[181] A. Dasari, S. Sarang, and R. Misra, "Strain rate sensitivity of homopolymer polypropylenes and micrometric wollastonite-filled polypropylene composites," *Materials Science and Engineering: A*, vol. 368, pp. 191-204, 2004.

[182] A. Dasari and R. Misra, "The role of micrometric wollastonite particles on stress whitening behavior of polypropylene composites," *Acta materialia,* vol. 52, pp. 1683-1697, 2004.
[183] R. Misra, R. Hadal, and S. Duncan, "Surface damage behavior during scratch deformation of mineral reinforced polymer composites," *Acta Materialia,* vol. 52, pp. 4363-4376, 2004.
[184] A. S. Luyt, M. D. Dramićanin, Ž. Antić, and V. Djoković, "Morphology, mechanical and thermal properties of composites of polypropylene and nanostructured wollastonite filler," *Polymer Testing,* vol. 28, pp. 348-356, 2009.
[185] S. Radhakrishnan and P. S. Sonawane, "Role of heat transfer and thermal conductivity in the crystallization behavior of polypropylene-containing additives: A phenomenological model," *Journal of applied polymer science,* vol. 89, pp. 2994-2999, 2003.
[186] M. Ichazo, C. Albano, J. Gonzalez, R. Perera, and M. Candal, "Polypropylene/wood flour composites: treatments and properties," *Composite structures,* vol. 54, pp. 207-214, 2001.
[187] S. M. Nachtigall, G. S. Cerveira, and S. M. Rosa, "New polymeric-coupling agent for polypropylene/wood-flour composites," *Polymer Testing,* vol. 26, pp. 619-628, 2007.
[188] Y. Wang, R. Qi, C. Xiong, and M. Huang, "Effects of coupling agent and interfacial modifiers on mechanical properties of poly (lactic acid) and wood flour biocomposites," *Iran Polym J,* vol. 20, pp. 281-294, 2011.
[189] B. L. Shah, S. E. Selke, M. B. Walters, and P. A. Heiden, "Effects of wood flour and chitosan on mechanical, chemical, and thermal properties of polylactide," *Polymer Composites,* vol. 29, pp. 655-663, 2008.
[190] S. K. Ozaki, M. B. B. Monteiro, H. Yano, Y. Imamura, and M. F. Souza, "Biodegradable composites from waste wood and poly(vinyl alcohol)," *Polymer Degradation and Stability,* vol. 87, pp. 293-299, 2// 2005.
[191] L. Huang, J. T. Arena, S. S. Manickam, X. Jiang, B. G. Willis, and J. R. McCutcheon, "Improved mechanical properties and hydrophilicity of electrospun nanofiber membranes for filtration applications by dopamine modification," *Journal of Membrane Science,* vol. 460, pp. 241-249, 6/15/ 2014.
[192] J. Yao, C. Bastiaansen, and T. Peijs, "High Strength and High Modulus Electrospun Nanofibers," *Fibers,* vol. 2, pp. 158-186, 2014.
[193] H. Ito, "Wood plastic composites using cellulose nanofiber technique," *Nippon Gomu Kyokaishi,* vol. 2, pp. 41-45, 2013.
[194] N. M. Stark and R. E. Rowlands, "Effects of wood fiber characteristics on mechanical properties of wood/polypropylene composites," *Wood and fiber science,* vol. 35, pp. 167-174, 2003.
[195] B. J. Saikia and G. Parthasarathy, "Fourier Transform Infrared Spectroscopic Characterization of Kaolinite from Assam and Meghalaya, Northeastern India," *Journal of Modern Physics,* vol. 01, pp. 206-210, 2010.
[196] R. Rošic, J. Pelipenko, P. Kocbek, S. Baumgartner, M. Bešter-Rogač, and J. Kristl, "The role of rheology of polymer solutions in predicting nanofiber formation by electrospinning," *European Polymer Journal,* vol. 48, pp. 1374-1384, 2012.

[197] T. Ke and X. Sun, "Melting behavior and crystallization kinetics of starch and poly(lactic acid) composites," *Journal of Applied Polymer Science*, vol. 89, pp. 1203-1210, 2003.

Appendix

There are four elements such as tets, bricks, prisms, and pyramids (shown in Figure A1) can be used, in various combinations, to mesh any 3D model.

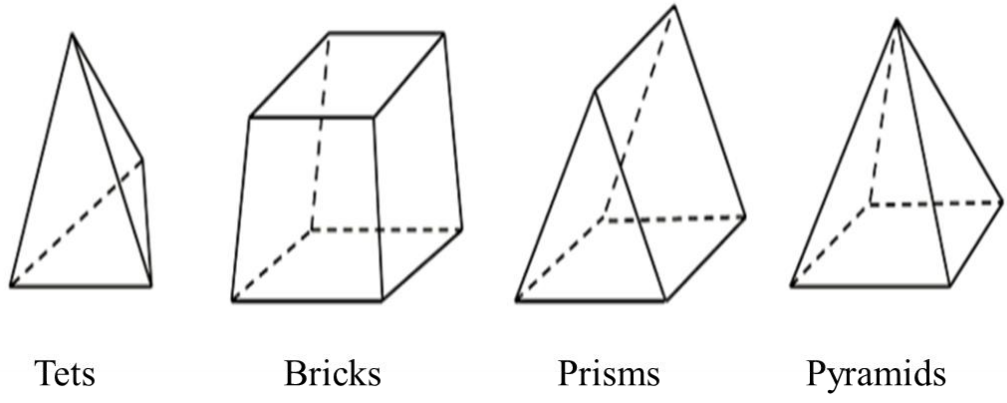

Figure A1 Three dimensional mesh elements

Tetrahedral elements are the most common used element type for any 3D model in FE analysis. They are known as a simplex because any 3D volume, regardless of shape or topology, can be meshed with tets. They can be used with adaptive mesh refinement. For these reasons, tets elements are the first choice of meshing. The other three element types (bricks, prisms, and pyramids) are normally used when it is driven to do so. The meshing algorithm usually needs some more user input to create such a mesh and with these elements it will not always be able to mesh all types of geometry.

In order to choose the tetrahedral element size for meshing of each geometry we carried out a quick simulation for three different cases which are listed in Table A1.

The distance between the needle and collector was 60 mm. A box 100 mm (L) x 55 mm (W) x 55 mm (H) was drawn to model the surrounding environment. The materials of needle, electrodes, and surrounding were stainless steel, copper, and air, respectively. At

the needle, a 10 KV positive voltage potential was applied and zero potential to electrodes. Three dimensional tetrahedral mesh generated for different cases is displayed in Figure A2.

Table A1 Different element configurations for meshing of geometry

	Needle	**Electrodes**	**Remaining Geometry**
Case 1	Extremely fine element (max. size – 2 mm Min. size – 0.02 mm)	Extra fine element (max. size – 3.5 mm Min. size – 0.15 mm)	Finer element (max. size – 5.5 mm Min. size – 0.4 mm)
Case 2	Finer element (max. size – 5.5 mm Min. size – 0.4 mm)	Fine element (max. size – 8 mm Min. size – 1 mm)	Normal element (max. size – 10 mm Min. size – 1.8 mm)
Case 3	Custom element (max. size – 1 mm Min. size – 0.005 mm)	Custom element (max. size – 2 mm Min. size – 0.02 mm)	Custom element (max. size – 3 mm Min. size – 0.2 mm)

Electrical field strengths are measured at the needle tip and electrode tip which are listed in Table A2. It is seen that the electrical field strengths are almost similar in case 1 and 3. In contrast, slightly higher electrical field strength was observed in case 2 where coarse elements were used for meshing. Therefore, we selected case 1 for further FE simulation.

Table A2 Electrical field strength for different cases

	Electrical field strength at needle tip (V/m)	**Electrical field strength at electrode tip (V/m)**
Case 1	5.5×10^6	1.2×10^6
Case 2	5.6×10^6	1.2×10^6
Case 3	5.5×10^6	1.2×10^6

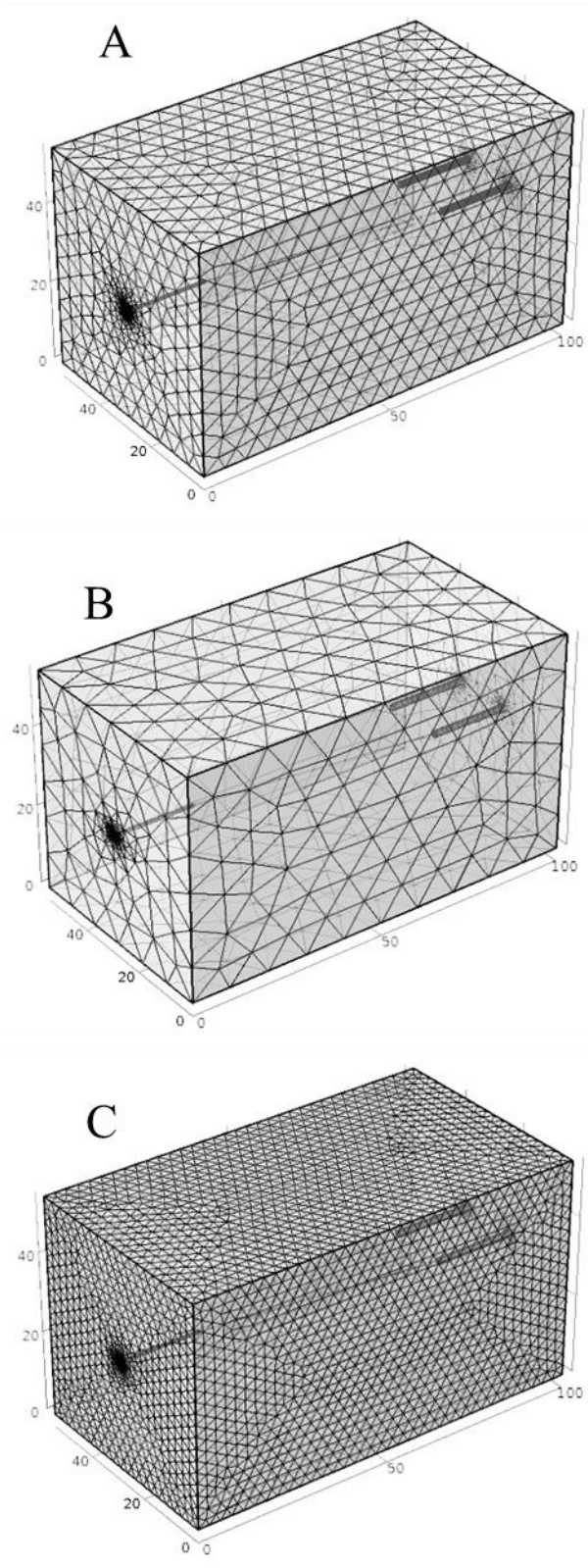

Figure A2 3D tetrahedral mesh A) case 1, B) case 2, and C) case 3.